AN ANALYSIS OF THE STRESS-STRAIN BEHAVIOR OF
SEVERAL GRADES OF POLYCRYSTALLINE
TITANIUM AND ZIRCONIUM WITH REFERENCE TO
DYNAMIC STRAIN AGING AND DEFORMATION
TWINNING BETWEEN 77 AND 1000°K

By

Anand Madhav Garde

A Dissertation Presented to the Graduate Council
of the University of Florida in Partial Fulfillment
of the Requirements for the Degree of Doctor of
Philosophy

UNIVERSITY OF FLORIDA

1973

AN ANALYSIS OF THE STRESS-STRAIN BEHAVIOR OF
SEVERAL GRADES OF POLYCRYSTALLINE
TITANIUM AND ZIRCONIUM WITH REFERENCE TO
DYNAMIC STRAIN AGING AND DEFORMATION
TWINNING BETWEEN 77 AND 1000°K

By

Anand Madhav Garde

A Dissertation Presented to the Graduate Council
of the University of Florida in Partial Fulfillment
of the Requirements for the Degree of Doctor of
Philosophy

UNIVERSITY OF FLORIDA

1973

To

My Parents

COPYRIGHT INFORMATION

This dissertation uses the contents of the paper,
"A Dual Analysis of Longitudinal and Transverse Zirconium
Tensile Stress-Strain Data," that was presented at the ASTM-
AIME Symposium on Zirconium in Nuclear Applications, August
21-24, 1973, Portland, Oregon and is accepted by ASTM for
publication in the Special Technical Publication 551 cover-
ing the Proceedings of the Symposium. All copyright and
publication rights are reserved for the American Society
for Testing and Materials.

ACKNOWLEDGMENTS

TABLE OF CONTENTS

LIST OF TABLES

LIST OF FIGURES

viii

xiii

AN ANALYSIS OF THE STRESS-STRAIN BEHAVIOR OF SEVERAL GRADES
OF POLYCRYSTALLINE TITANIUM AND ZIRCONIUM WITH REFERENCE TO
DYNAMIC STRAIN AGING AND DEFORMATION TWINNING
BETWEEN 77 AND 1000°K

By

Anand Madhav Garde

December, 1973

Chairman: Dr. Robert E. Reed-Hill
Major Department: Materials Science and Engineering

Constant strain rate tensile tests were conducted on
several grades of polycrystalline titanium and zirconium over
the temperature range 77 to 1000°K. With the help of a com-
puter, the data were analysed by both the Crussard-Jaoul
method and a modified method based on the Swift equation.
Though both the methods reveal similar deformation stages,
each method has advantages under specific conditions. While
the results of the Crussard-Jaoul analysis are independent
of the flow stress level, they are significantly affected by
the prestrain and manufacturing history of the metal.   The
converse is true in the case of the modified method.

The basic zirconium stress-strain curve when deforma-
tion primarily occurs by slip, as in longitudinal specimens
at high temperatures, conforms to a single stage behavior.
Whenever mechanical twinning or kinking occurs, additional
deformation stages are introduced. On the other hand,

titanium shows a two stage behavior above the "blue brittle" temperature. This difference in the deformation stage behavior can explain the difference in high temperature uniform elongations of titanium and zirconium.

The linear work hardening rate and high uniform elongations in titanium and zirconium at low temperatures are closely related to deformation twinning. Impurities suppress deformation twinning in these metals, the effect being stronger in zirconium than in titanium. The twin volume fraction measurements of the twinned structures reveal that a constant work hardening stage is associated with a high rate of build up of the twin volume fraction. A closer examination of these structures with the help of quantitative microscopic parameters implies that geometric hardening is probably mainly responsible for the effect of twinning on the work hardening behavior of titanium and zirconium at low temperatures.

At high temperatures (500-800°K) titanium exhibits significant dynamic strain aging effects. The DSA phenomena in zirconium, however, are very weak. These results indicate that while the impurity atoms interact strongly with the dislocations in titanium, this interaction is weak in zirconium. Considering the major known manifestations of dynamic strain aging, the DSA effects in titanium are comparable to those in steels.

The strain rate sensitivity data, obtained from differential strain rate tests, shed light on several features of

deformation of titanium and zirconium. First, they imply that the low temperature rate controlling thermally activated deformation mechanism is probably overcoming of the interstitial barrier atoms. They also indicate that below room temperature, where deformation occurs both by slip and twinning, titanium and zirconium obey the Cottrell-Stokes law. The temperature variations of the strain rate sensitivity and the work hardening rate parameter indicate that the deformation behavior of pure zirconium and pure titanium approach the characteristics of a fcc metal.

The effects of 77°K prestrain and prestraining in the dynamic strain aging interval on the room temperature properties of titanium were investigated. Work softening was not observed in either case. However, only the 77°K prestrain introduced significant strengthening at room temperature.

CHAPTER I
INTRODUCTION

The reductions in cost due to the recent advances in process metallurgy have made titanium and zirconium available for increasing numbers of industrial applications. Titanium is suitable for aerospace use because of its superior mechanical properties coupled with a high strength to weight ratio. Zirconium is used in the nuclear industry by virtue of its good strength and neutron cross-section. Therefore a better understanding of the mechanical behavior of titanium and zirconium is essential.

Some important factors, other than slip, that could influence the deformation characteristics of a metal are deformation twinning, dynamic recovery and dynamic strain aging. The objective of this investigation is to study these parameters with respect to the tensile deformation of titanium and zirconium over the temperature range 77 to 1000 °K. For this purpose tensile specimens of several grades of titanium and zirconium were strained to various levels up to fracture on an Instron machine at several strain rates. The resulting stress-strain data are analysed by two approaches based on empirical equations. An attempt is made to correlate the deformation stage behavior with microstructural changes, work hardening characteristics and elongation parameters.

There is some contradiction in the literature regarding the existence of mechanical twinning in the low temperature deformation of high purity titanium. The results obtained in this investigation demonstrate that deformation twinning influences significantly the mechanical properties of high purity titanium below 424 °K. With the help of quantitative microscopy, the role of twin nucleation and twin growth is evaluated in the 77 °K deformation of titanium and zirconium.

Although there are some reported examples of dynamic strain aging in titanium and zirconium, there is no comprehensive study of all aspects of dynamic strain aging. One of the objectives of the present investigation was to evaluate the significance of DSA effects in these metals compared to a well-known example of DSA phenomena in steels. For this comparison, all known major manifestations of dynamic strain aging were considered. One interesting outcome of this study is that although titanium and zirconium have similar crystal structures (hcp), similar c/a ratios, elastic moduli and slip modes, the strength of DSA phenomena in these two metals is quite different. Whereas the DSA effects in commercial titanium are strong and comparable to those observed in steels, these effects are much weaker in zirconium. Factors possibly responsible for this difference in DSA behavior will be discussed.

From the strain rate change experiments, the strain rate sensitivity of titanium and zirconium was evaluated at different temperatures. A study of the temperature and strain depen-

dence of the strain rate sensitivity was useful in investigating several aspects of deformation in these metals. These are the rate controlling thermally activated deformation mechanism at low temperatures, conformity to the Cottrell-Stokes law, the necking strain, the "blue brittle" effect and the strength of dynamic strain aging.

CHAPTER II
PREVIOUS INVESTIGATIONS

2.1 Deformation Twinning in Titanium

Although there are various investigations in the past dealing with mechanical twinning in titanium, there is a considerable disagreement in the literature concerning the existence and importance of deformation twinning in titanium at low temperatures. Orava, Stone and Conrad[1] indicated that fine grained commercial purity titanium specimens fail to reveal twins in the microstructure after 0.1 plastic strain at 77°K. This was attributed to the fine grain size and impurity content of the metal. Jones and Conrad[2] reported that twinning was not evident in the necked part of fine grained titanium specimen deformed at 4.2°K. The same authors neglect[3] the subject of deformation twinning completely in a paper related to the deformation of titanium at subambient temperatures and state in another publication[4] that no deformation twinning was observed in commercial purity A-70 titanium regardless of grain size or strain.

Nevertheless Rosi and Perkins[5] observed twins in coarse grained iodide titanium deformed at 77°K and at room temperature, the extent of twinning being higher at lower temperatures. Kula and DeSisto[6] showed mechanical twins in coarse grained commercial titanium specimen deformed at 4.2°K.

Burrier, Amateau and Steigerwald[7] reported thick twins on the surface of commercial purity fine grained specimens, which were ductile at low temperatures, when deformed below 175 °K. Apart from these works that demonstrate the existence of twinning at low temperatures, there are others that show that twinning not only occurs in titanium at low temperatures, but has a significant effect on the mechanical properties of this metal. In the commercial plate texture of titanium, the majority of grains are oriented with their basal plane parallel to the rolling plane. Longitudinal cylindrical specimens cut from such a plate, when deformed at elevated temperatures, show eliptical cross-section as deformation occurs primarily by $\{10\bar{1}0\}$ $\langle11\bar{2}0\rangle$ prism slip. Rosi and Perkins[8] observed that this elipticity of deformed cross-section decreased with decreasing deformation temperature. This observation implies that at low temperatures deformation modes are added that contribute a finite shear component normal to the basal plane (rolling plane of the plate) resulting in a more circular cross-section. These additional deformation modes could be either slip on systems with dislocations having Bergers vector with a component normal to the basal plane, i. e. (c+a) dislocations on pyramid planes or alternatively they could be mechanical twinning modes. The results of Lii et al.[9] are consistent with the latter possibility. They demonstrated that increasing twin volume fraction at low temperatures could account for the change in the strain anisotropy.

It has been reported in the literature that deformation twinning significantly affects the stress-strain behavior of titanium at low temperatures. A linear stress-strain curve in alpha titanium deformed at 77 °K was reported by Wasilewski[10] who attributed this "laminar flow" to a combination of slip and twinning. He further concluded that the large uniform elongation observed at 77 °K was a result of the ease with which twinning occured in this metal. These results have been recently confirmed by Santhanam.[11]

Thus although there is a strong evidence for low temperature deformation twinning in titanium, the absence of twinning in some cases has been attributed to fine grain size and swaged texture. Some of this latter work was done on high purity titanium. Therefore, a reexamination of the role of mechanical twinning in the low temperature deformation of fine grained high purity titanium specimens obtained from swaged rods was undertaken.

2.2 Dynamic Strain Aging in Titanium

The early investigations of Rosi and Perkins[8] and Kiessel and Sinnott[12] showed that strain aging influences both the tensile and creep properties of commercial purity titanium respectively. In recent years, however, the subject of strain aging in titanium has been largely ignored.[1,3,4,10,13] It is suggested in some publications[14-16] that strain aging in titanium is unimportant. Suiter[14] investigated the tensile defor-

mation of titanium solid solution alloys between 300 and 900° K and expressed doubts about the occurrence of strain aging in titanium. Turner and Roberts[15] associated an endurance ratio peak at 523 °K in titanium to a weak dynamic strain aging effect. They also indicated that while evidence exists for static strain aging in dilute titanium alloys, the effect appears small compared to that in low carbon steels. In a strain aging review paper, Baird[16] states that the yield point and strain aging effects in titanium are consistent with a relatively weak interaction between interstitial atoms and dislocations.

On the other hand, evidence[17-18] exists that dynamic strain aging is probably a very significant factor in the deformation of titanium. Since the basis for measuring the importance of dynamic strain aging in a metal has not been clearly defined in the past, a comparison of the tensile properties of two titanium grades, commercial purity and high purity, was deemed worthwhile. All known major manifestations of dynamic strain aging were considered for this purpose.

The principal characteristics of DSA phenomena are[19] the elongation minimum or "blue brittle" effect, low ($\simeq$zero) strain rate sensitivity, abnormal and rate dependent work hardening, plateaus or peaks in the flow stress-temperature diagrams, transients following a strain rate change in a constant temperature tensile test and serrated stress-strain curves (also known as the Portevin-LeChatelier effect, discontinuous yielding or jerky flow).

2.3 Dynamic Strain Aging in Zirconium

Although a comprehensive study considering all major aspects of the dynamic strain aging phenomena in zirconium has not been reported in the literature, there are some examples of individual aspects. These include differential strain rate transients and serrated stress-strain curves in iodide zirconium;[20] strain rate dependent peaks in flow stress-temperature diagrams of zirconium;[21-22] "blue brittle" effect in zirconium[21] and Zircaloy-2;[23-26] strain rate sensitivity-temperature curve minima in zirconium,[20,21,23] Zircaloy-2,[23-27] Zircaloy-4,[28] Zr-N alloys,[29] single crystals of Zr-O alloys[30-31] and Zircaloy-2 single crystals;[27-32] a decreasing creep rate with increasing temperature in Zircaloy-2;[26] apparent creep activation energy peaks in Zircaloy-2 at about 625 °K;[33] an anomalous stress-strain relationship near 625 °K in Zircaloy-2[23] and unusual thermal activation parameter variations with temperature above 300 °K in Zircaloy-2.[34]

2.4 Strain Rate Sensitivity

Two different definitions of the strain rate sensitivity are reported in the literature. The first definition of the strain rate sensitivity parameter, n, is based on an empirical equation

$$(\sigma_1 / \sigma_2) = (\dot{\epsilon}_1 / \dot{\epsilon}_2)^n \qquad (1)$$

Where σ_1 and σ_2 are the flow stresses at the strain rates $\dot{\epsilon}_1$ and $\dot{\epsilon}_2$ respectively. Under the assumptions that the Orowan equation ($\dot{\epsilon}=\rho_m bv$, where ρ_m is the mobile dislocation density, b is the Burgers vector and v is the average dislocation velocity) holds, that the thermally activated component dominates the flow stress and that ρ_m is not a function of strain rate, n defined in this manner is equal to the reciprocal of m , the stress-velocity exponent defined by the relation

$$(v_1 / v_2) = (\sigma_1 / \sigma_2)^m \qquad (2)$$

where v_1 and v_2 are the dislocation velocities at flow stresses σ_1 and σ_2 respectively.

The other definition of the strain rate sensitivity n'

$$n' = (d\sigma/d\ln\dot{\epsilon})$$

is based on the assumption that the deformation can be described by an equation

$$\dot{\epsilon} = A \cdot \exp-\left\{(H-v\sigma)/kT\right\} \qquad (3)$$

Where H is the activation enthalpy, v is the activation volume, T is the absolute temperature, k is the Boltzmann constant and A is a constant. The parameter n' is related to the reciprocal of the activation volume $(n'= kT/v)$. The first definition of the strain rate sensitivity is used in the present investigation.

There are three basically different methods of measuring the strain rate sensitivity of a metal : differential strain rate tests, stress relaxation and from the yield stress data. In the stress relaxation technique, a specimen is strained to a certain value of plastic strain and the crosshead of the testing machine is stopped. The mobile diclocations in the specimen continue to move even when the crosshead is stationary; therefore, the load relaxes and the drop of load is recorded as a function of time. The main advantage of the relaxation technique is that the amount of plastic strain involved in each test is small and therefore the same specimen can be used to obtain a number of data points. However, very accurate temperature control is necessary. This is a problem during high temperature relaxation tests. Also, analyses of the relaxation data involve assumptions that may not be valid under the dynamic strain aging conditions. For example, in one approach[35-36] the relaxation data are plotted as τ against log (t+c) where τ is the resolved shear stress, t is the time and c is a constant chosen over a certain time range to fit the data to a straight line. The positive value of the slope of this logarithmic relaxation plot is equal to n'. This curve fitting is objectionable[37] when dynamic strain aging or dynamic recovery effects are important. The assumption involved in this analysis is that the long range internal stress component τ_μ is practically constant during relaxation. It has been shown that for titanium[18] in the dynamic strain aging region the work hardening rate is strain rate

dependent and even a small increment in strain can give rise to significant change in the flow stress level. Thus the assumption of constant τ_μ may be questionable in the DSA range. The Li-Gupta[38-40] stress relaxation method plots $\log\left(d\sigma/dt\right)$ against $\log t$ and the slope of this plot is related to the stress-velocity exponent. This analysis assumes that the stress-velocity exponent is constant with velocity. The stress relaxation technique with high speed digital data recording proposed by Lee and Hart[41] is not based on any assumption and therefore seems to be widely applicable.

Sometimes the strain rate sensitivity is calculated from the yield stress data obtained from different constant strain rate tests. In the dynamic strain aging interval, where the work hardening is rate dependent, this method does not give the value of strain rate sensitivity at constant structure. Also due to the inverse rate dependence of the flow stress in DSA region, this analysis may give negative values of strain rate sensitivity. In a differential strain rate test, following an increase in the strain rate, the load normally does not drop instantaneously (even when transients are present) and therefore a negative value of the strain rate sensitivity is hard to rationalize.

In a differential strain rate test, the strain rate is changed during the test and the corresponding change in the flow stress is measured to calculate the strain rate sensitivity. On the load-elongation chart obtained from the machine, the change in the load following a change in the strain rate

in the DSA region is usually not smooth and therefore the value of n obtained in this region strongly depends on the extrapolation used to calculate the change in load. It has[42] been proposed that these transients observed after a strain rate change are due to dislocation multiplication. The steady state at the new strain rate probably involves a different dislocation substructure. Therefore extrapolation from the steady state at the new strain rate as used in the past[20] gives a strain rate sensitivity value with a change in the structure. On the other hand, an instantaneous change in the load indicates the value of the strain rate sensitivity without a change in the structure.

The strain rate sensitivity is a useful parameter to study several aspects of deformation. Firstly, since the strain rate sensitivity is related to the thermal component of the flow stress, it can be a tool to study the thermally activated deformation mechanisms in a metal. Secondly, the variation of the strain rate sensitivity with strain can determine the validity of Cottrell-Stokes law in a metal. The Cottrell-Stokes law states that

$$(\Delta \sigma / \sigma) = \text{Const.}$$

where $\Delta \sigma$ is the change in the flow stress σ following a change in the strain rate or temperature. Since

$$n = \log(\sigma_2/\sigma_1)/\log(\dot{\epsilon}_2/\dot{\epsilon}_1) \tag{4}$$

When $\quad \dot{\epsilon}_2 = 10\dot{\epsilon}_1$

$$n = \log(\sigma_2/\sigma_1) = \log(1 + \Delta\sigma/\sigma) \qquad (5)$$

Thus if the Cottrell-Stokes law is obeyed, n should remain constant with strain.

There is some disagreement in the literature regarding the validity of the Cottrell-Stokes law in Zr. Results of Soo and Higgins[30] indicate that zirconium-oxygen single crystals obey the Cottrell-Stokes law. Ramaswami and Craig[20] conclude that the Cottrell-Stokes law is obeyed in alpha-zirconium when plastic deformation occurs by twinning as well as slip. Gupta[43] working with Group IV B hcp metals, suggests that the application of the Cottrell-Stokes law to zirconium, titanium and hafnium is of questionable significance. Orava et al.[1] indicate that commercial Ti does not follow the Cottrell-Stokes relationship. One objective of the present investigation was to check the validity of the Cottrell-Stokes relationship in two grades each of titanium and zirconium in terms of the variation of the strain rate sensitivity with strain.

The variation of the strain rate sensitivity with temperature can reveal the regions of dynamic strain aging of a metal. There is a large amount of evidence showing a strain rate sensitivity minimum in the dynamic strain aging interval of different metals. A minimum on the n-T diagram has been

observed in 61-S aluminum alloy,[44] bcc metals like steels,[45,46] molybdenum,[47] carbide strengthened molybdenum,[48] tantalum,[49] vanadium[50] and hcp metals like titanium[1,17] and zirconium and zirconium alloys.[20,21,23,27-32] However, the effect of composition on the temperature variation of the strain rate sensitivity has not been evaluated in the past. One of the aim of the present study was to find the effect of composition on the strain rate sensitivity of titanium and zirconium and to determine the importance of low strain rate sensitivity as a measure of dynamic strain aging.

When a neck forms during the tensile testing of a specimen, the effective strain rate increases in the neck due to the localized deformation. One of the factors influencing the stability of the neck is the strain rate dependence of the flow stress i. e. the magnitude of the strain rate sensitivity of the metal. Consequently, a study of the strain rate sensitivity parameter over a broad temperature range may lead to a better understanding of necking phenomena.

2.5 Stress-Strain Analysis

A typical face centered cubic single crystal stress-strain curve usually reveals three deformation stages.[51] At small strains, in stage I, the deformation starts on the favorably oriented primary system. This region is also known as the easy glide region. This stage may or may not be present depending on crystal orientation and impurity content

of the metal. At intermediate strains, stage II of high
work hardening is characterised by a ratio of work hardening
to the shear modulus that is independent of the applied
stress, temperature, orientation and is of the same magni-
tude, 4×10^{-3}, for all fcc metals. In this stage there is
an interaction between primary and secondary slip systems.
Following stage II, due to dynamic recovery, the slope of
the stress-strain curve decreases with increasing strain and
this region is designated as stage III. The stress necessary
for the onset of stage III is strongly temperature dependent.

Deformation stages have been observed in the tensile
stress-strain curves of polycrystalline metals of all three
common crystal structures : face centered cubic,[52-59] body
centered cubic[60-62] and hexagonal close packed.[63-64] In the
fcc case, these stages have been related to the changes in
the processes that occur during deformation. For example,
in the case of copper and nickel, four stages have been iden-
tified.[52-57] In the microstrain region designated as the
accommodation stage, ($\epsilon < 0.001$), multiple slip starts in the
largest grains and spreads to the neighoring grains. It is
followed by stage I upto a strain $\epsilon = 0.01$ where all grains
deform by multiple slip. In stage II, slip concentrates on
primary systems with hardening interaction from secondary
systems. Subsequently, stage III appears where the work hard-
ening rate rapidly decreases due to dynamic recovery.

While the stage I of a polycrystalline fcc metal differs
fundamentally from the easy glide in fcc crystal, stages II

and III are analogous in two cases. However, there is one important distinction. Whereas the work hardening rate is constant during the stage II of a fcc single crystal, the work hardening rate continues to decrease during stage II of a polycrystalline fcc metal. Moreover, the magnitude of the ratio of the work hardening rate to the elastic constant is generally greater in stage II of a polycrystalline metal than in stage II of a single crystal. For example, it is well known[51] that $(1/G) \cdot (d\tau/d\gamma)_{II}$ for single crystals equals 4×10^{-3}. Using the relation

$$(d\tau/d\gamma) = (d\sigma/d\epsilon) \cdot m^2 \qquad (6)$$

where $m = \cos\theta \cdot \cos\phi$ (Schmidt factor) and taking the average value of $m = 0.4$ and $E = 2.5\,G$, one would expect that for polycrystals,

$$1/E \cdot (d\sigma/d\epsilon)_{II} = 10^{-2} \qquad (7)$$

The observed slope of the stage II of polycrystalline fcc metal is generally higher than this value everywhere but approaches this value at the end of stage II. This is probably due to the additional hardening introduced by the presence of grain boundaries.

While the deformation stages are directly evident on the stress-strain curve of a typical fcc crystal, an analysis is usually necessary to reveal the stages of a polycrystalline

curve. Three important empirical equations that can be used
for such an analysis are :

(a) the Hollomon equation[65] : $\sigma = k_1 \epsilon_p^{n_1}$ (8)

(b) the Ludwik equation[66] : $\sigma = \sigma_0 + k_2 \epsilon_p^{n_2}$ (9)

(c) the modified Swift equation[67] : $\epsilon_p = \epsilon_{p_0} + c\,\sigma^m$ (10)

where σ is the true stress, ϵ_p the true plastic strain, and ϵ_{p_0},
σ_0, k_1, k_2, c, m, n_1 and n_2 are constants. In the Hollomon
analysis, the constants k_1 and n_1 are usually determined
from a plot of $\log \sigma$ against $\log \epsilon_p$. When the stress-strain
curve has a finite proportional limit, as when the thermally
activated flow stress component is large, the Hollomon anal-
ysis may not give useful results and then a Crussard-Jaoul
analysis,[68-70] based on the Ludwik equation (9), is more suit-
able. In this case, the constants σ_0, k_2 and n_2 are evaluat-
ed from a $\log\,(d\sigma/d\epsilon_p)$ versus $\log \epsilon_p$ plot. Changes in the de-
formation behavior are also more readily detected by this
type of analysis because $(d\sigma/d\epsilon_p)$ is plotted rather than σ.

A new technique of stress-strain analysis based on the
modified Swift equation was recently proposed.[59] In this
approach $\log\,(d\sigma/d\epsilon_p)$ is plotted as a function of $\log \sigma$ and
the constants c, m and ϵ_{p_0} are evaluated from such a plot.
In the present investigation the relative advantages and lim-
itations of this method will be compared with those of the
Crussard-Jaoul method. An appropriate analysis will be used
to study the influence of dynamic strain aging and mechanical

twinning on the deformation stages of titanium and zirconium.

2.6 Quantitative Microscopic Study of Deformation Twinning

Although titanium and zirconium have similar deformation modes, nearly equal elastic moduli and (c/a) ratios, the longitudinal specimen stress-strain curves of these two metals are very different at low temperatures (77°K). This is particularly true at the commercial purity level, but significant differences also appear in the curves of zone refined iodide purity specimens. Of significance is the fact that the deformation twinning behavior differs markedly in these metals at 77°K. Therfore, an investigation of the 77°K deformation twinning involving quantitative microscopy and a Crussard-Jaoul analysis of the stress-strain curves was undertaken.

Deformation twinning involves both twin nucleation and twin growth. To determine the relative importance of these processes in the two high purity metals, several geometric parameters[71] were measured as functions of strain. These include V_v, the twin volume fraction, S_v, the twin-matrix surface area per unit volume, $\overline{\lambda}$, the mean twin intercept and N_A, the number of twins per unit area of a sample plane passed through the microstructure.

The mean twin intercept is the average length of the intercept made by lines passed randomly through the twins over all orientations and is calculated from the relation

$$\overline{\lambda} = 4V_v/S_v \qquad (11)$$

Assuming a given twin shape, this parameter is an index of the average twin size. For the present case, where twins normally cross a complete grain, the dominant factor acting to change $\overline{\lambda}$ is an increase in the twin thickness. Another quantitative microscopic estimate of relevance is

$$N_v = 1/C \cdot (N_A/\overline{\lambda}) \qquad (12)$$

where C is a shape factor and N_v is the number of twins per unit volume.

Equation (12) is based on the assumption that all twins are of the same size and shape. The application of this relation in the case of h.p. Ti is probably justifiable since most twins extend across the grains, are nearly flat sided (only slightly lenticular), and do not grow appreciably in thickness. In the case of h.p. Zr, the twins grow somewhat in thickness and therefore twin size varies with strain. However, the twin shape does not alter significantly. The use of Equation (12), therefore, is still deemed reasonable. Thus, N_v is assumed proportional to $N_A/\overline{\lambda}$.

2.7 Effect of 77°K Prestraining on the Tensile Properties of Titanium at Room Temperature

Some years ago it was demonstrated[72] that the room temperature mechanical properties of transverse commercial purity zirconium specimens could be significantly improved by small amounts of prestrain at 77°K. This prestrain caused $\{11\overline{2}1\}$ twins to nucleate in grains with basal planes steeply inclined

to the tensile stress axis. At 300°K the growth of these twins had a measurable effect on the stress-strain curve. In particular, the curve tended to become linear with a significant increase in tensile elongation.

In longitudinal commercial purity zirconium specimens, the effect of prestrain at 77°K on the room temperature mechanical properties was found to be very small. This was a result of the fact that $\{11\bar{2}1\}$ twinning is not favored in a longitudinal specimen and the $\{11\bar{2}2\}$ and $\{10\bar{1}2\}$ twins that do form do not occur in sufficient numbers to have a significant effect.

Because both commercial purity and high purity titanium longitudinal specimens twin readily at 77°K but only moderately at the room temperature, it was felt that an investigation of the effect of 77°K prestrain on the 300°K mechanical properties might yield significant results. That this hypothesis is correct has been demonstrated by the present study. A significant point, however, is that the amount of prestrain needed to improve the mechanical properties is about an order of magnitude higher in the longitudinal titanium specimens than was required in the earlier transverse zirconium specimens.

2.8 Prestraining Titanium in the DSA Interval

Deformation of steel in its dynamic strain aging interval near 500°K results in a dislocation density higher than that due to strain outside this interval.[73,74] Moreover the

dislocation substructure at this temperature contains poorly defined cell walls with a high degree of tangling resulting in a high work hardening rate. Based on these facts, pre-straining in the dynamic strain aging temperature interval has been proposed[73,74] as a strengthening mechanism for improving the yield strength and ultimate tensile stress of steel at temperatures lower than the prestraining temperature. However, it has also been demonstrated[75] that a steel structure obtained in this manner may be subject to work softening at room temperature. Since it has been shown[76] that the work hardening peak in titanium is comparable to that in steel, it was proposed to investigate the effect of prestraining in DSA interval on the room temperature properties of commercial purity titanium.

CHAPTER III
EXPERIMENTAL PROCEDURE

3.1 <u>Materials and Specimen Geometry</u>

Two grades of titanium and four grades of zirconium
were used in the present investigation. The titanium grades
were designated as high purity (h.p.) and commercial purity
(c.p.). The zirconium grades were labled as high purity
(h.p.), commercial purity A (c.p.A), commercial purity B
(c.p.B) and high oxygen (h.o.). The compositions of all
the materials as furnished by the suppliers are listed in
Table I.

The h.p. titanium was received from the Materials Re-
search Corporation, Orangeburg, New York as 13 mm diameter
cold swaged rods of zone refined iodide titanium (MARZ grade).
These rods were further cold swaged to 5.5 mm diameter and
tensile specimens with a gage section 3.64 mm in diameter
by 21.5 mm length were machined from the rods. The speci-
mens were annealed in a 10^{-6} mm of mercury vacuum for 1 hour
at temperatures 698, 773 and 908°K resulting in recrystaliz-
ed grain sizes 2.4, 3.8 and 22 micron respectively. The
specimens had a swaged texture with the majority of the grains
oriented with their basal plane parallel to and evenly dis-
tributed around the wire axis. The specimen dimensions are
given in Fig. 1(a).

Table I

Compositions of Materials Used
and Other Experimental Conditions

Metal and Texture	H.P.Ti long. swaged	C.P.Ti long. rolled	C.P.Zr A long.and trans. rolled	C.P.Zr B long. rolled	H.P.Zr long. swaged	H.O.Zr long. swaged
Grain size μM	22	16	45	33	18	25
Strain rate s^{-1} 10^{-4}	3.8	2.7	2.7	2.7	3.8	3.8
Oxy. Eq.	5×10^{-4}	5×10^{-3}	7×10^{-3}	6×10^{-3}	6×10^{-4}	2×10^{-2}
Comp.ppm						
C	78	200	110	70	43	80
N	6	100	39	32	5	150
O	63	1360	965	880	50	2400
H	4	54/92	---	5	---	--
Fe	50	1600	435	380	90	4000
Si	--	--	71	53	---	200
Al	15	--	44	53	35	100
Zn	--	--	50	50	---	--
Hf	12	--	40	40	---	--
Cu	8	--	25	25	---	--
Ti	bal.	bal.	20	--	42	--
Cr	25	--	10	--	---	380
Mg	15	--	--	--	---	--
Mo	5	--	--	--	---	--
Nb	6	--	---	--	---	--
Sn	5	--	---	--	---	--
Zr	20	--	bal.	bal.	bal.	bal.
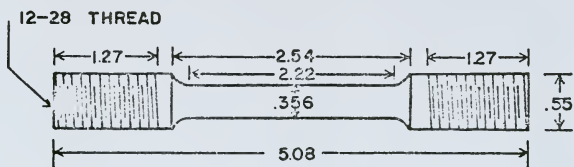
Fig. 1. The geometry of (a) h.p.Ti, h.p.Zr and h.o.Zr tensile specimens and of (b) c.p.Ti, c.p.Zr A and c.p.Zr B specimens. All dimensions are given in centimeters.

The c.p. titanium was obtained as a hot rolled annealed plate from Reactive Metals, Inc. The plate had a texture with the basal plane of the majority of the grains parallel to the rolling plane. The average grain size of the as received plate was 16 microns. Only longitudinal specimens, with their axis parallel to the rolling direction, were used in this investigation. Cylindrical tensile specimens with a 5 mm diameter by 31.75 mm gage length were machined. The specimen geometry is shown in Fig. 1(b).

The h.p. zirconium was obtained as a crystal bar from the Bettis Atomic Laboratory, Westinghouse Corporation and was zone melted by Dr. T. R. Cass at the Martin-Marietta Corporation, Orlando, Florida. The resulting 13 mm diameter bars were swaged to 5.5 mm diameter and 21.5 mm long by 3.64 mm diameter gage section specimens were machined from the rods. The specimens were annealed in vacuum at 888°K to an 18 micron grain size. Oxygen, nitrogen and carbon concentrations in the final specimens were determined by chemical analysis by the Armco Steel Corporation, Middletown, Ohio. The oxygen content was also analysed by neutron activation by Union Carbide, Tuxedo, New York. Analyses of all other elements were given by the supplier. The specimens had a wire texture.

The first grade of commercial purity zirconium (c.p.A) was an arc-melted sponge zirconium plate with an ASTM grain size 6 (45 microns) obtained from the Wah Chang Corporation in the form of a 13 mm thick plate. The plate had a texture

with a majority of the grains strongly aligned parallel to the rolling direction. The basal poles were nearly uniformly distributed about the rolling direction. This texture is similar to the wire texture. Both longitudinal and transverse specimens were used. The specimen geometry for both the c.p. A and c.p. B zirconium specimens was similar to that of c.p. titanium specimens.

The other grade of commercial purity zirconium (c.p. B) was purchased from the Reactive Metals, Inc. as an annealed hot rolled plate of 33 micron grain size. It had the same texture as that of c.p. Zr A. Only longitudinal specimens were used.

The high oxygen zirconium alloy (h.o.) was donated by the AMAX Specialty Metals, Akron, New York as a 26 mm thick cast plate. Cylindrical bars of 23 mm diameter were machined from this plate and then swaged down to 6 mm with intermittent annealing. Tensile specimen 3.64 mm in diameter and 21.5 mm long were machined and annealed in vacuum at $1118°K$ for 12 hours resulting in a 25 micron grain size.

3.2 Oxygen Equivalent

In order to compare the relative interstitial compositions of different grades of titanium and zirconium, an oxygen equivalent [77] was calculated for each grade. The oxygen equivalent is the effective atomic fraction of oxygen that will increase the flow stress to the same extent as caused

by the total interstitial content of the metal. The weight fraction of each interstitial element was converted to the atomic fraction by the relationship

$$\text{At. Fraction} = \text{Weight Fraction} \times \frac{\text{At. Weight of Matrix}}{\text{At. Weight of Interstitial}}$$

The oxygen equivalent total interstitial atomic fractions (O_{eq}) were then calculated using the empirical formula

$$O_{eq} = \text{At. Frac.(O)} + 2 \text{ At. Frac.(N)} + (3/4) \text{ At. Frac.(C)}$$

The equivalence factors 2 and (3/4) were originally calculated for titanium by Conrad[77] based on yield stress data. Using the flow stress data of Tyson[32] for Zr-O and Zr-N alloys, it was concluded that the factor 2 for nitrogen is also valid for zirconium. No data could be found in the literature for the effect of carbon content on the flow stress of zirconium. It is assumed here that the factor (3/4) calculated for carbon in titanium is also applicable for carbon in zirconium.

As indicated in Table 1, the oxygen equivalents were 5×10^{-4}, 5×10^{-3}, 6×10^{-4}, 7×10^{-3}, 6×10^{-3} and 2×10^{-2} for h.p.Ti, c.p.Ti, h.p.Zr, c.p.Zr A, c.p.Zr B and h.o.Zr materials respectively.

3.3 Apparatus and Testing Procedure

Cold Swaging : Cylindrical rods of as received materials h.p.Ti, h.p.Zr and h.o.Zr were cold swaged in a Fenn rotary swaging machine model 3F. Intermittent annealing was used

in the case of h.o.Zr to avoid fracture initiation. Nearly horizontal feeding was necessary for the ease of feeding and to avoid bending the rod. Swaged rods were machined into the tensile specimens. The tensile specimens were annealed in vacuum to obtain a desired grain size.

Vacuum Annealing : The vacuum annealing was done in a Minivac furnace assembly shown in Fig. 2. This assembly is equipped with a resistance heated tantalum hearth, $2\frac{1}{4}$ inches internal diameter by 4 inches high, that can work continuously at temperatures upto $2273°K$. The mechanical and diffusion pumps can maintain a vacuum of 0.001 micron mercury. A low voltage 7 KVA unit supplies power to the vacuum furnace. At one time as many as 16 tensile specimens, supported on a stand, could be annealed together. The vacuum was monitored by thermocouple and ionization gauges.

Specimen Profile Measurements : A Jones and Lamson Optical Comparator, capable of measuring 0.0001 inch vertical and 0.001 inch horizontal motion of the specimen platform, was used to measure the profile of the tensile specimen before and after the deformation. In this apparatus, a magnified image of the specimen edge is projected on the screen with cross hair lines. The relative movement of the specimen edge with respect to the cross hair line is used to determine the specimen dimensions accurately.

Tensile Testing : All tensile testing was carried out on

Fig. 2. The Minivac Vacuum Furnace Assembly.

two Instron machines, a 10,000 lbs capacity TT-C model and a 20,000 lbs capacity FDL model. The model FDL is shown in Fig. 3.

Constant strain rate tests to fracture were carried out over the temperature interval 77 to 1000°K. The low temperature pull rod and capsule assembly, used for testing at and below room temperature, is shown in Fig. 4. At 77°K, the capsule containing the specimen was immersed in a liquid nitrogen bath. At 193°K, an acetone bath containing solid dry ice was used to maintain the specimen temperature. The high temperature pull rod assembly is shown in Fig. 5. During a test, the temperature was maintained within $\pm$ 2°K of the test temperature. Prior to the actual straining, the capsule was held in the furnace for a sufficient time to attain a uniform temperature throughout the specimen. High purity argon gas was circulated around the specimen to avoid oxidation at high temperatures. In the case of titanium specimens, the oxidation was further suppressed by enclosing clean zirconium chips near the specimen in the capsule. Crosshead speeds of 0.051 and 0.51 mm/min were used (strain rates 10^{-5} and 10^{-4} per second respectively). Zero suppresion of the load was sometimes used to reveal and magnify serrations on the load-elongation chart. For a metallographic study of the specimens deformed at low temperatures, tensile specimens were strained to specific amounts of plastic strain.

Strain rate change experiments were conducted between 77 and 1000°K. A change in the crosshead speed from 0.051

Fig. 3. The 20,000 lbs. capacity Instron Testing
Machine Model FDL.
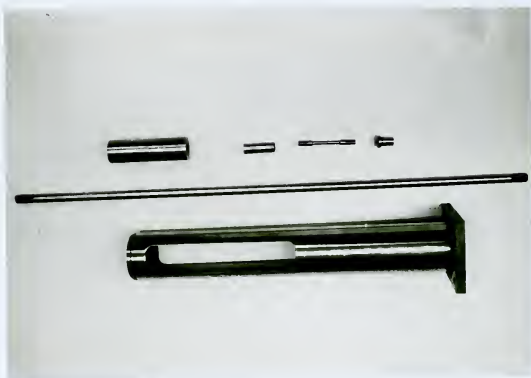
Fig. 4.   The low temperature tensile testing
         assembly showing the capsule, pull rod,
         grips and the specimen.

Fig. 5. The high temperature tensile testing
pull rods and the specimen.

mm/min to 0.51 mm/min resulted in a strain rate change from 10^{-5} to 10^{-4} per second. In a single test, these strain rate changes were reversely applied after specific strain interval to study the effect of strain on the strain rate sensitivity parameter. The next strain rate change was applied only after a steady has reached at the earlier strain rate. During a strain rate change, both the crosshead speed and chart speed were changed by the same factor for an easy correlation between movements of the chart and the crosshead.

3.4 Computation of the Data

A reasonable number of (load, displacement) points were fed to the computer. These points were chosen from the Instron load-displacement chart to represent it fully and adequately. Other input data to the computer include the original gage length of the specimen and its cross-section, the Young's modulus of the specimen material at the test temperature and the total number of data points taken from the Instron chart. The initial linear portion of the experimental load-displacement data was used to calculate the resultant elasticity of the machine, specimen and the linkage. For the given load points, the computer calculates the engineering and true stresses and strains. Then the program fits a parabola through the three consecutive points and calculates the flow stress and the slope of the stress-strain curve at specific plastic strain values.

The computer output was plotted as log ($d\sigma/d\epsilon_p$) vs log ϵ_p for the Crussard-Jaoul analysis and as log ($d\sigma/d\epsilon_p$) vs log σ for the modified method. A least squares straight line fit was imposed on the segments of such plots where the data conform to an approximate linear behavior. Different empirical constants related to the Ludwik equation (9) and the modified Swift equation (10) were then evaluated.

3.5 Metallography

Metallographic techniques involve three steps : mechanical polishing, chemical polishing or electropolishing and anodizing. Metallographic practice followed in this investigation is identical for titanium and zirconium except for the second step. Whereas titanium specimens were electropolished, the zirconium specimens were chemically polished.

First the specimen was mounted in a cold mount like the Nuweld dental compound. After allowing approximately one hour setting time for the mount, the specimen was mechanically polished on 240, 320, 400 and 600 grit silicon carbide papers using standerd metallographic procedures. After cleaning the specimen thoroughly in water, it was polished on a microcloth with 6 micron diamond paste. The specimen was again cleaned in water.

The zirconium specimen was chemically etched[78] in a solution containing 5 parts HNO_3, 5 parts H_2O and 1 part HF and after washing in water it was immediately anodized. The

titanium specimen was electropolished at - 40°C in a fresh solution of 118 ml Methanol, 70 ml N-Butanol and 12 ml Perchloric acid. This mixture is explosive at temperatures above the room temperature and it was continuously cooled to - 40°C by a bath alcohol with dry ice. A D. C. power supply was used at 28 Volts. Electropolishing was done for about 6 to 8 minutes with a stainless steel cathode. The specimen was thoroughly cleaned in water, dried and anodized.

The anodizing bath[79] consists of 60 ml ethyl alcohol, 35 ml distilled water, 20 ml glycerine, 5 ml phosphoric acid, 10 ml lactic acid and 2 grams citric acid. A 20-24 Volts D.C. power supply was used for 5 seconds. Stainless steel was used as the cathode. Anodizing was followed by a through wash in water. The specimen was then dried in hot air. Normally a properly anodized titanium or zirconium specimen attains a uniformly colored purple or brown surface. Anodizing improves the contrast between different grains, especially when the microstructure is examined under polarized light. Typical microstructure of annealed h.p.Ti is shown in Figure 6.

For the quantitative metallographic measurements, a square grid was superimposed on a random portion of a polished metallographic specimen and P_P, N_A and N_L counts were measured. The point count P_P is the fraction of the number of random points that lie in a region of interest in the microstructure, e.g. fraction of grid points that lie inside twins in a microstructure. N_A is the number of units of a
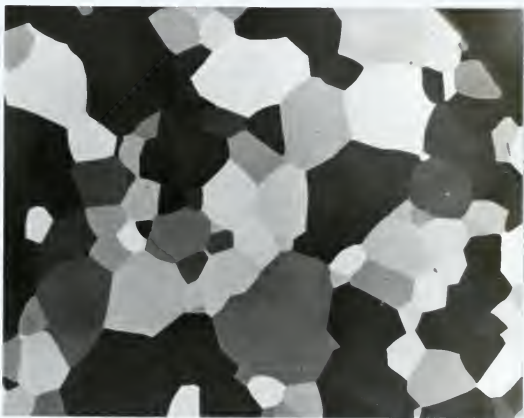
Fig. 6.   The microstructure of annealed high
          purity titanium specimen. Magnification
          416 times.

certain feature per unit area of the microstructure, e.g. the number of twins per unit area of the sample. N_L is the number of intersections of a random line with certain feature in the microstructure per unit length of the sampling line, e.g. number of intersections of a sampling line with the twin-matrix interface per unit length of the line. Following relationships were used to calculate the volume fraction, V_V, and surface area per unit volume S_V.

$$V_V = P_P \tag{13}$$

$$S_V = 2 \ N_L \tag{14}$$

CHAPTER IV

EXPERIMENTAL RESULTS

4.1 Deformation of H.P.Ti below 424°K

Figure 7 shows a set of true stress-true strain curves,
(to the point of maximum load), that illustrate the effect
of temperature on the stress-strain curve of high purity
titanium. These correspond to the temperatures 77, 193, 298
and 424°K and a 22 micron grain size. Notice the approximate
linear shape of the 77°K stress-strain curve upto 0.3 strain.
The uniform and total elongations of these specimens are
plotted in Fig. 8 Attention is called to the fact that duc-
tility rises below room temperature (uniform elongation 0.55
at 77°K).

Figure 9 shows the effect of grain size on the stress-
strain curve at 77°K. The true stress-true strain curves of
high purity titanium of three different grain sizes deformed
at 77°K are illustrated in this figure. All three curves
show a characteristic nearly linear work hardening behavior.

Typical micrographs of regions of a fractured 22 micron
grain size specimen deformed at 77°K are shown in Fig. 9.
The local strain at these regions was calculated from the
diameter changes. The microstructure in the shoulder region
was similar to the annealed structure shown in Fig. 6.

39
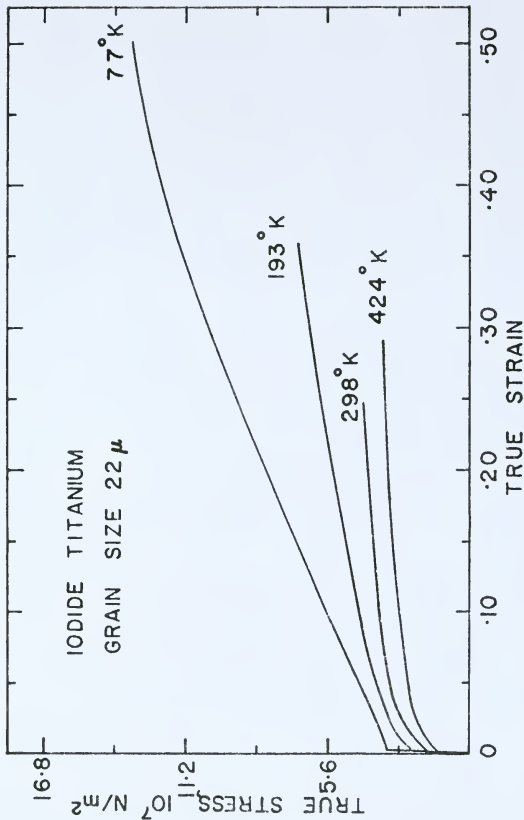
Fig. 7. True Stress-True Strain curves, upto the point of maximum load on the load-elongation diagram, of high purity tita-nium at different temperatures. Strain Rate 3.9×10^{-4} sec^{-1}.
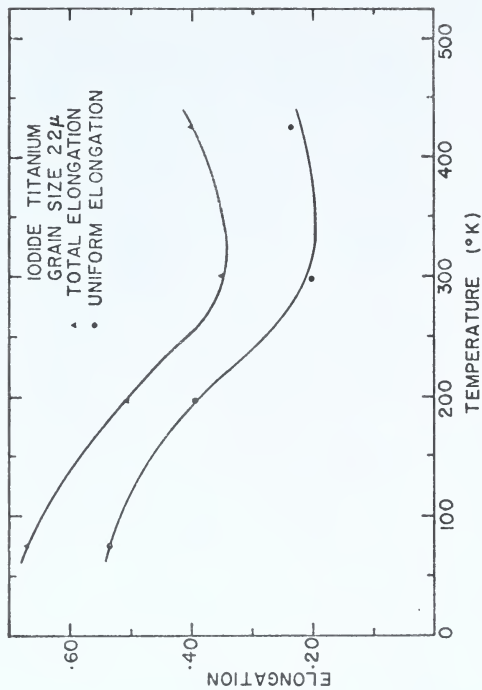
Fig. 8. The temperature variation of the uniform and total elongations of high purity titanium. Strain Rate 3.9×10^{-4} sec^{-1}.
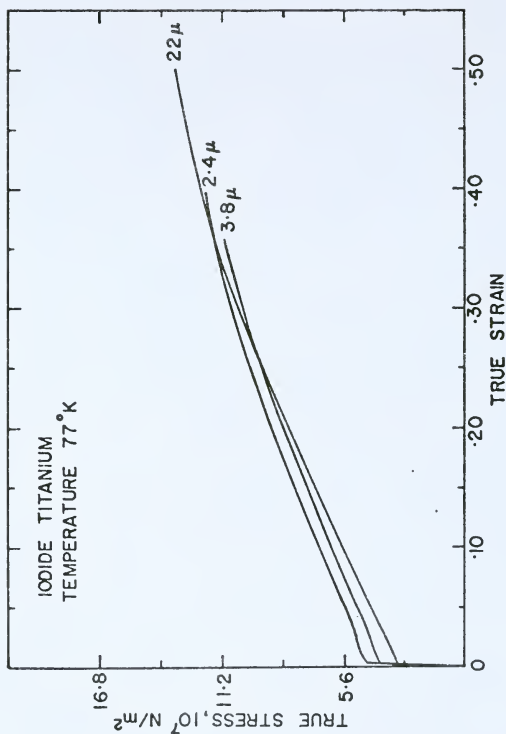
Fig. 9. The 77°K true stress-true strain curves of high purity titanium specimens of several grain sizes. Strain Rate 3.9 X 10⁻⁴ per second.

(a)

(b)

Fig. 10.   Microstructures of **h.p. titanium specimen**
deformed at 77°K. Grain size 22 microns.
Strain rate 3.9 X 10⁻⁴ per second.
(a) at 0.4 true strain (b) near the fractured
end. Magnification 416 times in both cases.

Therefore, the twins shown in Fig. 10 were formed due to the deformation and not by specimen preparation. The volume fraction of twins, as measured in the fractured specimens, for the 22 micron grain size material is plotted in Fig. 11. The volume fraction increases at a higher rate at lower temperatures and at $77°K$ it was so high near the fractured end that it was difficult to distinguish between the twinned and the untwinned regions. Hence, a twin volume fraction measurement was not possible at this position. The lowest twin volume fraction values correspond to a region near the specimen shoulder. A single fractured specimen was used at each temperature for twin volume fraction measurements.

Microstructures showing deformation twins corresponding to fine grained specimens are shown in Figs. 12 and 13. Though it is generally believed that fine grained material does not twin easily, these micrographs show that deformation twinning is significant even at a grain size of 2.4 micron. Quantitative measurements of mechanical twinning at this grain size was not possible by optical microscopy as a surface suitable for quantitative measurements was not obtained.

4.2 Deformation Stages at $77°K$

In order to relate the deformation twinning and stress-strain behavior of titanium and zirconium at $77°K$, a simultaneous stress-strain analysis and quantitative microscopic study of microstructure was undertaken.
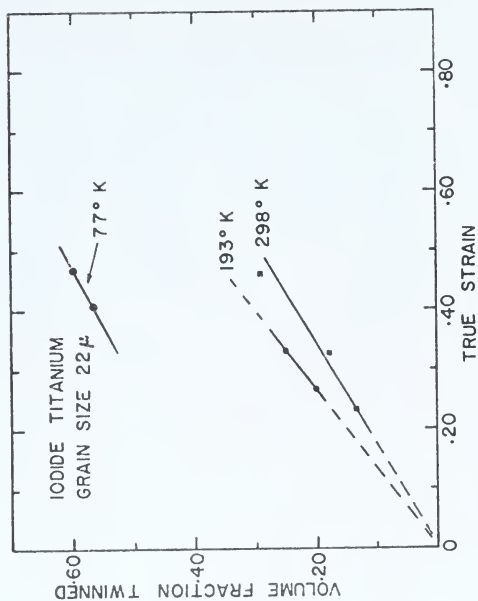
Fig. 11. The volume fraction of twins as a function of true strain in h.p.Ti specimens deformed at several temperatures. Strain rate 3.9 X 10-4 per second.

Fig. 12. The microstructure of a 3.8 micron
grain size h.p.Ti specimen deformed
at 77°K. Strain rate 3.9 X 10^{-4}
per second. Magnification 528 times.
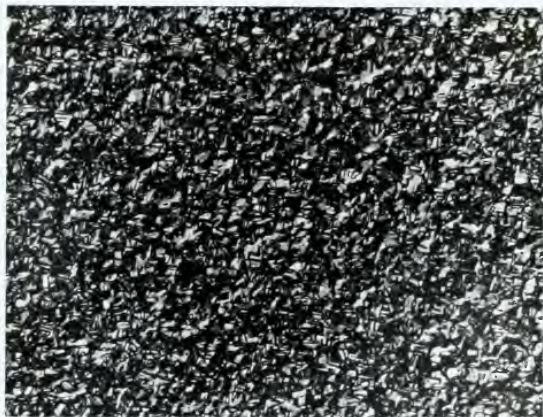
Fig. 13. The microstructure of a 2.4 micron
grain size h.p.Ti specimen deformed
at 77°K. Strain rate 3.9 X 10⁻⁴ per
second. Magnification 528 times.

The 77°K engineering stress-strain curves of h.p.Ti, c.p.Ti, h.p.Zr and c.p.Zr are given in Fig. 14 while Fig. 15 shows the corresponding true stress versus true strain curves. Since the flow stress level of these four metals varied considerably, it was more appropriate to use the Crussard-Jaoul method for the stress-strain analysis.

Differentiating Eq. (9) with respect to strain and taking the logarithm of both sides gives :

$$\log (d\sigma/d\epsilon_p) = \log (kn) + (n-1) \log \epsilon_p \qquad (15)$$

Therefore, the slope of a $\log(d\sigma/d\epsilon_p)$ against $\log \epsilon_p$ curve is $(n-1)$, where n is designated as the work hardening exponent.[65]

All data on Crussard-Jaoul diagrams were plotted over a strain interval selected to exclude the yield point and the necking regions. A least squares analysis was used to fit straight lines over those intervals of each plot where the data were judged to conform to a linear behavior. A work hardening exponent n was calculated from the slope of these lines. The parameter k was calculated from the Eq. (15), and an average value of σ_o over the selected strain range was calculated using the Eq. (9).

The Crussard-Jaoul plots for four metals are shown in Fig. 17 and are reproduced individually in Figs. 17, 18, 19 and 20 so as to clearly define the stages of each stress-strain curve where the deformation behavior differed. Values of the parameters n, k and σ_o, calculated for these intervals, are listed in Table 2. These regions are also indicated in
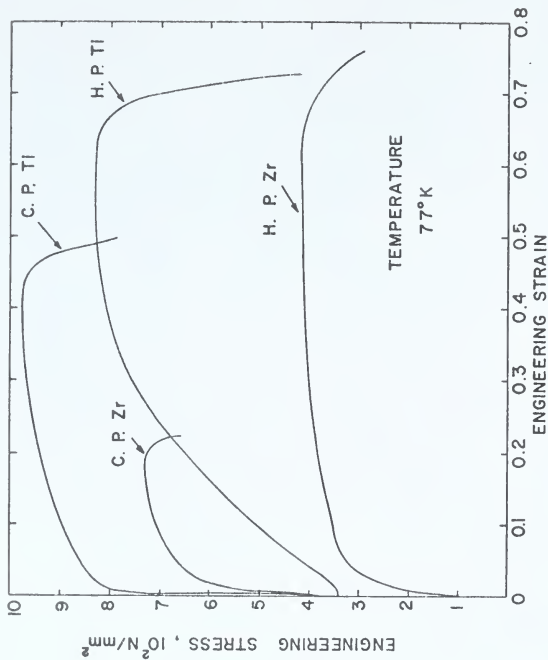
Fig. 14. The 77°K engineering stress-engineering strain curves of high purity and commercial purity titanium and zirconium. The h.p. Zr data are due to Aigeltinger.
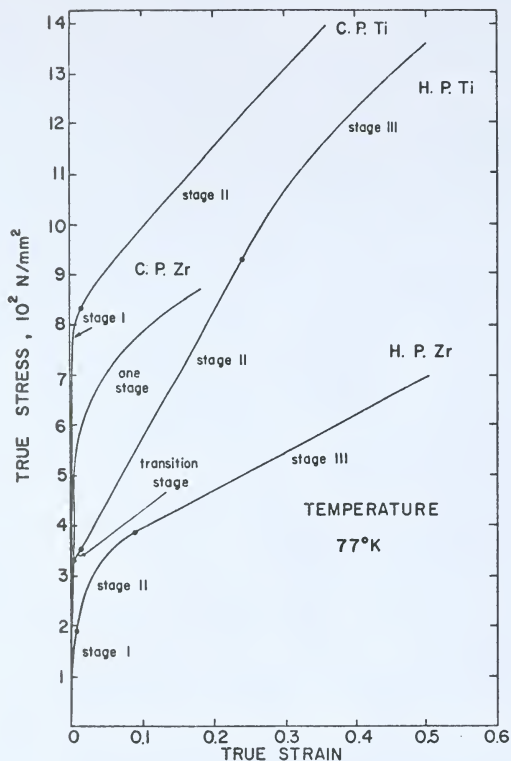
Fig. 15. The true stress versus true strain diagrams for curves in Fig. 14. The dots on each curve indicate the limits of Crussard-Jaoul stages. The h.p. Zr data are due to Aigeltinger.
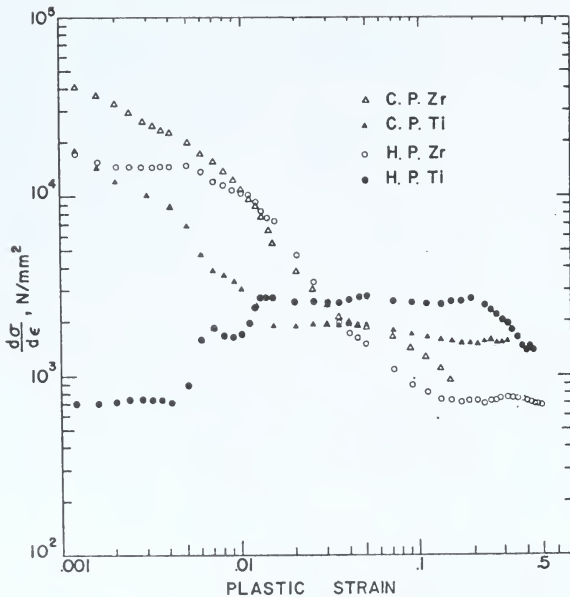
Fig. 16.   Crussard-Jaoul plots for the curves in Figs.
14 and 15.
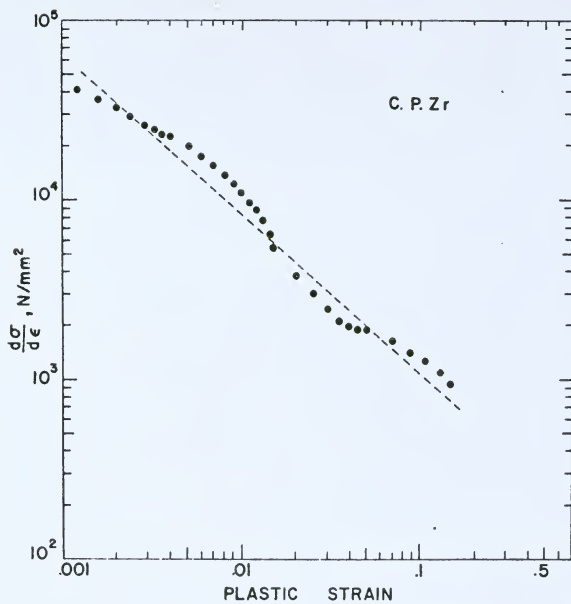
Fig. 17. Crussard-Jaoul diagram for c.p.Zr.
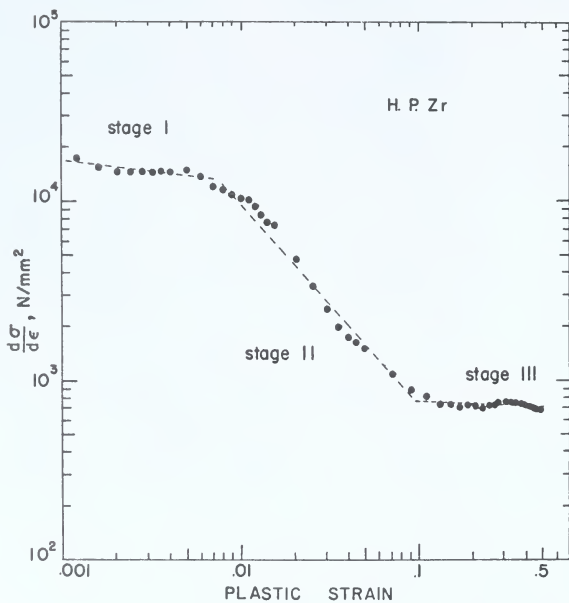
Fig. 18. Crussard-Jaoul diagram for h.p. Zr. The data
are due to Aigeltinger.
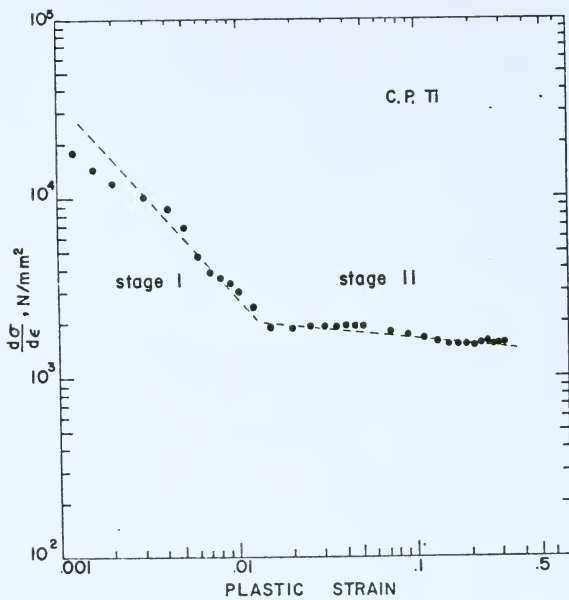
Fig. 19. Crussard-Jaoul diagram for c.p.Ti.
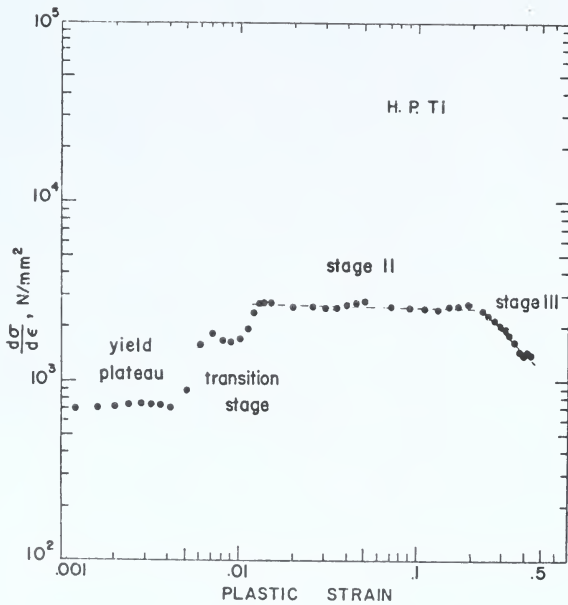
Fig. 20. Crussard-Jaoul diagram for h.p.Ti.

Table II

Values of Parameters n, k and
Average σ_0 calculated from the
least squares straight line fits
to segments of Crussard-Jaoul plots

		n	k	Ave. σ_0	Prop. limit
			10^2 N/mm^2	10^2 N/mm^2	10^2 N/mm^2
H.P.Ti	Yield Plateau	--	--	--	
	Trans. Stage	--	--	--	3.3
	Stage II	0.98	24.8	3.1	
	Stage III	-0.02	-273.8	291.0	
C.P.Ti	Stage I	-0.15	-1.0	10.2	
	Stage II	0.89	14.8	8.0	7.5
H.P.Zr	Stage I	0.87	80.6	0.6	0.7
	Stage II	-0.13	-4.3	9.7	
	Stage III	0.94	7.1	3.1	
C.P.Zr	Stage I	0.11	15.0	-2.3	3.5

Fig. 15 where the limits of each stage are defined by dots placed on the curves.

The variation of the volume fraction of twins as a function of true strain is shown in Fig. 21. The initial portion of Fig. 21 covering strains less than 0.1, is shown in Fig.22 Figures 23, 24 and 25 represent the variation with strain of S_V, $\overline{\lambda}$ and $N_A/\overline{\lambda}$, respectively, for h.p.Ti and h.p.Zr. The effects of strain on the h.p.Ti and h.p.Zr microstructures are presented in Figs. 26 to 29.

4.3 Deformation Stages in Longitudinal and Transverse Zr

A problem of the Crussard-Jaoul method is that the values of the constants σ_o, k_2 and n_2 depend on where a power law curve, that fits a range of experimental data, intercepts the strain axis, i. e. when the curve is extrapolated back to $\epsilon = 0$. In Fig. 30 (a), three stress-strain curves of identical shape are shown displaced horizontally with respect to each other by a strain ϵ_{p_o}. When the data of these stress-strain curves are plotted on a $\log (d\sigma/d\epsilon_p) - \log \epsilon_p$ diagram, all three curves will not yield straight lines. However, for the sake of the following qualitative argument, we can assume them to be straight lines as shown in Fig. 30 (b). These hypothetical Crussard-Jaoul plots have different slopes and correspond to three different n_2 values. This is important because in a multi-stage stress-strain curve, the stages after the initial stage often conform to power law equations
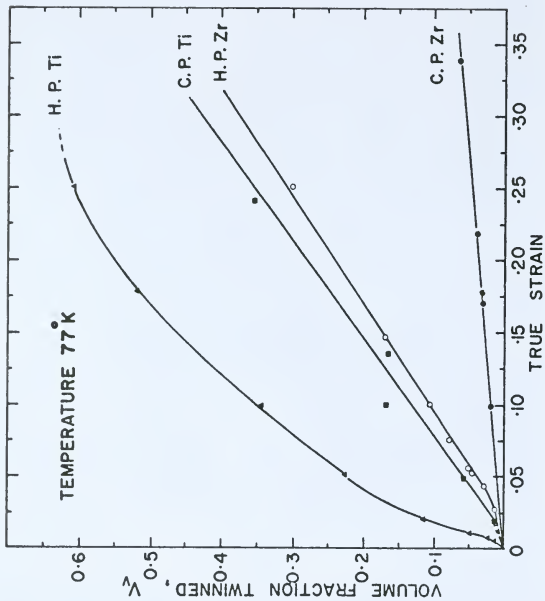
Fig. 21. The volume fraction of twins as a function of tensile strain for h.p.Ti, c.p.Ti, h.p.Zr and c.p.Zr. The h.p.Zr data are due to Aigeltinger, the c.p.Ti data are due to Cetlin and c.p.Zr data are due to Santhanam and Ramachandran.
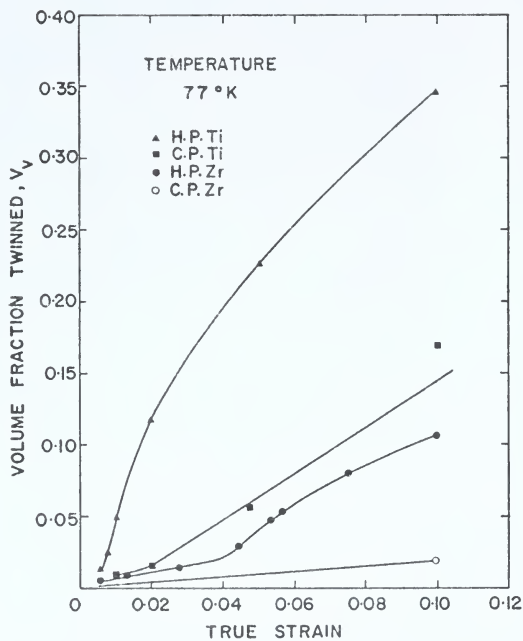
Fig. 22. Volume fraction of twins as a function of
strain for strains less than 0.1.
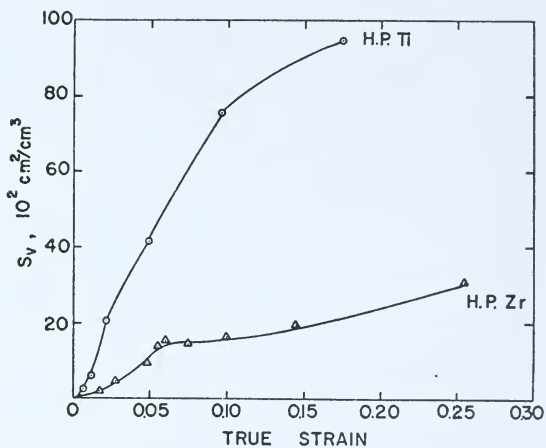
Fig. 23. The dependence of the twin-matrix interface area per unit volume (S_v) on the true strain for h.p.Ti and Zr. The h.p.Zr data are due to Aigeltinger.
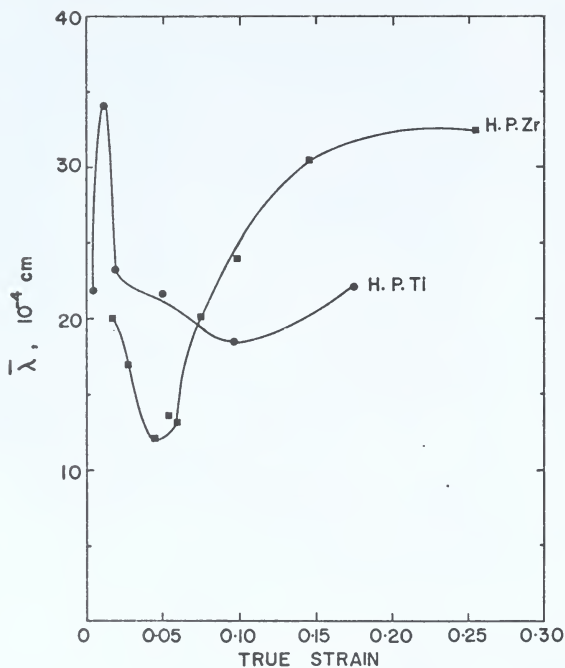
Fig. 24. The variation of the mean twin intercept ($\overline{\lambda}$) with strain for h.p.Ti and Zr. The h.p.Zr data are due to Aigeltinger.
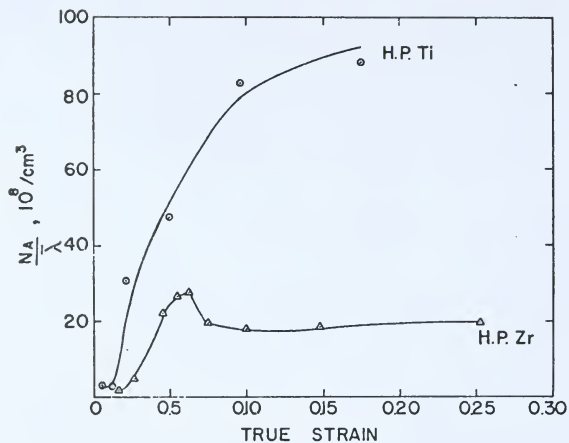
Fig. 25. The effect of strain on the parameter $(N_A/\overline{\lambda})$ for h.p.Ti and Zr. The h.p.Zr data are due to Aigeltinger.

(a)
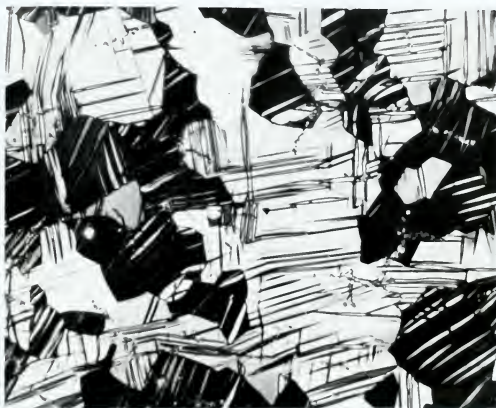
(b)

Fig. 26. The microstructures of h.p.Ti specimens
deformed at 77°K. Magnification 457 times.
(a) at 0.02 strain. (b) at 0.05 strain.
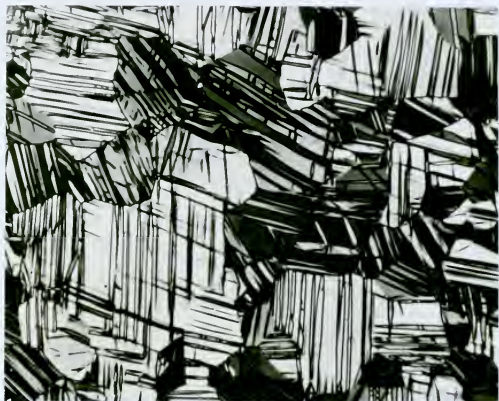
Fig. 27. The microstructure of h.p.Ti specimen
          deformed at 77°K. Magnification 457 times.
          0.1 strain.
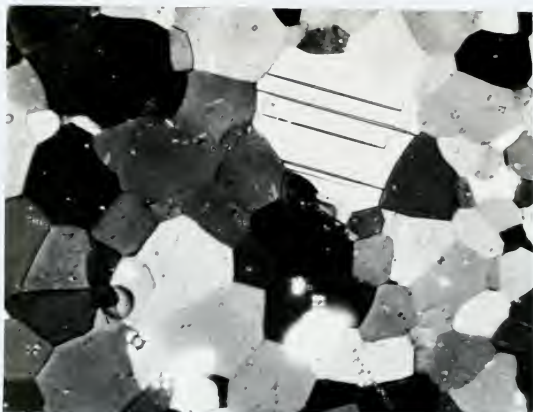
(a)

(b)

Fig. 28.   The microstructures of h.p.Zr specimens
deformed at 77°K. Magnification 457 times.
(a) $\epsilon = 0.02$. (b) $\epsilon = 0.05$.

Fig. 29.   The microstructure of h.p.Zr specimen
deformed at 77°K.   Magnification 457
times. $\epsilon = 0.1$.
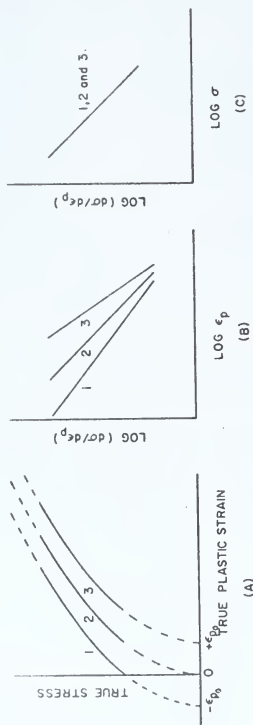
Fig. 30. (a) Three hypothetical stress-strain curves of similar shape but displaced with respect to each other horizontally by ϵ_{p_0}. (b) The corresponding Crussard-Jaoul plots. All three curves in this diagram will not be straight lines. This figure, however, is only qualitative. (c) The three curves plot as a single line on a $\log(d\sigma/d\epsilon_p)$ versus $\log \sigma$ coordinates.

of the Ludwik type where the $\sigma = 0$ intercept does not pass through $\epsilon_p = 0$. In addition, during the manufacture of metals, unknown amounts of prestrain may be introduced and therefore two specimens of the same metal, with different effective prestrains, may yield different results in a Crussard-Jaoul analysis.

The influence of the strain axis intercept on the Crussard-Jaoul analysis is not a problem if an analysis is carried out based on Eq. (10), as implied in Fig. 30 (c). Here $\log (d\sigma/d\epsilon_p)$ is plotted against $\log \sigma$. Such an analysis also has the advantage that the flow stress is normally defined by the present state of a material[80] and not by the path of attaining that state as is ϵ_p. Thus the plot of $\log (d\sigma/d\epsilon_p)$ against $\log \sigma$ seems more characteristic of the material than the alternate plot of $\log (d\sigma/d\epsilon_p)$ versus $\log \epsilon_p$.

Though an analysis based on the modified Swift equation is not affected by a prestrain, the parameters of such an investigation should be influenced by the general flow stress level. Thus a vertical shift of a stress-strain curve will give rise to different m values, while the Crussard-Jaoul n_2 will remain unchanged. This dependence on the stress level should be considered in evaluting the results of an analysis based on the Swift equation.

Both n_2 and m are measures of the rate of change of the work hardening rate with strain or stress. In fact, a simple expression may be obtained in each case relating m and n_2 to

($d\theta/d\sigma$) where θ is ($d\sigma/d\epsilon_p$). For example, by differentiating Eq. (9) twice, one obtains

$$d\theta/d\sigma = (n_2 - 1)/\epsilon_p = -q/\epsilon_p \qquad (16)$$

where q equals $-(n_2 - 1)$. A similar operation on Eq. (10) yields

$$d\theta/d\sigma = (1-m)/m \cdot 1/(\epsilon_p - \epsilon_{p_o}) = -p/(\epsilon_p - \epsilon_{p_o}) \qquad (17)$$

where p equals $-(1 - m)/m$.

A Crussard-Jaoul analysis of zirconium stress-strain data covering a range of temperature and composition and a difference in texture has not been previously reported. It was felt that useful information might be obtained from such an investigation, especialy if a complementary analysis based on the Swift equation were to be made simultaneously. The result of such a twofold analysis are presented in Figs. 31 through 39.

A linear region on a log ($d\sigma/d\epsilon_p$) - log ϵ_p or log ($d\sigma/d\epsilon_p$) - log σ diagram was designated as a "stage" in the present investigation. While it is understood that a stage will not always yield a linear plot in such diagrams, (e.g. the stage near the maximum load in fcc polycrystalline metals), the deformation behavior of zirconium could be represented by approximate linear regions over the entire range of temperature, composition and texture used in this study. Though the labeling of stages is arbitrary to some extent, it is based on the average behavior covering finite portions

of the stress-strain curve. Local variations (possibly due to the scatter in the data) are not considered as a basis for stage designation.

Figure 31 shows log $(d\sigma/d\epsilon_p)$ against $\log \sigma$ plots for longitudinal zirconium specimens at representative temperatures. Note that at 4 and 77°K, a three stage behavior is observed. The bumps observed in stages 2 and 3 at 4°K conform to the discontinuous and irregular nature of the plastic deformation at this temperature.[81] A two stage behavior is observed at room temperature and at 573°K. The stress-strain response at 813°K can be approximated by a single stage. The stages are identified in Table III and in the figures by numbers from 1 to 3. In the cases where two stages were observed, one of the stages normally had a slope comparable to the intermediate or second stage of the three stage behavior. This stage of the two stage curve was labled as stage 2. Also the slope of a single stage curve was usually comparable to the intermediate stage of the three stage behavior and accordingly it was labeled as stage 2. The values of parameters m, ϵ_{p_o} and c, calculated for these curves, are given in Table III. While m takes only positive values greater than one, the parameter ϵ_{p_o} can take both positive and negative values and c is always positive. The Crussard-Jaoul plots for these longitudinal specimens are given in Fig. 32. Note that the stress-strain curve stages in Fig. 32 correspond to those in Fig. 31. Calculated values of n_2, k_2 and σ_o, given in Table III, show that n_2, k_2 and σ_o can take
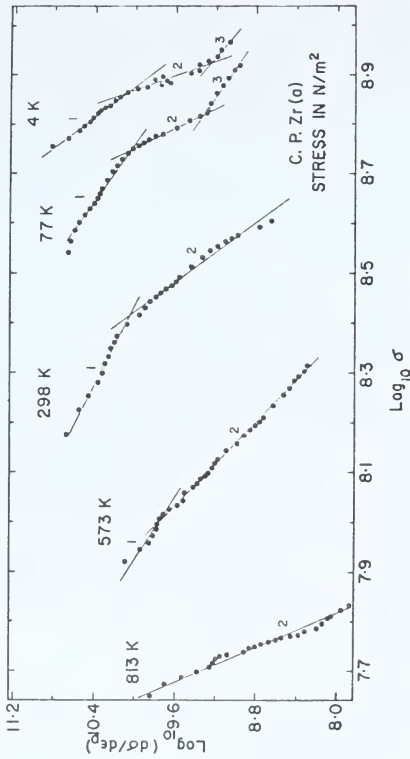
Fig. 31. Log($d\sigma/d\epsilon_p$) against logσ diagrams for longitudinal zirconium specimens.
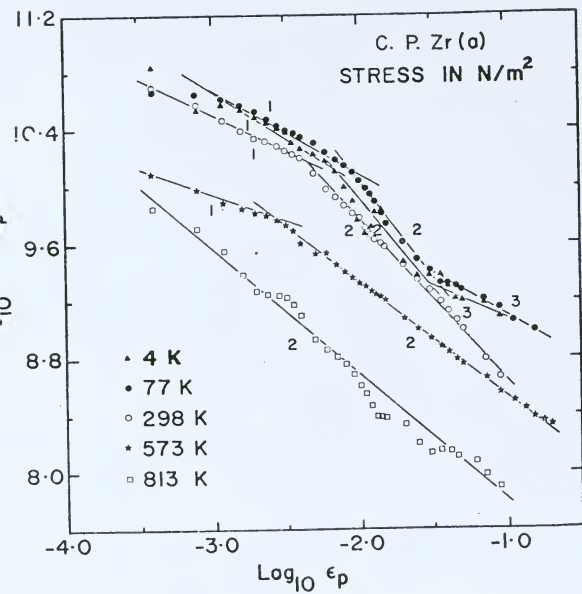
Fig. 32. Crussard-Jaoul diagrams for longitudinal zirco-
nium specimens.

both positive and negative values.

The log $(d\sigma/d\epsilon_p)$ - log σ and log $(d\sigma/d\epsilon_p)$ - log ϵ_p plots for transverse zirconium specimens appear in Figs. 33 and 34 respectively. In both figures, a three-stage behavior below the room temperature is recorded. Serrated flow[81] was observed in stages 2 and 3 at 4°K. At room temperature an additional transition or fourth stage appears in the microstrain region. At 560 and 813°K, a two stage behavior is depicted. The calculated values of the various parameters are also given in Table III. Figures 35 and 36 show the effect of composition on the tensile behavior of zirconium in the temperature range 550 to 595°K. Note that while iodide and commercial purity zirconium specimens show one stage behavior, the high oxygen specimen shows a three stage behavior. The values of the constants derived from these figures are given in Table III.

The variation of p and q as functions of temperature for all three major stages are plotted in Fig. 37. In general, values of the parameter q show much greater variation than do these of parameter p. The significance of this will be discussed in the next chapter.

The effect of a small amount of 77°K prestrain on the room temperature stress-strain behavior of longitudinal and transverse zirconium specimens is shown in Figs. 38 and 39 respectively. As demonstrated in Fig. 38, prestrain does not produce any significant change in the log ($d\sigma/d\epsilon_p$) - log σ plot of a longitudinal specimen. On the other hand, a small

Fig. 33. Log($d\sigma/d\epsilon_p$) against logσ plots for transverse zirconium specimens.
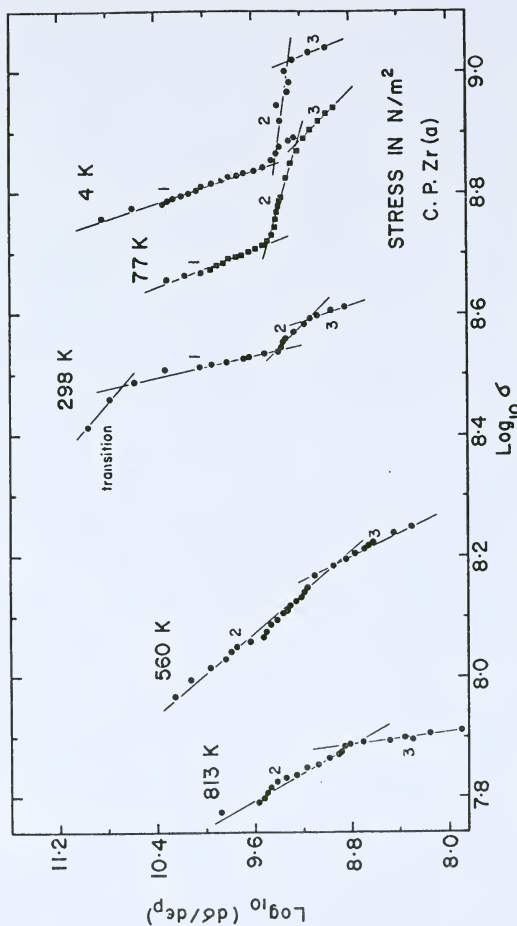
Fig. 34. Crussard-Jaoul diagrams for transverse zirconium specimens.
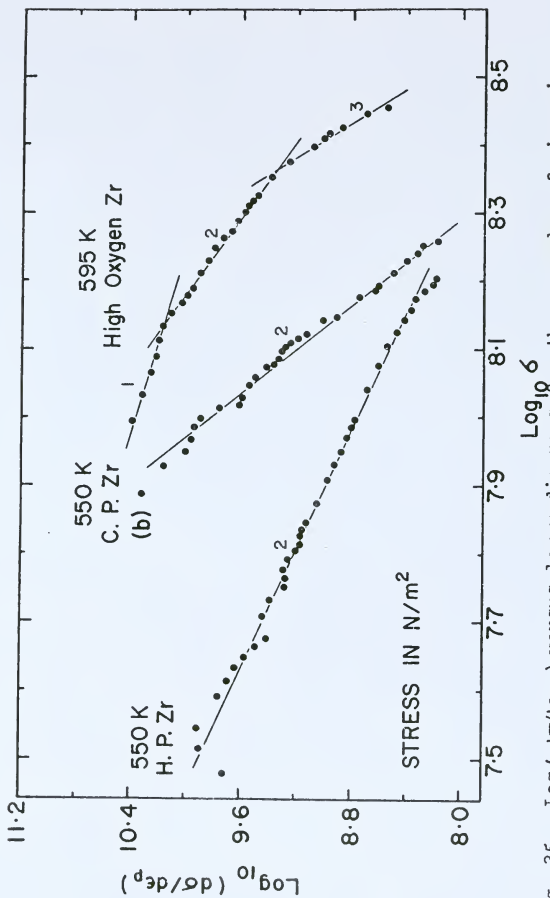
Fig. 35. Log ($d\sigma/d\varepsilon_p$) versus log σ diagrams for three grades of zirconium at an intermediate temperature.
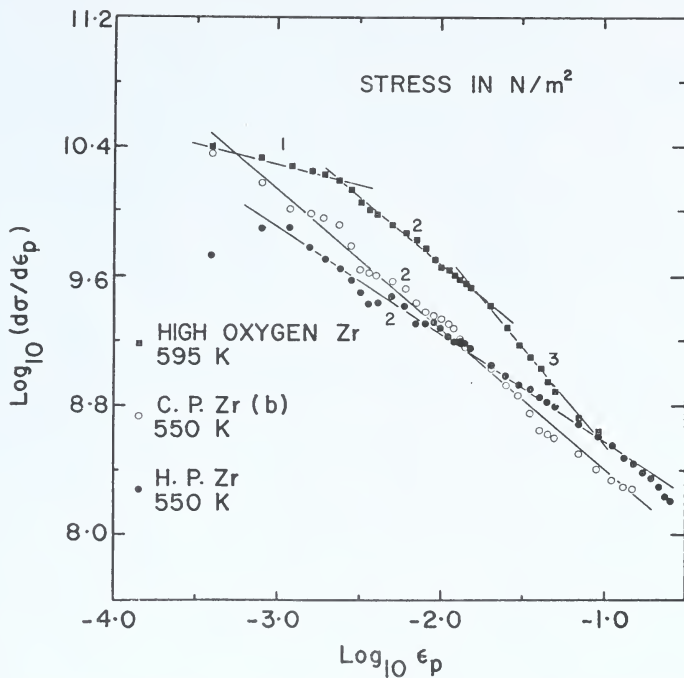
Fig. 36. Crussard-Jaoul plots for three zirconium grades.
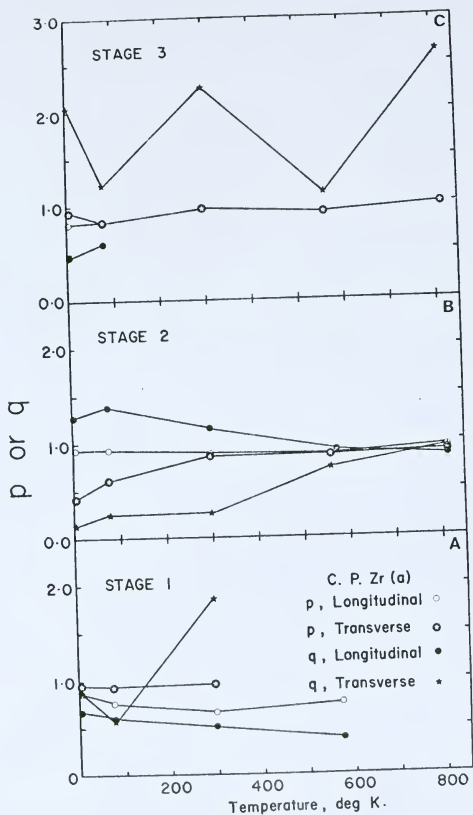
Fig. 37. Variation of p and q as function of temperature for the three major stress-strain curve stages of both longitudinal and transverse c.p.Zr specimens.
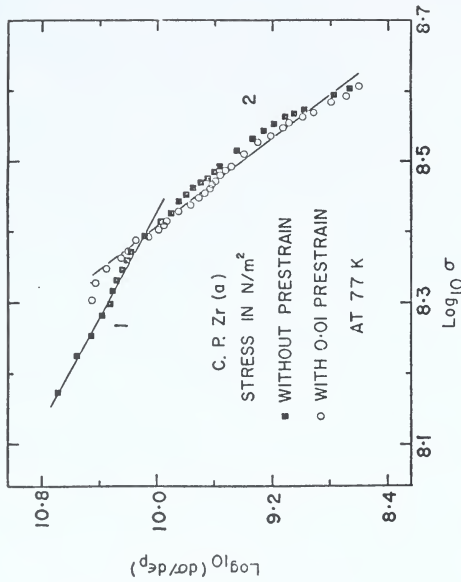
Fig. 38. Effect of 0.01 prestrain at 77°K on the 298°K log($d\sigma/d\epsilon_p$) against log σ diagram of longitudinal zirconium specimens.

amount of prestrain significantly changes the stress-strain
stage behavior of a transverse specimen (Fig. 39). The
values of the parameters evaluated from these curves are given
in Table III. Note that the curves with and without prestrain
in Fig. 39 are similar to the 77 and 298°K curves respective-
ly in Fig. 33.

4.4 The Strain Rate Sensitivity

The strain rate sensitivity, defined by Eq. (4), was
calculated from strain rate change test data. Whenever tran-
sients appeared two values were calculated. Transients ap-
peared in c.p.Ti data in the temperature range 573 to 760°K
and in c.p.Zr data in the interval 600 to 675°K. The effect
was, however, much weaker in zirconium. As shown in Fig. 40,
one value was based on an instantaneous change in the load
giving rise to a stress change $\sigma_2' - \sigma_1$. The other value
was related to the extrapolated steady state stress change,
$\sigma_2'' - \sigma_1$. The significance of the latter value will be dis-
cussed in the next chapter. The strain rate sensitivity was
calculated as a function of tensile strain. Figure 41 shows
the temperature variation of the strain rate sensitivity for
the two titanium grades calculated from a strain rate change
near 2 percent strain. Note that both the curves show a
peak near 450°K and a minimum in the range 600 to 700°K.
Corresponding curves for a strain rate change near 12
percent strain are given in Fig. 42. It was not possible
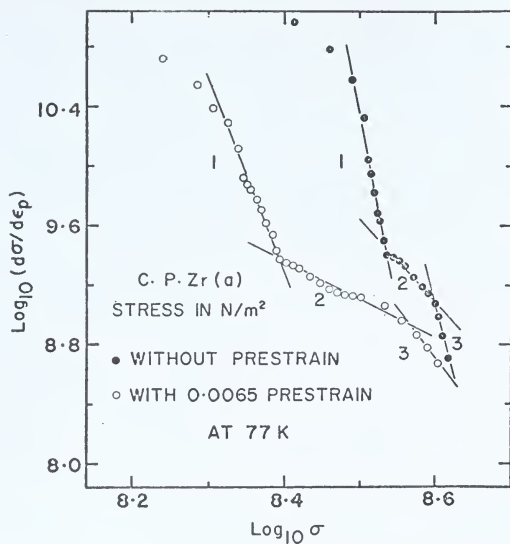
Fig. 39. Effect of 0.0065 prestrain at 77°K on the 298°K $\log(d\sigma/d\epsilon_p)$ versus $\log\sigma$ diagram of transverse zirconium specimens.

Table III

Calculated Values of Parameters for the Stress-Strain Curve Stages

Grade and Texture	Temperature, Deg. K	Stage No.	n_2	k_2, N/m²	σ_o, N/m²	m	c, (N/m²)$^{-m}$	ϵ_{p_o}	Uniform Strain expt.	Uniform Strain cal.
C.P. Zr A Longitudinal.	4	1	0.34	1.14×10^9	4.92×10^8	7.4	2.19×10^{-68}	1.1×10^{-3}	----	----
		2	-0.27	-9.1×10^7	1.07×10^9	14.8	8.0×10^{-134}	4.5×10^{-3}	----	----
		3	0.53	7.1×10^8	7.10×10^8	5.0	2.39×10^{-46}	-6.1×10^{-2}	0.09	0.14
	77	1	0.41	2.7×10^9	2.50×10^8	4.3	7.53×10^{-40}	-1.1×10^{-3}	----	----
		2	-0.38	-4.9×10^7	8.30×10^8	10.6	9.32×10^{-96}	5.5×10^{-3}	----	----
		3	0.40	8.0×10^8	4.50×10^8	4.6	4.97×10^{-42}	-3.3×10^{-2}	0.18	0.18
	298	1	0.49	1.9×10^9	1.07×10^8	3.5	4.23×10^{-32}	-1.6×10^{-3}	----	----
		2	-0.15	-1.9×10^8	6.70×10^8	7.7	1.23×10^{-67}	-1.0×10^{-2}	0.12	0.12
	573	1	0.62	9.9×10^8	7.60×10^7	4.0	4.19×10^{-35}	-1.6×10^{-3}	----	----
		2	0.09	3.8×10^8	-1.20×10^8	5.6	5.43×10^{-48}	3.0×10^{-3}	0.19	0.18
	813	2	0.11	7.2×10^7	1.30×10^7	12.3	1.03×10^{-97}	3.0×10^{-3}	0.10	0.09

Table III (cont.)

Grade and Texture	Temperature, Deg. K	Stage No.	n_2	k_2 N/m^2	σ_o N/m^2	m	c, (N/m^2)-m	ϵ_{p_o}	Uniform strain expt.	Uniform strain cal.
	4	1	0.13	5.8×10^8	3.6×10^8	15.5	1.4×10^{-139}	-3.5×10^{-4}	----	----
		2	0.87	1.9×10^9	6.4×10^8	1.7	1.4×10^{-16}	-1.3×10^{-1}	----	----
		3	-1.04	-4.5×10^7	1.3×10^9	13.7	1.2×10^{-125}	1.3×10^{-1}	0.20	0.20
	77	1	0.43	5.9×10^8	4.3×10^8	14.4	1.2×10^{-127}	-1.2×10^{-3}	----	----
		2	0.76	1.4×10^9	4.7×10^8	2.6	4.0×10^{-24}	-5.5×10^{-2}	----	----
		3	-0.22	-5.8×10^8	1.7×10^9	6.0	4.0×10^{-55}	4.6×10^{-2}	0.21	0.21
C.P.Zr A Transverse	298	1	-0.85	-1.6×10^5	3.6×10^8	28.8	2.9×10^{-245}	1.0×10^{-3}	----	----
		2	0.74	8.7×10^8	3.3×10^8	6.9	2.2×10^{-61}	-1.1×10^{-3}	----	----
		3	-1.25	-5.1×10^5	4.3×10^8	24.5	3.7×10^{-213}	2.3×10^{-2}	0.06	0.06
	560	2	0.28	2.6×10^8	6.4×10^7	6.9	3.3×10^{-59}	2.0×10^{-4}	----	----
		3	-0.12	-1.2×10^8	3.3×10^8	11.1	2.5×10^{-93}	9.3×10^{-3}	0.11	0.10
	813	2	0.09	1.3×10^8	-9.7×10^6	9.7	9.6×10^{-75}	2.0×10^{-5}	----	----
		3	-1.61	-4.2×10^3	8.1×10^7	41.7	4.6×10^{-332}	1.0×10^{-2}	0.04	0.04

Grade and Texture	Temperature, Deg. K	Stage No.	n_2	k_2 N/m^2	σ_o N/m^2	m	c, $(N/m^2)^{-m}$	ϵ_{p_o}	Uniform Strain expt.	Uniform Strain cal.
H.P.Zr longitudinal	550	2	0.33	2.4×10^8	9.9×10^6	3.4	8.0×10^{-29}	5.0×10^{-4}	0.25	0.29
C.P.Zr B Longitudinal	550	2	0.13	2.7×10^8	-4.2×10^7	7.3	2.1×10^{-61}	1.0×10^{-4}	0.17	0.14
H.O.Zr Longitudinal	595	1	0.73	4.2×10^9	8.4×10^7	2.6	6.6×10^{-24}	-1.2×10^{-3}	----	----
		2	0.13	6.0×10^8	-1.4×10^8	4.7	3.0×10^{-41}	6.0×10^{-4}	----	----
		3	-0.31	-4.8×10^7	3.9×10^8	9.2	3.5×10^{-79}	1.0×10^{-2}	0.12	0.12
C.P.Zr A, Long. 0.01 Prest. at 77°K	298	2	-----	-----	----	7.7	1.3×10^{-67}	1.0×10^{-3}	0.12	0.13
C.P.Zr A, Trans. 0.0065 Pre-strain at 77°K		1	-----	-----	----	14.4	3.5×10^{-123}	8.0×10^{-4}	----	----
		2	-----	-----	----	3.7	6.3×10^{-33}	-1.6×10^{-2}	----	----
		3	-----	-----	----	7.7	1.7×10^{-67}	4.0×10^{-2}	0.17	0.17

Fig. 40. Schematic diagram showing the instantaneous stress change $\sigma_2' - \sigma_1$ and the extrapolated steady state stress change $\sigma_2'' - \sigma_1$ following a strain rate change from $\dot{\epsilon}_1$ to $\dot{\epsilon}_2$.
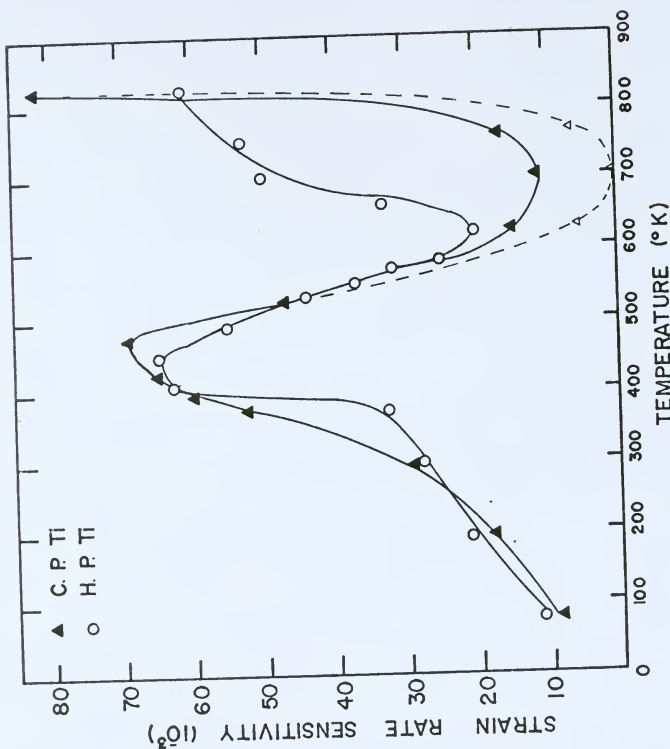
Fig. 41. The temperature dependence of the strain rate sensitivity of h.p. and c.p. titanium. Calculated from a strain rate change near 2 percent strain. The dotted curve for c.p.Ti is based on the extrapolated steady state stress values when transients appeared.
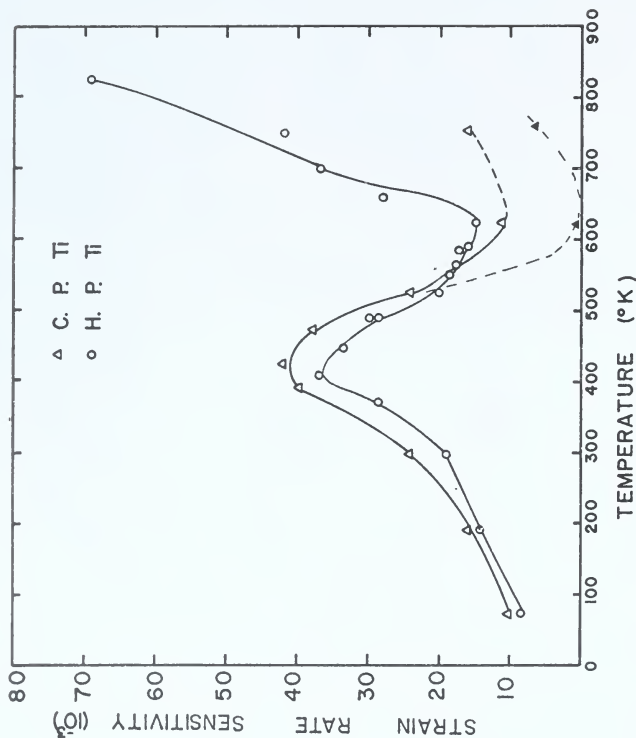
Fig. 42. The temperature dependence of the strain rate sensitivity of h.p. and c.p. Ti based on a strain rate change near 12 percent strain. The lower dotted curve is for c.p. Ti based on the extrapolated steady state stress values where transients appeared.

to obtain data points above $700°K$ on the c.p.Ti curve in
Fig. 42 as the uniform strain was less than   12   percent.
While the value of the strain rate sensitivity minimum has
not changed significantly from Fig. 41 to Fig. 42 the peak
height has considerably decreased with increasing strain.
This decrease is more significant for high purity titanium
curve. The n – T curves shown in Fig. 43 are for c.p.Ti
specimens deformed between different sets of strain rates.
The values were calculated from the instantaneous changes in
the load. Note that an increase in the strain rate does not
change the magnitude of the peak height or the minimum. For
temperatures below the peak temperature, two sets of data
points follow the same curve. However, at higher temperatures
the faster strain rate data points shift to a higher tempera-
ture thereby shifting the minimum to a higher temperature.
The variation of the strain rate sensitivity of high purity
titanium specimens with strain is shown in Fig. 44. Disre-
garding the curves in the first few percents of strain, below
room temperature the strain rate sensitivity remains constant
with strain. Above room temperature the strain rate sensiti-
vity generally continues to decrease with increasing strain,
a greater decrease occuring near temperatures corresponding
to the peak in Figs. 41 and 42. The n – T (based on the in-
stantaneous change in load) curves for commercial purity tita-
nium specimens are shown in Fig. 45. Only at $77°K$ does the
strain rate sensitivity remains constant after 4   percent
strain. At room temperature the strain rate sensitivity of
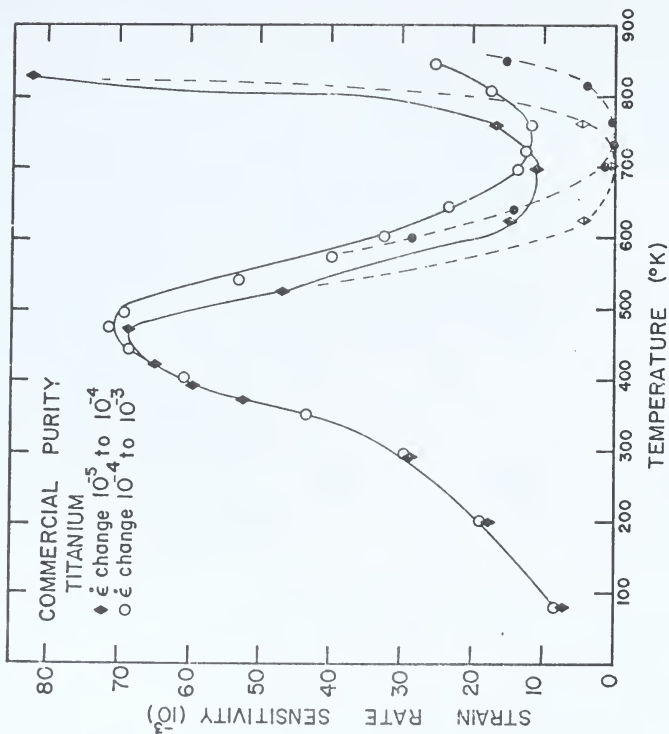
Fig. 43. The strain rate sensitivity-temperature curves for c.p. Ti. The two curves correspond to a tenfold strain rate change from different initial values of strain rate. The dotted curves are for extrapolated steady state stress change.
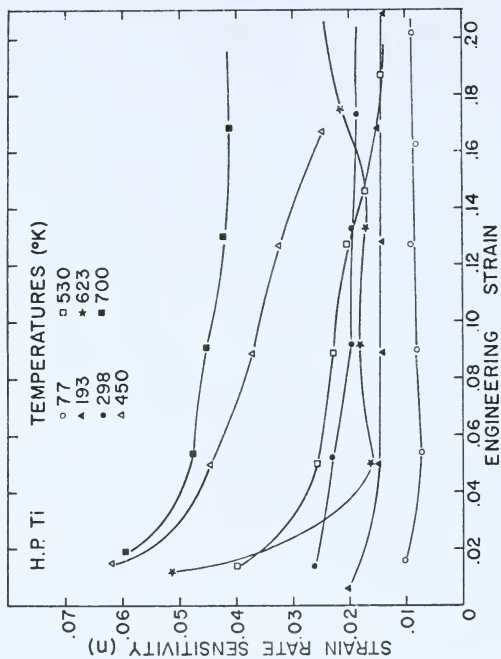
Fig. 44. The strain rate sensitivity of h.p.Ti as a function of strain.
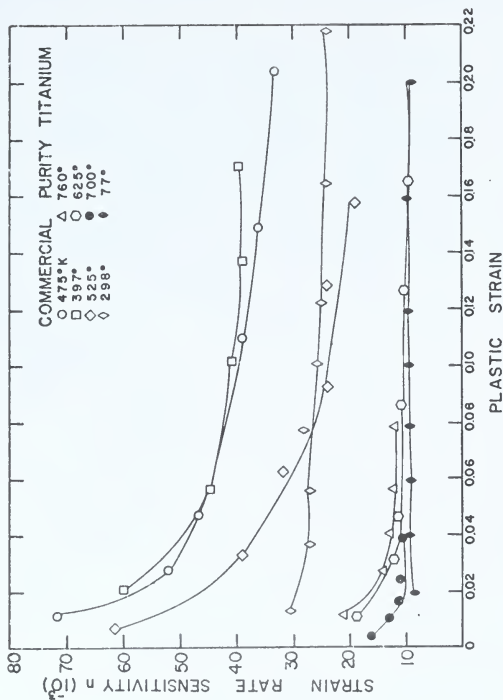
Fig. 45. The strain dependence of the instantaneous strain rate sensitivity of c.p.Ti.

c.p.Ti continues to decrease with increasing strain.

The temperature variation of the strain rate sensitivity of h.p.Zr and c.p.Zr based on a strain rate change near 8 percent strain is shown in Fig. 46. Since transients were observed in c.p.Zr data between 600 and 675°K, two values of strain rate sensitivity (that is from an instantaneous load change and from an extrapolated steady state load change) were calculated in this temperature range. Note that the n - T curves for both zirconium grades show a peak near 450°K. However, the height of the peak is considerably higher in c.p. Zr data. While the h.p. Zr n - T curve shows a minimum of 0.01 at 600°K, the c.p.Zr minimum has a higher value($\simeq 0.02$) and it occurs at a higher temperature ($\simeq 650$°K). Note that the h.p.Zr n - T curve approaches the shape of a n - T curve of a typical fcc metal like polycrystalline silver shown in Fig.47 (data of Carreker[82]).

The effect of strain on the strain rate sensitivity of h.p.Zr and c.p.Zr is shown in Figs. 48 and 49 respectively. Observe that below room temperature, both zirconium grades exhibit a strain rate sensitivity parameter that is independent of strain. At higher temperatures the strain rate sensitivity generally decreases with increasing strain.

The strain rate sensitivity - temperature diagram for the h.o.Zr specimens is shown in Fig. 50. Although the shape of this curve is similar to that of the c.p.Zr curve in Fig. 46 both the peak at 450°K and the minimum near 600°K are less pronounced in the h.o.Zr data. An exceptionally high
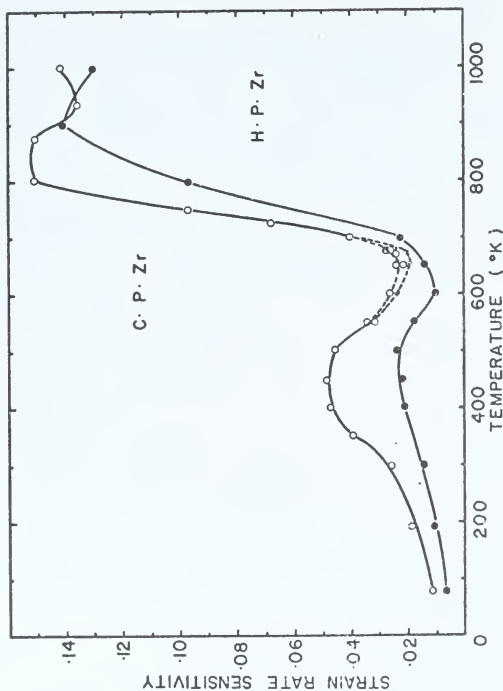
Fig. 46. The temperature dependence of the strain rate sensitivity of c.p. Zr and h.p.Zr calculated from a strain rate change near 8 percent strain. Between 600 and 675°K the lower values for c.p.Zr are based on extrapolated steady state stress change following a transient. Data of Aigeltinger and Woodruff.
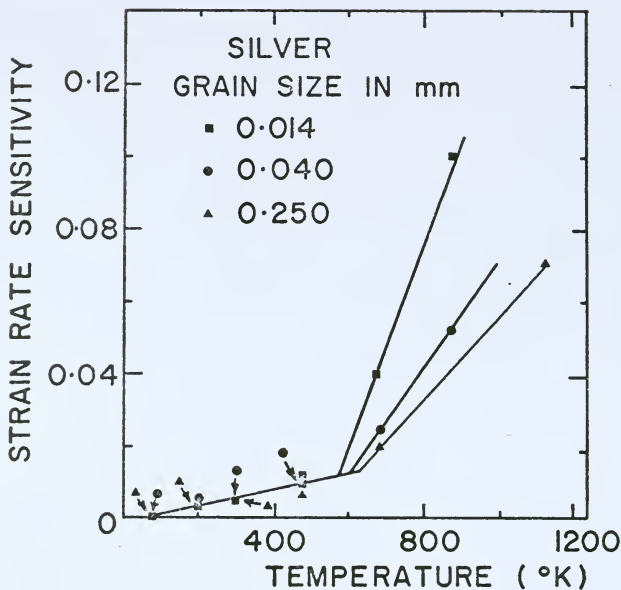
Fig. 47. Temperature dependence of the strain rate sensitivity of polycrystalline silver. Data of Carreker.
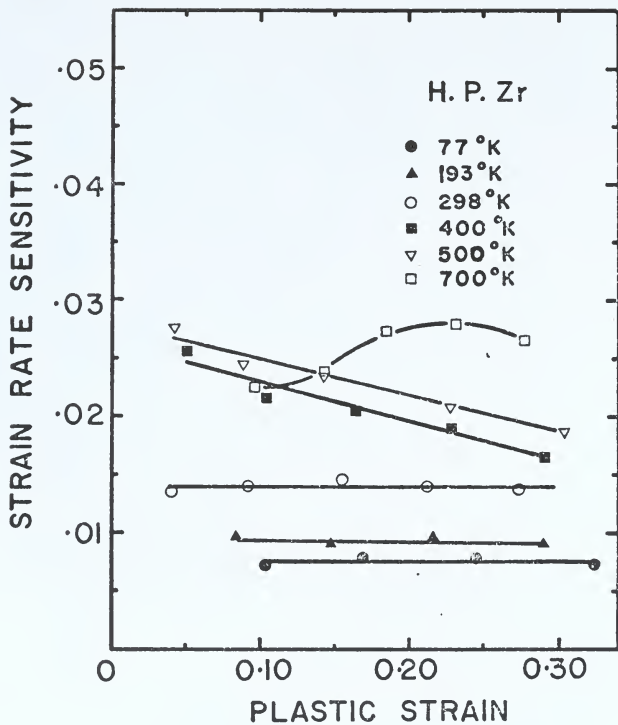
Fig. 48. The variation of the strain rate sensitivity of h.p.Zr as a function of tensile strain. Data of Aigeltinger.
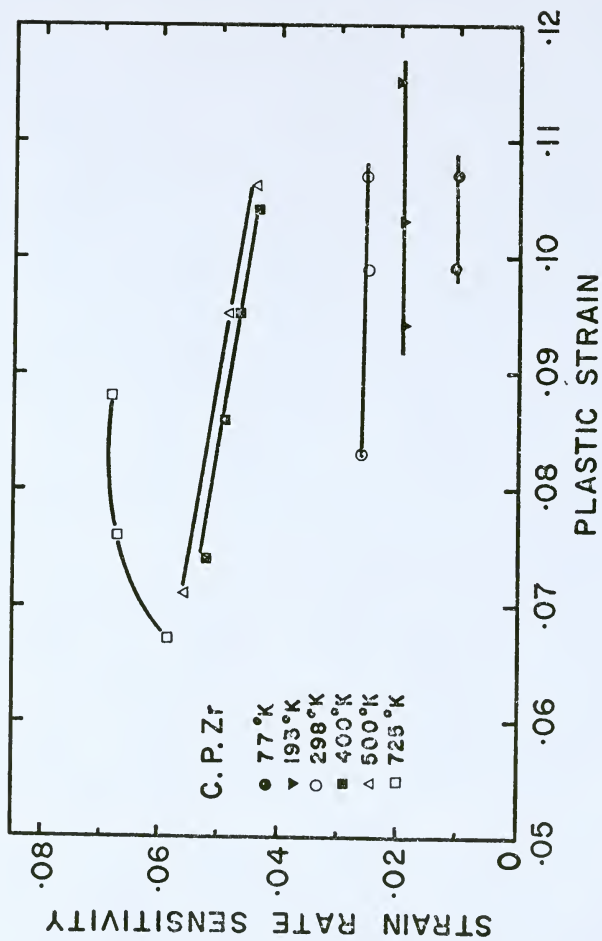
Fig. 49. The strain rate dependence of the strain rate sensitivity of c.p.zr. Data of Woodruff.
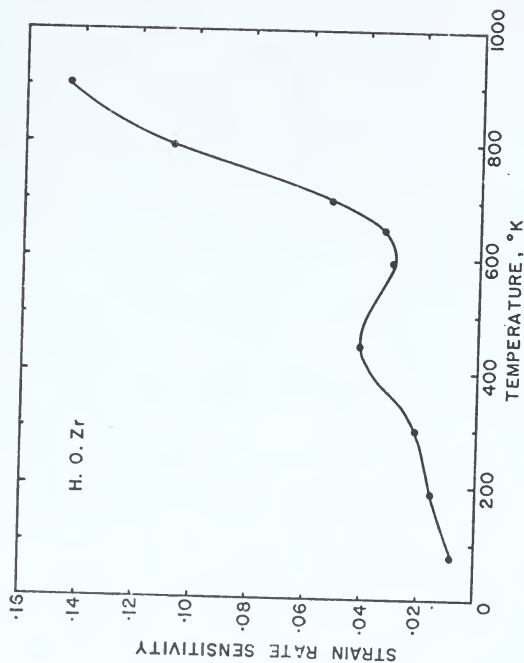
Fig. 50. The temperature variation of the strain rate sensitivity of the h.o.Zr specimens.

iron content in the h.o.Zr specimens may be responsible for this difference.

4.5 Tensile Elongations

The uniform and total elongations of the h.p.Ti and c.p. Ti specimens are plotted against the deformation temperature in Figs. 51 and 52 respectively. Both grades of titanium show large uniform elongations below 300°K. At higher temperatures, Figs. 51 and 52 show three different features in the mechanical behavior of the two specimen types. First note that the well-defined total elongation minimum at the "blue brittle" temperature on the commercial purity curve in Fig. 52 is almost completely missing in the high purity data (Fig. 51). Although there is apparently a ductility minimum at 675°K in Fig.51, it is shallow and the minimum total elongation is large, 40 percent. Whether or not this minimum is equivalent to that of the commercial purity metal in Fig. 52 is also debatable since it occurs at a temperature 75°K below the 750°K minimum in Fig. 52. Normally, the temperatures at which dynamic strain aging phenomena are observed tend to rise with increasing purity.[83,84] However, speculation in this regard is questionable because of the number of composition parameters involved in comparing the two present grades of titanium. The significant feature is that in the high purity metal the "blue brittle" ductility minimum is either missing or is only of a minor importance.
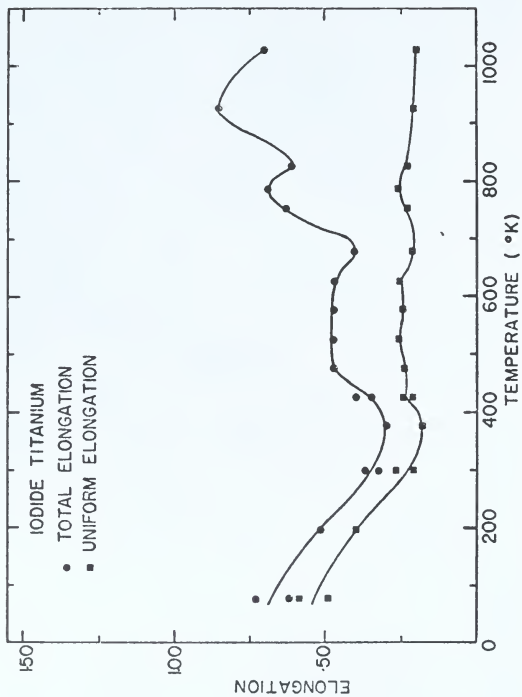
Fig. 51. The uniform and total elongations of h.p.Ti specimens as a function of the deformation temperature.
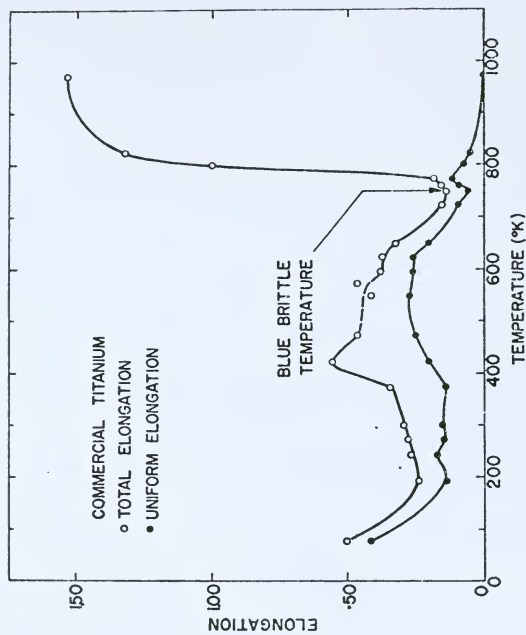
Fig. 52. The temperature dependence of the uniform and total elongations of c.p.Ti. Data of Santhanam.

Another important difference between the data in Figs. 51 and 52 relates to the uniform elongations (strain to the maximum load) as shown in Fig. 53. In high purity titanium, this parameter is nearly constant at 20 percent over a broad temperature range from 300 to 1026°K, whereas in the c.p.Ti data it varies widely. In this latter the uniform elongation is 15 percent at 300°K, rises to 28 percent at 440°K, falls to 6 percent at the "blue brittle" temperature, then passes through a small maximum to become very small above 800°K.

The third difference in the tensile ductility parameters of c.p.Ti and h.p.Ti is evident in Fig.54. The necking strain (strain after maximum load) is plotted as a function of deformation temperature in this diagram. Note that the rise in the necking strain at temperatures just above the elongation minimum is much more rapid in the c.p.Ti specimens. Thus at 75°K above the minimum, the necking strain is almost three times greater in c.p.Ti than that in h.p.Ti. Also note that whereas the c.p.Ti necking strain shows a pronounced peak at 425°K, such a peak is either missing or subdued in the h.p.Ti necking strain curve.

Figure 55 shows the temperature dependence of the uniform and total elongations of h.p.Zr. Observe that at 77°K both ductility parameters are very high, o.65 and 0.80 respectively. However, between 200 and 750°K, the uniform elongation becomes approximately constant at 0.30 and then decreases to about 0.10 between 900 and 1000°K. The total elongation also varies little between 200 and 750°K. However,
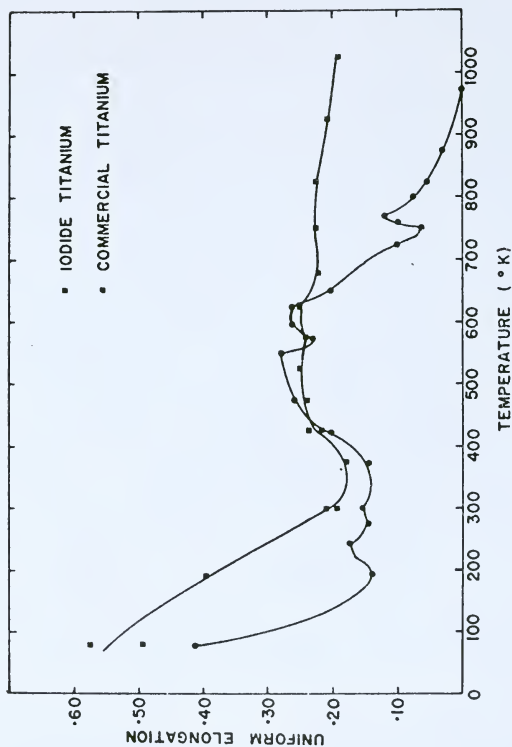
Fig. 53. The variation of the uniform strain of c.p. and h.p. titanium with temperature.
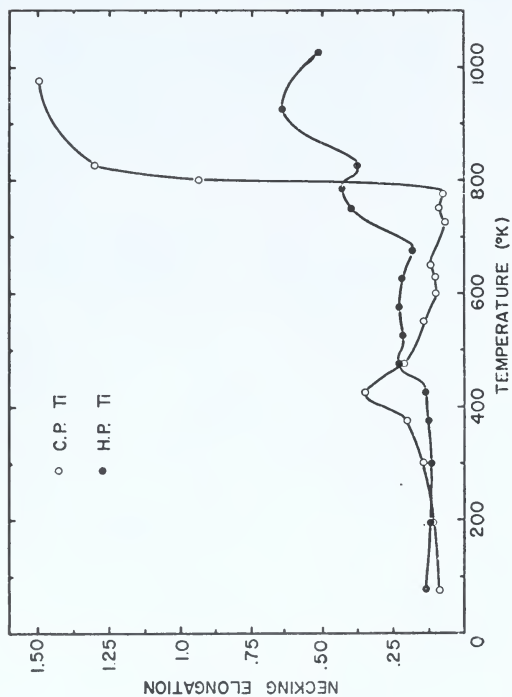
Fig. 54. The temperature dependence of the necking strain of h.p. and c.p. Ti.
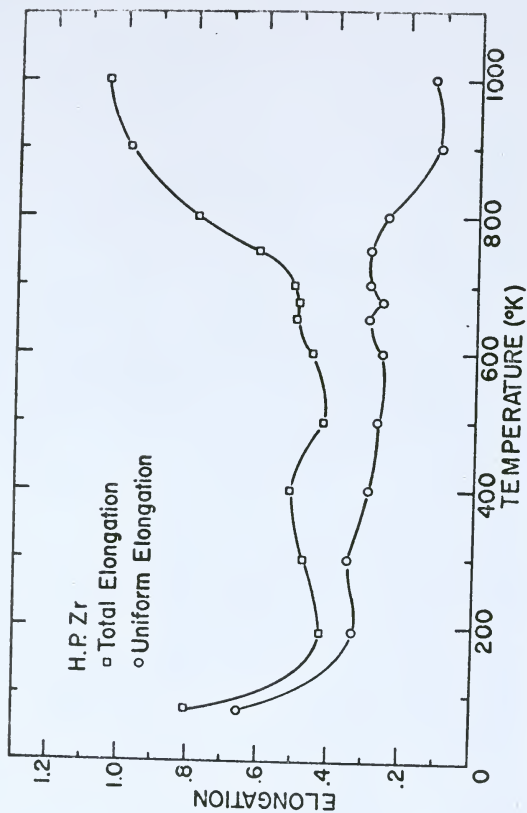
Fig. 55. The uniform and total elongations of h.p.Zr as a function of the deformation temperature. Data of Aigeltinger.

above 750°K it rises rapidly so that the necking strain, or the difference between total and uniform elongations, increases significantly above 750°K.

The corresponding uniform and total elongations of the c.p.Zr specimens are plotted against temperature in Fig. 56. At 77°K, both c.p.Zr elongation parameters are smaller than those of h.p.Zr by about a factor of three. Another significant difference between Figs. 55 and 56 is the larger variation of the total elongation of c.p.Zr between 200 and 750°K. The average uniform elongation of c.p.Zr in this temperature interval is less than half that of h.p.Zr. At the "blue brittle" temperature, 720°K, the c.p.Zr total elongation shows a minimum which is not present in Fig. 55. Above the "blue brittle" temperature, the uniform elongation decreases to remain between 5 and 8 percent to 1000°K, while the necking strain increases more abruptly in c.p.Zr than in h.p.Zr so that at 1000°K it is about 50 percent greater.

Figure 57 presents the temperature dependence of the uniform and total elongations of h.o.Zr. At 77°K, both elongation parameters are much smaller in the h.o.Zr than in the other two Zr grades. Also the uniform elongation of the h.o. Zr is almost constant between 200 and 650°K. These data do not reveal a blue brittle elongation minimum.

A comparison of the uniform and necking strains of the three zirconium grades is shown in Fig. 58. A significant feature of Fig. 58. that was not apparent in the earlier diagrams, is the close similarity between the necking strain -
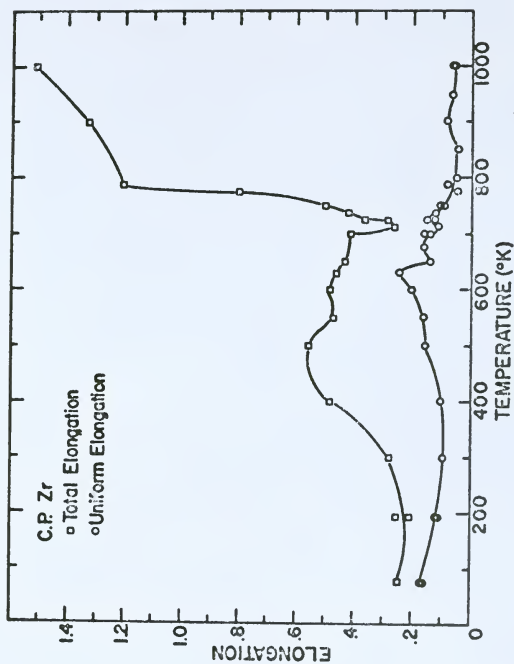
Fig. 56. The variation of the total and uniform elongations of c.p.Zr specimens with temperature. Data of Woodruff.
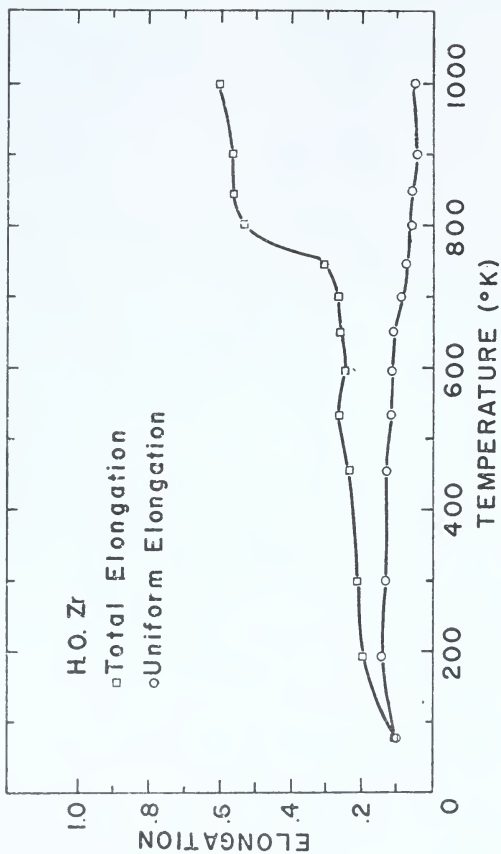
Fig. 57. The temperature dependence of the uniform and total elongations of h.o.Zr specimens.
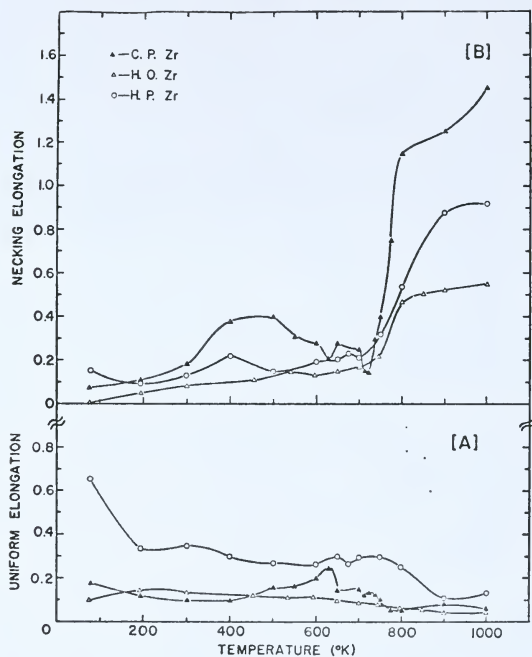
Fig. 58. The uniform and necking elongations of the three zirconium grades as a function of the deformation temperature.

temperature curves of c.p.Zr and h.p.Zr in Fig. 58 (b) and
the corresponding strain rate sensitivity - temperature curves
in Fig. 46.

Perhaps the best way to illustrate the effect of tem-
perature on the ductility parameters is to compare the shapes
of the stress-strain curves at several temperatures. Figures
59 and 60 show such comparison for the two titanium grades.
The three temperatures chosen are representative of behavior
below the DSA temperature range, within the DSA interval and
above it. As shown in Fig. 59 (a), at 473°K where the DSA
effects are small, except for the higher flow stress level
of the commercial purity curve with the presence of a small
yield point, the stress-strain curves of the two titanium
grades have the same basic shape. When dynamic strain aging
effects are significant, the shape of the stress-strain curves
becomes very different (Figs. 59(b) and 60).

At the blue brittle temperature (750°K), c.p.Ti speci-
men has a much smaller uniform and total elongation than does
the h.p.Ti (Fig. 59 (b)) whose stress-strain curve,except for
the lower flow stress level and an increased elongation, is
similar to that at 473°K. Further increasing the deformation
temperature by only 73 to 823°K again does not alter the h.p.
Ti stress-strain curve significantly (Fig.60). However c.p.
Ti specimen shows a 900 percent increase in total elongation
that is almost entirely due to an increase in necking strain.

A similar comparison of the stress-strain curves of two
zirconium grades is shown in Figs. 61 and 62. Though the
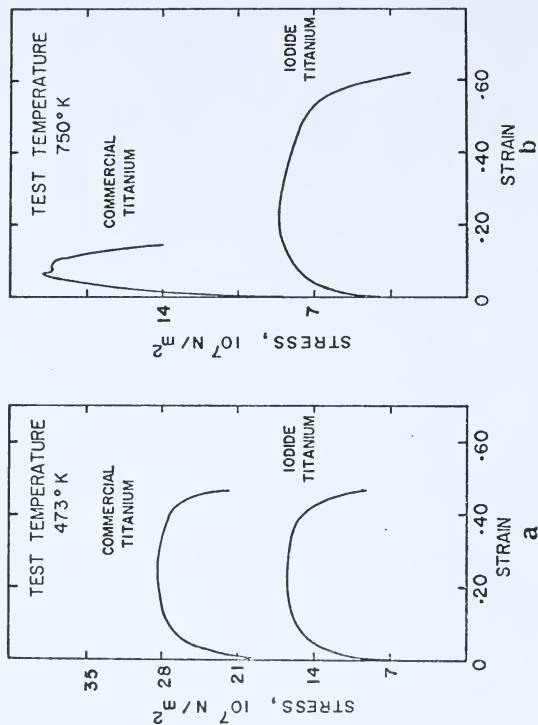
Fig. 59. The stress-strain curves of c.p. and h.p.Ti. (a) at 473°K and (b) at 750°K.
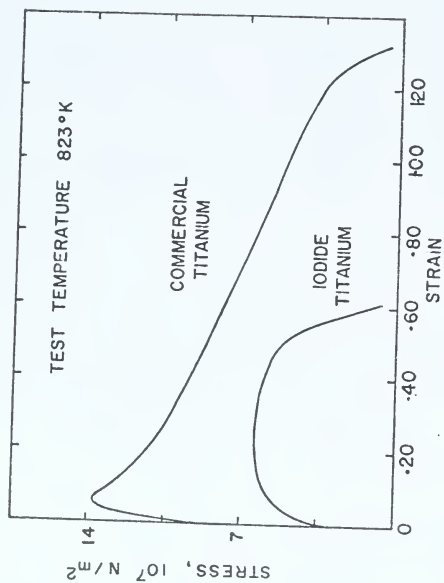
Fig. 60. The stress-strain curves of h.p. and c.p. Ti at 823°K.
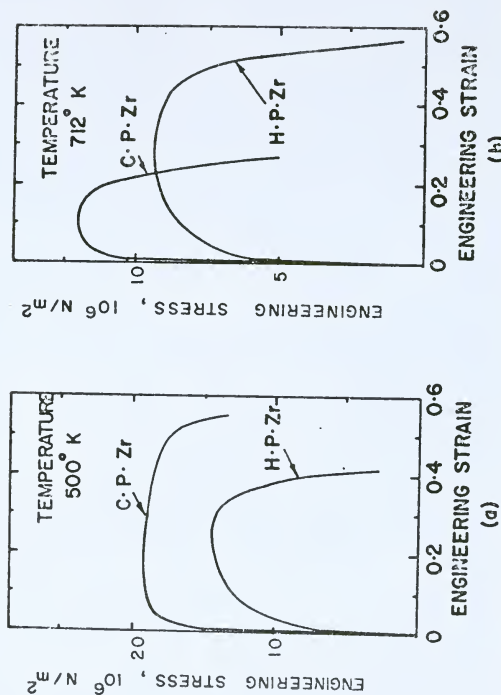
Fig. 61. The stress-strain curves of h.p.Zr and c.p.Zr. (a) at 500°K and (b) at 712°K. Data of Aigeltinger and Woodruff.
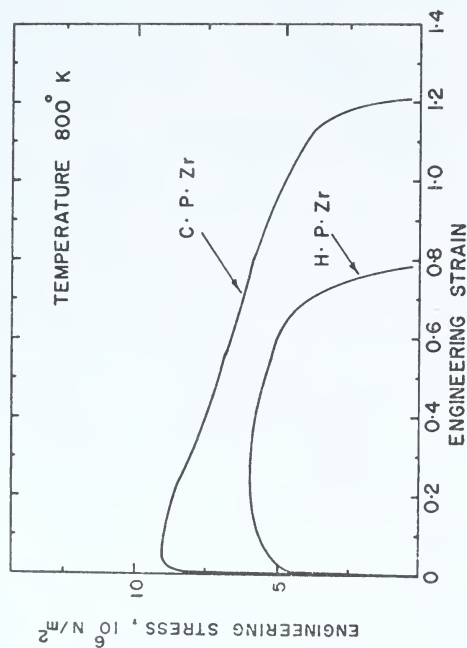
Fig. 62. The stress-strain curves of h.p.Zr and c.p.Zr at 800°K. Data of Aigeltinger and Woodruff.

trends in Figs. 61 and 62 are similar to those in Figs. 59 and 60, it is clear that the variation of the shape of the stress-strain curve is more significant in titanium than in zirconium.

4.6 The Work Hardening Rate

Although the work hardening rate is an important mechanical property of a metal, a simple measure of the work hardening rate is difficult to define. A direct measure of the work hardening rate is the slope of the true stress-true strain curve. Figure 63 shows the variation of the slope of the h.p.Zr stress-strain curve with temperature. The slope is evaluated at fixed values of plastic strain and was divided by the modulus to remove the variations due to the temperature variation of the modulus. The plots for different strains in Fig. 63 indicate a tendency for the work hardening rate to peak near $700°K$. Since the value of $(1/E).(d\sigma/d\epsilon_p)$ at any perticular point on the stress-strain curve is strongly affected by scatter in the data and the accuracy of measurements, a more reliable measure will probably be the parameter $(1/E).(\Delta\sigma/\Delta\epsilon_p)$ over a selected strain interval. A strain interval between 0.005 and 0.05 plastic strain was chosen so as to exclude the yield point load drops at lower strains and necking at higher strains.

Figure 64 shows the variation of the work hardening rate parameter $(1/E).(\Delta\sigma/\Delta\epsilon_p)$ with temperature for h.p.Ti, c.p.Ti
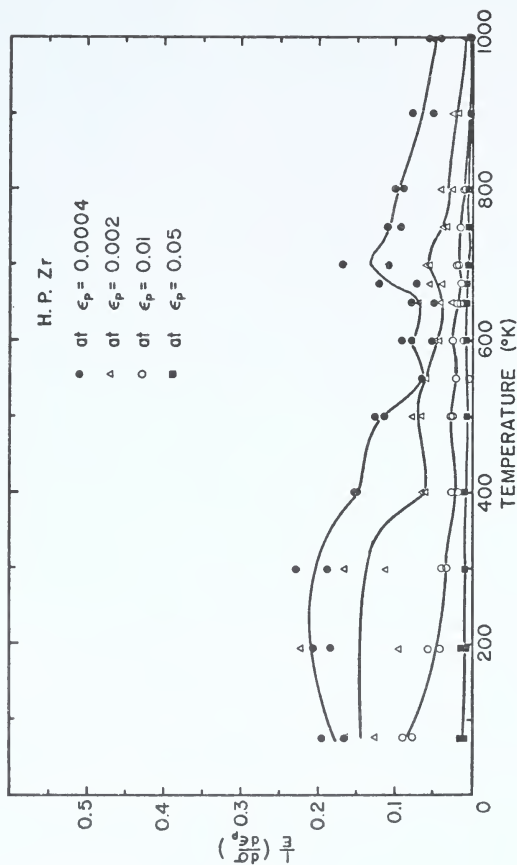
Fig. 63. The temperature variation of the parameter $1/E$, $(d\sigma/d\epsilon_p)$ for h.p.Zr. The slope of the stress-strain curve is calculated at different strain levels. Data of Aigeltinger.
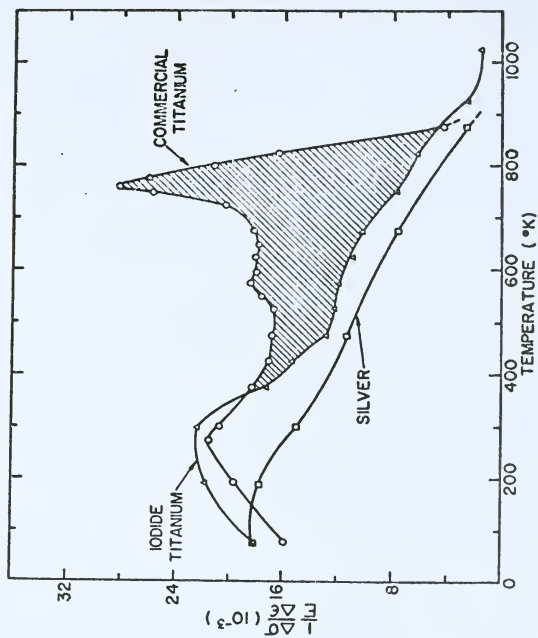
Fig. 64. The temperature dependence of the work hardening rate parameter $1/E.(\Delta\sigma/\Delta\epsilon_p)$ for h.p.Ti, c.p.Ti and silver.

and silver.[82] Observe that while the c.p.Ti curve shows a pronounced work hardening rate peak at 760°K, such a peak is absent in h.p.Ti data. Also note that the high temperature work hardening rate of h.p.Ti is similar to that of a typical fcc metal like silver where dynamic recovery effects are important. At and below room temperature, the work hardening rates of the two titanium grades are comparable. Figure 65 depicts the variation of the work hardening rate of h.p. Zr. Note that above room temperature these data are similar to those of h.p.Ti in Fig. 64. Figure 65 does not show any work hardening peak. Figure 66 shows the work hardening rate of c.p.Zr at two strain rates differing by an order of magnitude. Observe that unlike the c.p.Ti data in Fig. 64, the c.p.Zr data in Fig. 66 do not show a work hardening peak. The weak plateau observed between 600 to 700°K ($\dot{\epsilon} = 10^{-5} \mathrm{sec}^{-1}$) shifts to higher temperatures (650 to 750°K) with a tenfold increase in strain rate to 10^{-4} sec.$^{-1}$. A similar strain rate dependence of work hardening rate has been reported for c.p.Ti.[18]

A comparison of temperature variation of the work hardening rate of c.p.Ti, c.p.Zr and steel (of comparable grain size[85]) is possible from the curves in Fig. 67. Note that the steel data shows a work hardening rate peak at about 423°K ("blue brittle" temperature for steel). Also note that while the work hardening peak is almost absent in c.p.Zr data, the heights of the work hardening rate peaks in c.p.Ti and steel are almost comparable.
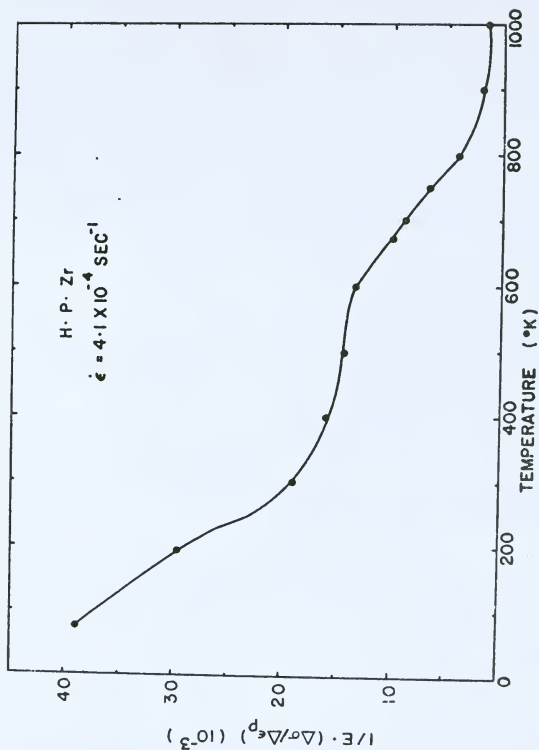
Fig. 65. The work hardening parameter $1/E \cdot (\Delta\sigma/\Delta\epsilon_p)$ as a function of deformation temperature for h.p.Zr data of Aigeltinger.
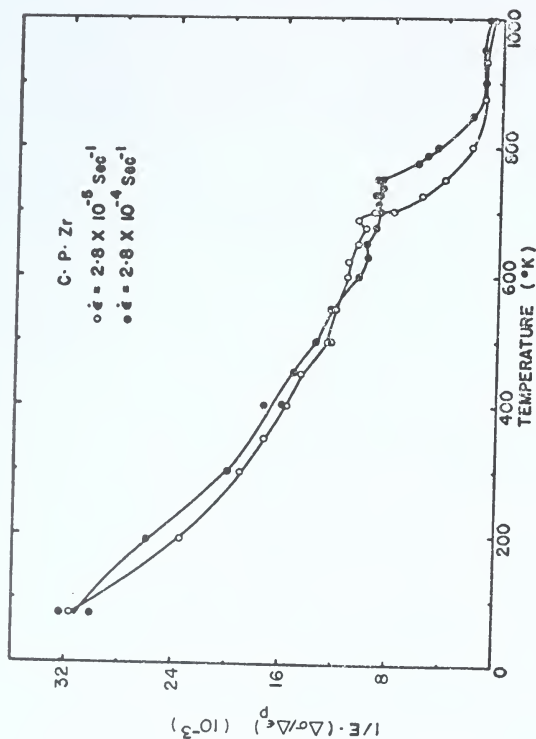
Fig. 66. The variation of the work hardening rate parameter $1/E \cdot (\Delta\sigma/\Delta\epsilon_p)$ for c.p.Zr with temperature. The two curves are for different strain rates. Data of Woodruff.
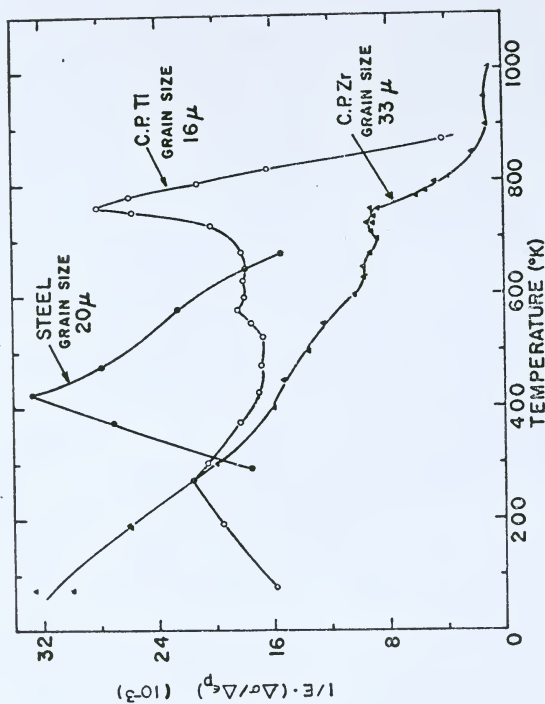
Fig. 67. The work hardening rate parameter $1/E \cdot (\Delta\sigma/\Delta\epsilon_p)$ – temperature diagrams for steel, c.p.Ti and c.p.Zr.

The absence of a work hardening rate peak in the c.p.Zr data demonstrates the weak interaction between dislocations and interstitial atoms. In order to investigate the effect of a still greater amount of impurities on the deformation behavior of zirconium, the work hardening rate parameter of h.o.Zr was compared with that of c.p.Zr (Fig. 68). The h.o. Zr material has a exceptionally high iron content whose effects on the tensile properties of the h.o.Zr are unknown. In any case, however, the important feature of Fig. 68 is that although the work hardening rate level of the h.o.Zr specimens is higher than that of the c.p.Zr specimens, the h.o.Zr data fail to reveal a pronounced work hardening rate peak as observed in the c.p.Ti data.

Another way of analysing the work hardening behavior is a plot of ($d\sigma/d\epsilon_p$) against plastic strain ϵ_p. The area under this curve gives the net increase of flow stress over the strain interval under consideration. Such plots for c.p.Zr and c.p.Ti in the dynamic strain aging interval are given in Fig. 69. Note that among the three c.p.Ti curves, the inter-mediate temperature curve has the highest level of work hard-ening (temperature corresponding to the work hardening rate peak in Fig. 64). The three zirconium curves on the other hand fall regularly with increasing temperature. Also observe that the work hardening rate level at any given temperature is higher in c.p.Ti than in c.p.Zr.

An indirect way of analysing the work hardening behavior
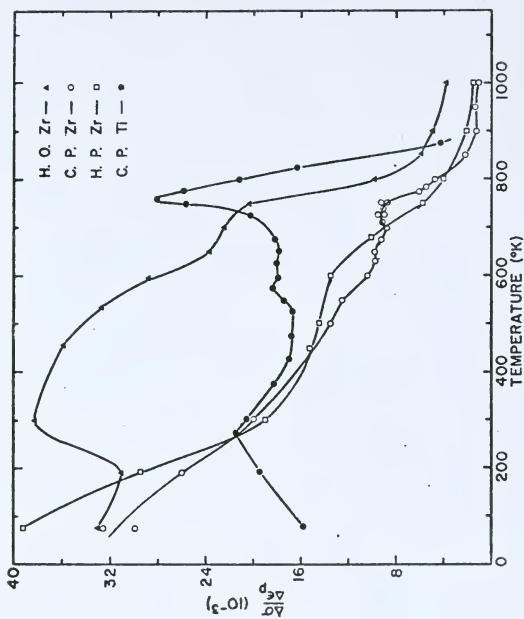
Fig. 68. A comparison of the temperature variation of the work hardening rate parameter $1/E \cdot (\Delta\sigma/\Delta\epsilon_p)$ of the three zirconium grades and c.p.Ti.
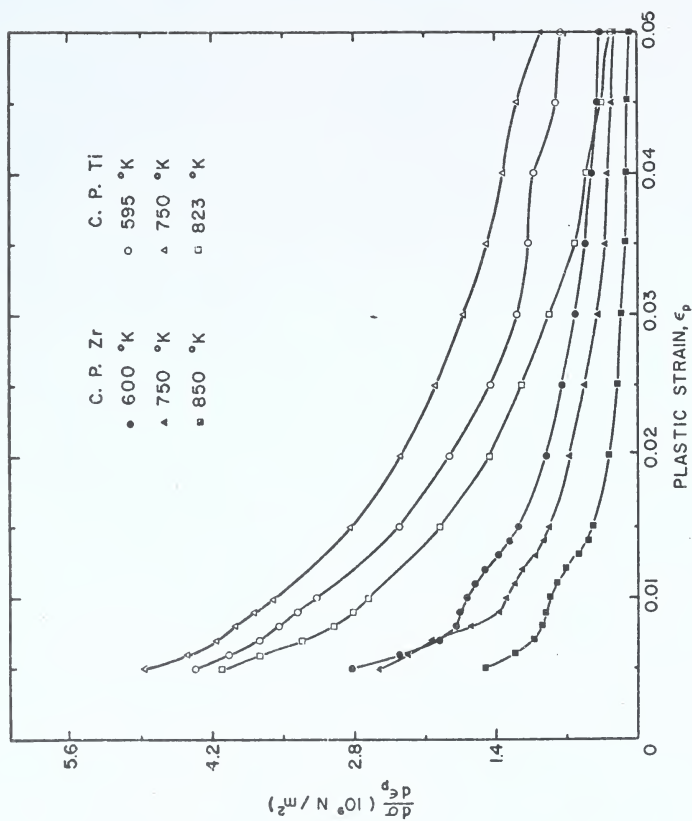
Fig. 69. The variation of the slope of the stress-strain curve as a function of strain for c.p.Zr and c.p.Ti at three different temperatures.

is a set of flow stress-temperature diagrams for different strains. Figure 70 shows σ/E - temperature plots for c.p. Zr specimens at plastic strains 0.0004, 0.002. 0.01 and 0.05. Since the curves do not diverge from each other significantly at any temperature, the work hardening rate peak is almost absent in c.p.Zr. For c.p.Ti,[11] it has been shown that such curves diverge significantly at 760°K (the extent of diversion increases as the strain increases) giving rise to a work hardening rate peak.

Though the exponent n in the empirical Equations (8) and (9) has been designated[65] as a "work hardening exponent ," a simple differentiation of Eq. (8) and (9) reveals that the work hardening is not simply related to the exponent and that the constants k_1 and k_2 also enter into the work hardening rate.

4.7 The Yield Stress

Commercial purity titanium specimens showed yield point load drops between 373 and 773°K, whereas none were observed in this interval in h.p.Ti. Yield point phenomena were observed, however, in the h.p.Ti between 77 and 298°K. None of the zirconium grade showed yield points over the entire temperature range of investigation 77 to 1000°K. The yield stress was taken as the lower yield stress when yield point occured or as the flow stress at 0.2 percent strain when it did not occur.

125
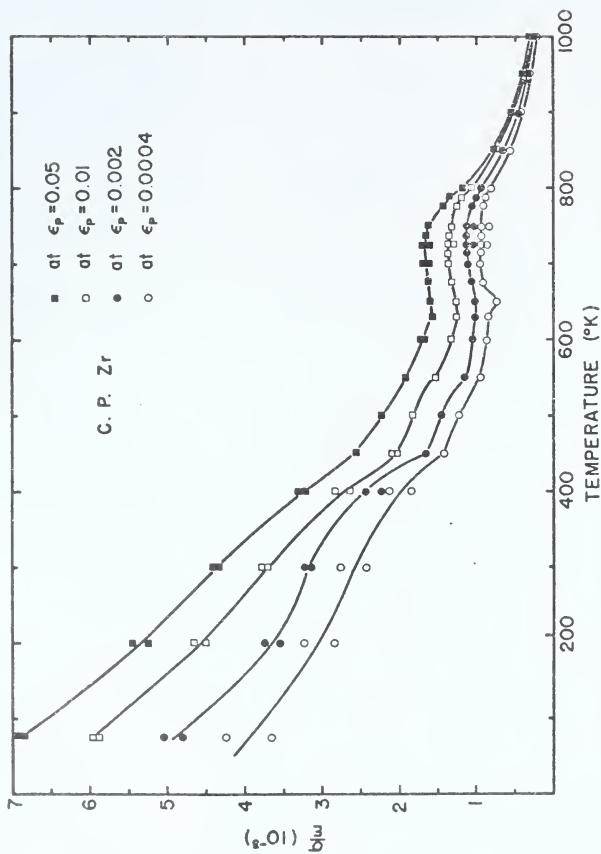
Fig. 70. The temperature variation of the parameter (σ/E) at different strains for c.p.Zr. Data of Woodruff.

The dependence of the parameter, yield stress divided by the Young's modulus , on the temperature for the two Zr and Ti grades is shown in Fig. 71. Notice that the c.p.Zr, c.p.Ti and h.p.Ti data indicate a tendency for plateau formation in the temperature range 575 to 775°K. Due to the negligible temperature dependence of the yield stress of h.p. Zr, it is difficult to detect any plateau. In fact the yield stress parameter of h.p.Zr almost remains constant from 77 to 800°K.

Since both the c.p. and h.p.Ti data in Fig. 71 showed a tendency for plateau formation, these data were further analysed by a ln (τ/μ) versus temperature diagram shown in Fig. 72. In this figure, τ is the critical resolved shear stress computed from the 0.2 percent yield stress assuming a 0.5 Schmid factor and μ is the shear modulus. Straight lines have been superimposed on both curves passing through the data points at low (77°K) and high temperatures (above 900°K) where the strain aging phenomena are known to be weak. This does not account for a possible effect of twinning on the yield stress below 300°K which could change the slopes of the two straight lines. Note that both curves in Fig. 72 deviate from the straight lines in two temperature intervals centered near 350 and 800°K. However, the high temperature deviation (600 to 1000°K) is more pronounced in c.p.Ti, being at 750°K about 5.5×10^6 N/m^2 compared to 1.2×10^6 N/m^2 in the case of h.p.Ti.
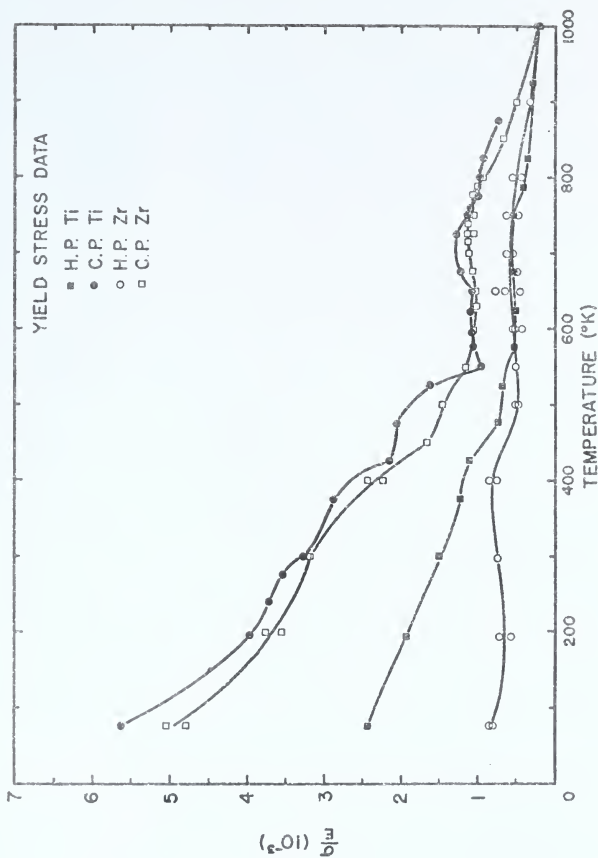
Fig. 71. The temperature variation of the yield stress (normalized with respect to the elastic modulus) of h.p. and c.p. Ti and Zr.
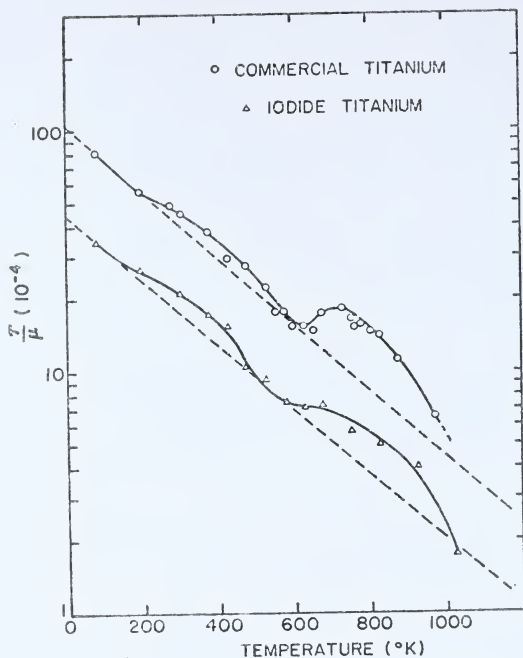
Fig. 72. A plot of $\ln(\tau/\mu)$ against temperature for
c.p. and h.p. titanium.

4.8 The Portevin-LeChatelier Effect

The Portevin-LeChatelier effect (also known as discontin-
uous yielding or serrated yielding) was observed in the c.p.
Ti tensile data over the temperature range 650 to 730°K.
However the stress drops were much smaller in the c.p.Ti speci-
mens (300 psi) than the corresponding stress drops observed
in steel[85] (2500 psi). Serrations were not observed in the
stress-strain curves of h.p.Ti,or any zirconium grade.

4.9 Effect of 77°K Prestrain on Room Temperature
Stress-Strain Curve of Titanium

Mechanical twins introduced during 77°K prestraining
improve both the room temperature yield stress and the ulti-
mate tensile strength while still yielding respectable duc-
tility values, as may be seen in Fig. 73. This figure shows
the effects of various amounts of prestrain on the room tem-
perature stress-strain curve of h.p.Ti. A 40 percent 77°K
prestrain increased the room temperature high purity yield
stress by about 300 percent and the ultimate tensile strength
by about 200 percent. Prestraining was also observed to in-
crease the room temperature work hardening rate resulting in
higher uniform elongations. As far as can be determined, the
microstructure with deformation twins is stable during room
temperature restraining. Yield drops or premature necking
associated with work softening were not observed. A Crussard-
Jaoul plot of log ($d\sigma/d\epsilon_p$) against log ϵ_p revealed that
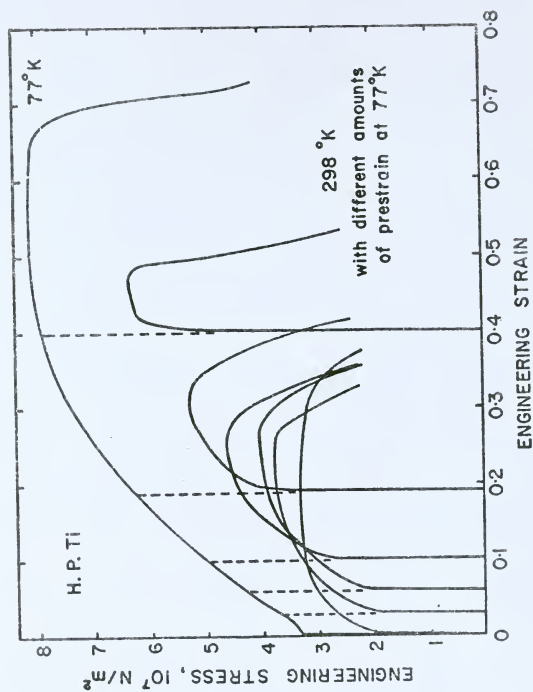
Fig. 73.   The effect of various amounts of 77°K prestrain on the room temperature stress-strain curve of h.p.Ti.

prestraining introduces constant slope regions in the room temperature stress-strain curve. Similar curves for c.p.Ti are shown in Fig. 74. A comparison of Figs. 73 and 74 reveals that the effect of prestrain is more pronounced in h.p.Ti than in c.p.Ti.

4.10 Effect of Small Amounts of Prestrain in the DSA Region on the Room Temperature Properties of C.P.Ti

Figure 75 shows the influence of prestraining in the dynamic strain aging interval on the room temperature stress-strain of c.p.Ti. Notice the absence of a yield point on the stress-strain curve of the specimen without prestrain and the presence of yield points in the prestrained specimens. Though the yield points (one of the characteristics of work softening phenomena) are observed after prestraining, there is no loss of ductility as normally observed in work softening. In fact, while there is no change in the uniform elongation after prestrain, the total elongation is increased after the prestrain.
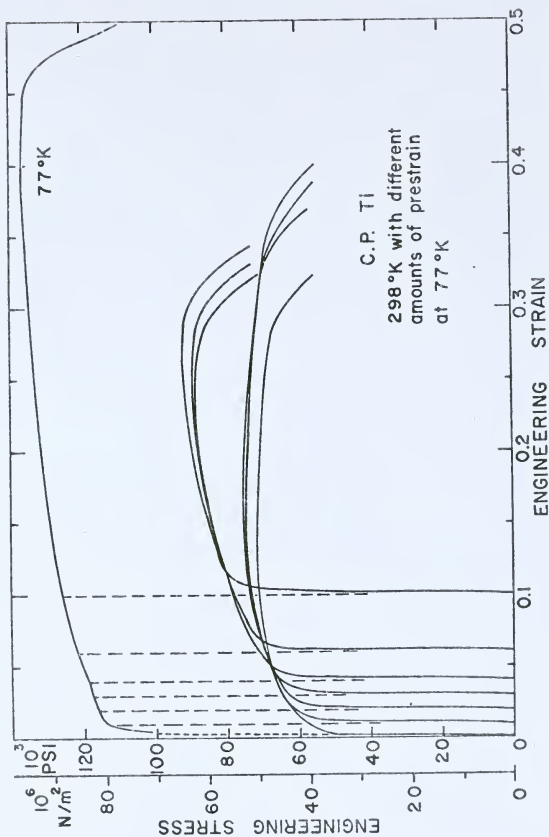
Fig. 74. The influence of various amounts of 77°K prestrain on the room temperature stress-strain curve of c.p. Ti.
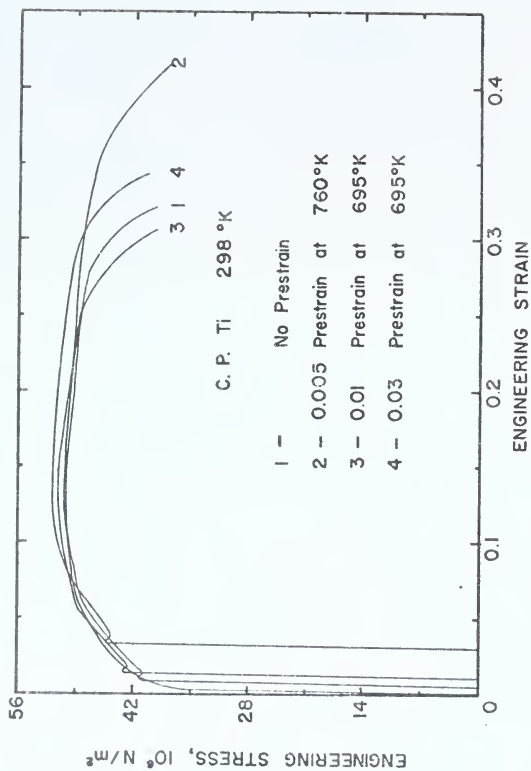
Fig. 75. The effect of a small amount of prestrain in the DSA interval on the room temperature stress-strain curve of c.p.Ti.

CHAPTER V

DISCUSSION

5.1 The Importance of Deformation Twinning in Ti[86]

The results presented in Figs. 7 through 13 are consis-
tent with those of Wasilewski[10] and Santhanam[11] on c.p.Ti.
The stress-strain curves are similar (approximately linear
work hardening rate at low temperatures). Both deformation
twinning and high ductility are observed at 77°K. These data,
combined with those reported earlier, have covered a range
of composition from 99.6 to 99.96 percent Ti and have involved
specimens cut from rolled plates and swaged rods and grain
sizes ranging from 22 to 3 microns. In summary, it would ap-
pear that there is little doubt that deformation twinning
occurs significantly and is important in the low temperature
deformation of various grades of titanium of different longi-
tudinal textures (basal planes parallel to the stress axis)
over a range of grain sizes. The preparation of properly
electropolished and anodized titanium specimens suitable for
twin-trace observation is a difficult process. It is much
harder to prepare a titanium specimen than one of zirconium
or hafnium. In the cases where twinning has not been detect-
ed in longitudinal titanium tensile specimens deformed at
77°K, it may be possible that the problems associated with

the metallographic preparation have prevented the observtion of twins.

As a result of the present observations, an activation analysis of the deformation of titanium based on the extrapolation of data obtained below $424°$K to this temperature should be considered inadequate if it does not consider the effect of deformation twinning on the low temperature flow stress. Similarly, the conclusion of Sargent and Conrad[87] that the complete deformation dynamics of titanium at low homologous temperatures ($T < 0.4\ T_m$) can be determined by a relatively small number of stress relaxation tests at room temperature is questionable.

5.2 Effect of Twinning on the $77°$K Stress-Strain[88] Behavior of Titanium and Zirconium

The twin volume fraction data in Figs. 21 and 22 show that impurities tend to suppress deformation twinning in both Ti and Zr, the effect being much stronger in zirconium. Thus, even though the impurity concentration of the commercial purity zirconium specimen is comparable to that of the corresponding titanium specimens, the average twinning rate is about four times lower in the zirconium. As discussed later in this chapter, this effect is opposite to that at higher temperatures (500 to $900°$K) where impurities introduce weaker[89] dynamic strain aging phenomena in zirconium than in titanium.[76] As compared to zirconium, the higher twinning rate in titanium may be related to the higher flow stress level in titanium.

An important effect of a high twinning rate in zirconium and titanium may be seen in Figs. 16 through 20. The three metals (h.p.Ti, h.p.Zr and c.p.Ti) that twin moderately or heavily at large strains all show stages of approximately constant work hardening rate (linear true stress-true strain diagram stages) on their Crussard-Jaoul diagrams. On the other hand, the c.p.Zr specimen that twins only to a limited extent, fails to develop a constant work hardening rate stage and its true stress-true strain curve has a continuous curvature. The introduction of linear work hardening stages with purification has also been observed by Mannan and Rodriguez[90] in zirconium and its alloys at room temperature. The magnitude of the work hardening rate in the constant slope stage is evidently related to the degree of twinning. Thus, in Fig. 20, stage II of h.p.Ti has a work hardening rate nearly double that of stage II of c.p.Ti (Fig.19), which is about twice that of stage III of h.p. Zr (Fig.18). Figure 22 shows that the corresponding $V_V - \epsilon$ curves follow the same order.

Large elongations are normally associated with linear stress-strain curves because a constant $(d\sigma/d\epsilon_p)$ tends to delay the Considere's criterion for necking to larger strains.[91] Thus, a nearly constant work hardening rate and a low initial flow stress act to produce large uniform elongations in h.p. Ti and h.p.Zr specimens. Linear stress-strain curves with large uniform elongations are not restricted to titanium[10,11] and zirconium, but are also formed in other metals[83,92-94]

that twin significantly during deformation at low temperatures.

5.3 Relationship between the Work Hardening Stages and the Twinning Behavior

The strong effect that deformation twinning has on the mechanical properties of titanium and zirconium at 77°K is further demonstrated by the close correlation between the stages in the Crussard-Jaoul plots and comparable stages in the quantitative microscopic data diagrams.

Commercial Purity Titanium : In c.p.Ti a constant work hardening stage (stage II) starts to develop near $\epsilon_p = 0.015$, as shown in Fig. 19. Figure 22 shows that the corresponding twin volume fraction curve has an increase in slope at approximately this same strain. Thus, the start of the constant work hardening rate region of the stress-strain curve is associated with an increase in $dV_V/ d\epsilon_p$.

High Purity Titanium : The h.p.Ti stress-strain curve shows a well-defined yield plateau (See Fig.14) that extends to about 0.005 strain, shown in Fig. 20, may not be meaningful. Figure 22 shows that at 0.005 strain, the twin volume fraction is about 1.3 percent, implying that the yielding process involves significant amount of twinning and that the yield plateau may be largely associated with twin formation. From $\epsilon_p = 0.005$ to $\epsilon_p = 0.010$ the volume fraction of twins increases very rapidly and, in this interval, the work hardening rate actually increases, as may be seen in Fig.20.

Above $\epsilon_p = 0.01$ and to $\epsilon_p = 0.24$, the work hardening rate is constant, while V_v in Fig. 21 increases less rapidly but still at a large, roughly constant rate.

Near 0.24 strain, the work hardening rate of h.p.Ti starts decreasing, as shown in Fig.20. This is accompanied by a corresponding decrease in $dV_v/d\epsilon_p$, as indicated in Fig. 21. At this strain, the twin volume fraction becomes greater than 0.6 and therefore, the fraction of untwinned matrix becomes less than 0.4. Above $\epsilon_p = 0.24$, high purity titanium becomes more and more saturated with twins.

High Purity Zirconium : In the h.p.Zr data, $dV_v/d\epsilon_p$ is very low, to about 0.04 strain (Fig.22), and then increases to about the same value as in c.p.Ti at higher strains. The other three quantitative microscopic parameters diagrams (Figs. 23, 24 and 25) for h.p.Zr all show breaks in their curves near $\epsilon_p = 0.05$. In addition, the Crussard-Jaoul plots (Fig. 18) also show that the constant work hardening rate (stage III) begins to develop near this strain. Though the twinned volume fraction versus strain curve shows a break point at a slightly lower strain (0.04), there is certainly a reasonable correspondence between the constant work hardening rate and a moderate rate of increase of twinned volume fraction with strain.

Commercial Purity Zirconium : The volume fraction of twins in the c.p.Zr specimens was less 0.05 even at a 0.10 strain and in agreement with this small $dV_v/d\epsilon_p$, the c.p.Zr stress-strain curve does not develop a constant slope stage, and

the work hardening rate decreases continuously with strain.

5.4 Evolution of Twin Structure with Deformation

On the basis of the quantitative metallographic data, the evolution of twinning with strain in high purity titanium and high purity zirconium can be evaluated as follows :

High Purity Titanium : At the beginning of the test and extending to $\epsilon_p = 0.005$, there is a yield plateau in which many fine twins are formed. The data in Figs. 24 and 25 indicate that immediately after the yield plateau, from $\epsilon_p = 0.005$ to $\epsilon_p = 0.010$, the most important effect is the growth of these twins. Note that $\overline{\lambda}$ increases sharply by a factor of about 50 percent, whereas $N_A/\overline{\lambda}$, a measure of N_V, the number of twins per unit volume, does not change. The fact that S_V also rises in this interval suggests, however, that there is probably some nucleation of new twins. Above this interval, where the yield plateau twins grow rapidly, twin nucleation apparently becomes the dominant factor. Thus, above $\epsilon_p = 0.01$, $N_A/\overline{\lambda}$ rises rapidly with strain, while $\overline{\lambda}$ drops sharply at first (to about $\epsilon_p = 0.015$) and then varies only slowly with strain. At the same time, S_V and V_V grow progressively and rapidly. A plausible explanation for the decrease in $\overline{\lambda}$ is that when new thin twins are nucleated in a structure containing twins which have already grown appreciably in thickness, the average twin thickness may decrease if there are sufficient new twins. The importance

of continued twin nucleation in titanium may be seen in the microstructures of Figs. 26 and 27, which indicate that as the strain is increased from 0.02 to 0.1, a significant rise in the number of twins occurs with only a moderate growth in the average twin size.

High Purity Zirconium : The development of the twin structure can be divided into two regions below and above $\epsilon_p = 0.05$. Below this strain, the twin volume fraction increases slowly with strain (Fig. 22), the twin-matrix interface area increases rapidly (Fig. 23), the mean twin intercept, $\overline{\lambda}$, decreases (Fig. 24) and $N_A/\overline{\lambda}$ (i.e. N_v) increases rapidly (Fig. 25). All these observations imply that twin nucleation is important at low strains. Above 0.05 strain, V_v increases rapidly, S_v rises slowly, $\overline{\lambda}$ increases and $N_A/\overline{\lambda}$ decreases to some extent. These observations imply that twin growth is more important at higher strains. That some change in the twin evolution is occuring near 0.05 strain is also implied by the break in the slope of the $\ln(d\sigma/d\epsilon_p) - \ln\epsilon_p$ curve in Fig.18 .

The role of twin growth in zirconium is evident in the microstructures shown in Figs.28 and 29. The twin structure at 0.02 strain was non-homogeneous and, since the twin volume fraction was small, it was difficult to obtain a representative picture. Between $\epsilon_p = 0.02$ and $\epsilon_p = 0.05$, both twin growth and twin nucleation were effective, as shown in Fig. 28. However, from $\epsilon_p = 0.05$ to 0.1 strain, there is a significant growth in the thickness of the twins without a signi-

ficant increase in their number.

5.5 The Mechanism of Work Hardening Due to Twinning

The action of deformation twinning on the work harden-ing behavior of a metal may arise from several factors. Two of the more important are orientiation (geometric) hardening and hardening due to the subdivision of the structure by the twins. Since the lattice inside the twin has a different orientiation from that outside the twin, the twinned region may be unfavorably oriented for slip, which is the case for $\{11\bar{2}2\}$ and $\{11\bar{2}4\}$ twinning in Ti and Zr.[91] The evolution of the twinned structure is different in titanium and zirco-nium at high strains. Twin nucleation seems to be important in titanium, while twin growth is more significant in zirco-nium. The large number of twins in titanium would imply that hardening due to the subdivision of structure is dominant. Both the titanium and zirconium results, however, indicate that a constant work hardening rate is closely related to a high twin volume fraction and a large $dV_v/d\epsilon_\rho$. Whether the large twin volume fraction is achieved by a large number of small twins or growth of a moderate number of thick twins seems to be of secondary importance. These results imply that orientiation hardening is probably of greater signifi-cance than the grain subdivision.

5.6 Contribution of Tensile Strain due to Twinning

About one third of the total strain can be accounted
for by the twin volume fraction in the 77°K deformation of
h.p.Ti. For example, in a specimen deformed to 0.097 strain
at 77°K, the twin volume fraction is about 0.35. Assuming
an average Schmid factor of 0.4 and a twinning shear of
0.22,[91] the strain contributed by twinning alone is 0.4 X
0.22 X 0.35 = 0.031. A similar calculation for iodide zirco-
nium, assuming a twinning shear of 0.225,[95] shows that at 0.1
strain, mechanical twinning can account for only 10 percent
of the total strain.

5.7 Significance of p and q in the Analysis[96] of Deformation Stages

By Eqs. (16) and (17), both p and q are directely relat-
ed to the decrease in the slope of the stress-strain curve
with stress, i.e. ($d\theta/d\sigma$). A high value of p or q indicates
a stress-strain curve slope that decreases rapidly with in-
creasing stress. This implies a significant continuing
change in the nature of the structure development with in-
creasing stress. A low value of p or q means that the slope
of the stress-strain curve decreases slowly with increasing
stress and, therefore, Considere's criterion for necking
($d\sigma/d\epsilon_p$) = σ tends to be deferred to higher strains. A
small p or q, other factors remaining the same, implies a
large uniform elongation.

While comparing the stress-strain behavior of zirconium at different temperatures, it is appropriate to first consider stage 2 since it normally covered a major portion of each stress-strain curve. The results in Fig.37 (b) show that expect in transverse specimens at or below 300°K, all zirconium specimens show high values of q. Similarly, except for the transverse specimens at 4 and 77°K, all specimens show high values of p, averaging about 0.9. This value of p is much higher than the average value of p in stage 2 (0.4) or stage 3 (0.66) of a typical fcc metal like Nickel 270.[97] Consistent with this fact is the observation that Nickel 270 specimens show uniform elongations about twice those observed in zirconium specimens. Higher values of p in zirconium, compared to those in fcc metal, imply a difference in the buildup of the dislocation structure in the two cases.

5.8 Deformation Stages in Zirconium

Longitudinal zirconium tends to show three stages below room temperature, two stages at intermediate temperatures and a ingle stage at high temperatures. As indicated earlier,[88] the deformation behavior below room temperature is probably influenced by deformation twinning. Note that when deformation occurs primarily by multiple prism slip, as at high temperatures, deformation tends to proceed along a single stage.

Thus in the absence of other effects, prism slip appar-

ently tends to conform to a single basic deformation stage
behavior. This contrasts sharply with the three different
basis behaviors in fcc metals like nickel and copper:[53-57]
multiple slip in stage 1, predominantly single slip in stage
2 and the occurrence of cross slip in stage 3.

Transverse specimens twin heavily[72] at low temperatures
and kink[98] at high temperatures. Both effect apparently lead
to multi-stage behavior, although of a different sort. Yield-
ing in transverse specimens at 77°K is probably closely asso-
ciated with deformation twinning. Earlier measurements[72] in-
dicate that at 77°K the initial deformation is accomplished
primarily by twinning. In longitudinal specimens that twin
at lower temperatures, deformation is primarily by slip ac-
companied by a moderate amount of twinning. This has a dif-
ferent effect on the curve, as may be seen by comparing Fig.
31 with Fig. 33. Note that in these diagrams there is a re-
versal in the appearence of the curves at low temperatures.
Thus, in longitudinal specimens, the slope in stage 2 is
steeper or more negative than that in the other two stages.
In transverse specimens the reverse is true. Here the slope
in stage 2 is less negative than that in stages 1 and 3.

The strong effect of twinning in transverse specimens
at low temperatures is visible at intermediate strains. For
example, transverse specimens at 77 and 4°K develop stage 2
with an almost constant work hardening rate and accompanying
small values of p and q. This corresponds to an increased
ductility. At high temperatures where kinking occurs, the

second stage has a large negative slope that becomes more
negative in stage 3, corresponding to an increase in p and
q. This results in a very limited uniform elongation of the
order of 0.04 at 813 K contrasting with 0.21 at 77°K.

5.9 Comparison of the Two Types of Analysis

The results show that the two methods of analysis
(Crussard-Jaoul and the modified) are in qualitative agree-
ment. Both reveal stages covering the same stress-strain
curve regions. Further notice that the trends of the p and
q values in Fig. 37 tend to be similar, although differences
between the p and q values are rather large in some instances.
These variances, however, show a good correlation with the ϵ_{p_o}
values given in Table III. As may be deduced from Fig. 30,
a positive ϵ_{p_o} or strain axis intercept of the power law
equation tends to make the slope of the log ($d\sigma/d\epsilon_p$) versus
log ϵ_p curve, which equals $(n_2 - 1)$, steeper or more nega-
tive, while a negative ϵ_{p_o} value has the opposite effect.
Since q equals $-(n_2 - 1)$, the value of q increases if ϵ_{p_o} be-
comes positive and decreases if ϵ_{p_o} becomes negative. In
accord with these conclusions is the fact that, in Fig. 37,
the values of q are larger than those of p everywhere that
ϵ_{p_o} is positive and are smaller everywhere that ϵ_{p_o} is nega-
tive. Furthermore, the degree of divergence between q and p
is atleast qualitatively related to the absolute magnitude
of the ϵ_{p_o} values. Thus the differences between the p and

q values in Table III and Fig. 37 are probably largely de-
termined by the ϵ_{p_o} values. Alternatively, it would appear
that plots such as those in Fig. 37 give a good indication
of the magnitude of the ϵ_{p_o} values. This in turn tells some-
thing about the nature of the power law fit to the stress-
strain curve. Thus considering Fig. 37 (b), corresponding
to stage 2, it is apparent that, for this stage, all the
longitudinal specimens correspond to curves whose $\sigma = 0$ inter-
cepts are positive, while the transverse specimens yield
curves in stage 2 that extrapolate back to negative values
of ϵ_{p_o}. This implies a difference in deformation behavior
between the two textures.

An additional advantage of an analysis based on the mod-
ified Swift equation is that the uniform elongation can be
simply related[59] to the parameters of the stage in which
necking occurs. Since it may be shown that

$$\epsilon_{p_u} = (1/m) + \epsilon_{p_o} \qquad (18)$$

where ϵ_{p_u} is the uniform strain defined as the strain corre-
sponding to the maximum load. Such a simple correlation of
uniform strain is not possible in the Crussard-Jaoul analy-
sis, although ϵ_{p_u} may be determined in terms of Eq.(9) by nu-
merical methods.[99] A good correspondence between the predict-
ed and observed uniform elongations is shown in Table III.

That the results of an analysis based on the Swift equa-
tion are not influenced by prestrain but are affected by the
changes in the deformation processes is shown by Figs. 38 and

39 . Longitudinal zirconium specimens deform by slip and $\{11\bar{2}2\}$ twinning, both at room temperature and at 77°K. There-fore, a small 77°K prestrain does not significantly change the room temperature deformation characteristics. On the other hand, transverse zirconium has a different dominating twinning mode at 77°K and at 298°K, changing from $\{11\bar{2}1\}$ to $\{10\bar{1}2\}$.[100] In accord with this, a small 77°K prestrain changes the deformation characteristics at room temperature and dif-ferent results are obtained with a prestrain. With the pre-strain, the 298°K deformation stage behavior becomes similar to that of a 77°K specimen without prestrain (Fig. 33).

5.10 Dynamic Strain Aging in Titanium[76]

The Tensile Ductility : From the data presented in Fig. 53 , we may conclude that the impurities have a very strong influ-ence on the uniform elongation. They cause a "blue brittle" elongation minimum in c.p.Ti at 760°K. Moreover, above 800°K, in the c.p.Ti specimens necking instability occurs at strains of 0.05 or less. Impurities also strongly affect the necking strain, as shown in Fig. 54 . In particular the rise in the necking strain just above the ductility minimum is much more rapid in c.p.Ti. In general a large necking strain is asso-ciated[101] with a strain rate dependent flow stress whose rate dependence may take several forms.[102] First the flow stress itself may be rate dependent. The large necking strains ob-served in superplasticity conform to this case. Here the

work hardening rate is effectively zero,[103] and n, the strain rate sensitivity parameter is large (> 0.3).[103] On the other hand, just above the blue brittle temperature in commercial purity titanium the work hardening rate is large and strain rate dependent, while n is small (≃ 0.01). In this case the large necking strain has been associated[102] with the rate dependence of the work hardening rate. Figure 54 shows that the necking strain is large in the commercial purity titanium not only just above the blue brittle temperature, but also at temperatures near the transformation point where this latter form of rate dependence would not be expected to hold. In this case n is about 0.2 and the work hardening rate is almost zero so that here the necking strain is probably developed in the same manner as superplasticity. The peak in Fig. 54 and Fig. 42 at 425°K imply the influence of the rate dependence of flow stress on the necking strain. However the work hardening rate at this temperature is not zero and it may have some rate dependence. Therefore, the necking strain at 425°K in c.p.Ti is probably influenced by both types of rate dependence. It may, therefore, be concluded that impurities in titanium tend to increase both types of flow stress dependence. Figures 59 and 60 clearly demonstrate the considerable effect of a fractional percent of impurities on titanium stress-strain curve shape.

The Work Hardening Rate : The large necking strain in c.p. Ti just above the minimum total elongation temperature can be explained in terms of a rate dependent work hardening rate

peak.[102] The much smaller h.p.Ti necking strain implies that in this material the rate dependent work hardening phenomena may be largely eliminated. Evidence for this is shown in Fig. 64 where the c.p.Ti curve shows a work hardening peak at 760°K that is absent in the h.p.Ti data. Moreover, Fig. 64 shows that lowering the impurity concentration in titanium to 300 ppm produces a work hardening rate-temperature curve, above 300°K, like that of silver whose work hardening rate decreases almost linearly with temperature. A similar result is obtained when nitrogen and carbon are removed from steel as can be seen if the data of Baird and Jamieson[104] are plotted in the manner of Fig. 64. The higher impurity level in c.p.Ti not only produces a peak at 760°K but increases the work hardening rate from approximately 300 to 900°K as revealed by the cross-hatched area between the two titanium curves in Fig. 64. Note that at the peak temperature (760°K) the work hardening rate in the commercial purity metal is about four times larger than that in the high purity metal.

Below 300°K, titanium twins heavily,[9,86] which has a strong effect on the shape of its stress-strain curve. The decrease in its work hardening rate parameter at low temperatures may be due to this cause. Above 300°K, where deformation primarily occurs by slip in titanium, the $1/E \cdot (\Delta\sigma/\Delta\epsilon_p)$ curves of high purity silver and high purity titanium are similar. It is often assumed[51,80,105,106] that the continuous decrease in work hardening rate with increasing deformation temperature observed in fcc metals is primarily due to

an increasing rate of dynamic recovery with rising temperature. On this basis, it may be assumed that above $300°K$, dynamic recovery is probably the major factor in determining the shape of the titanium work hardening rate - temperature curve.

The anomalous work hardening in titanium will be compared with those in zirconium and steel in a later section of this chapter.

Effect of Dynamic Strain Aging on Yielding : The deviations from a straight line on a $\ln(\tau/\mu)$ - temperature diagram in Fig. 72 correspond to temperature intervals where strain aging phenomena are observed. The low temperature deviation is probably due to hydrogen and the high temperature deviation is possibly due to a combined effect of carbon, nitrogen and oxygen. Note that the deviations, especially the high temperature deviation where the strongest strain aging effects are observed, is more significant in c.p.Ti. This indicates that while lowering the impurity concentration does not remove the effect on the yield stress, it seriously reduces it in the upper temperature range. Furthermore, Figs. 64 and 72 show clearly that whereas the small amount of interstitial impurities present in h.p.Ti is enough to influence the yield stress, it is insufficient to produce a measurable work hardening rate peak. With a low impurity concentration, the effects of dynamic strain aging should decrease with increasing strain because the available number of impurity atoms is fixed while the total dislocation line

length increases with strain. Therefore, the dilocation -
impurity interactions should be less effective at higher
strains, in agreement with an argument presented by Glen[107]
for steel.

No definite conclusion can be drawn from these results
regarding the relative importance of the impurity elements
responsible for dynamic strain aging in c.p.Ti. It is gen-
erally accepted that carbon and nitrogen are responsible
for strain aging in iron. The solubilities of carbon and ni-
trogen in iron at 473°K (near the iron blue brittle tempera-
ture) are 10^{-5} and 10^{-2} atomic percents respectively,[108]
so very small concentrations of these elements produce very
large dynamic strain aging effects. On the other hand, strain
aging phenomena have been associated with oxygen in vanadium[83]
and oxygen in tantalum[109] where the oxygen solubilities equal
several atomic percents. These observations are significant
as nitrogen and oxygen have high solubilities in titanium
(34 atomic percents O and about 5 atomic percents N at 800 K)[110]
while carbon and hydrogen have low solubilities (0.5 atomic
percent C[110] at 800°K and approximately 0.25 atomic percent
H[111] at 350°K). Thus all four interstitial elements may cause
strain aging. The hydrogen diffusion activation energy is
only 12,380 cal/mole[112] or about one fourth that of C, N or O.
Therefore, hydrogen is probably not associated with the strain
aging phenomena centered around 800°K, but may cause those
observed near 350°K. The high temperature phenomena therefore
probably represent the combined effects of C, N and O, all

of which are present in commercial purity titanium.

In iron the activation energy for the start of serrations on the stress-strain curve is close to that for the diffusion of carbon and nitrogen in iron.[84] This information has been used to associate the strain aging phenomena in iron with these elements.[84] In titanium, the activation energy for the start of the serrations is 41,000 cal/mole,[11] while the activation energy for the strain rate dependent work hardening peak is 59,000 cal/mole.[113] However, it has not been possible to relate these values unambiguously with the diffusion activation energies of any of the interstitial elements because in titanium these energies are nearly the same for nitrogen and carbon (45,250 $\pm$ 2,250 cal/mole for N[114] and 48,500 $\pm$ 3,000 cal/mole for C[115]). Furthermore, it has been shown[115] that the oxygen activation energy for diffusion (58000 cal/mole), as measured by internal friction, can be strongly affected by substitutional elements in solution. This is an important point since the present commercial purity titanium contains 1,600 ppm of iron whose effects are unknown.

5.11 Dynamic Strain Aging in Zirconium[89]

Tensile Ductility : Below 400°K and especially at 77°K, h.p. Zr specimens show larger uniform and necking elongations than the other two Zr specimens (Fig. 58). This is due to the effect of impurities on deformation twinning. Decreasing impurity content increases[88] the twinning rate in Zr, with the

result that the h.p.Zr stress-strain curve becomes approximately linear. In this type of curve because the work hardening rate is constant with strain, Considere's necking criterion ($d\sigma/d\epsilon = \sigma$) is delayed to large strains.

At intermediate temperatures, 400 to 750°K, the uniform strain of c.p.Zr specimens shows a greater variation than in the other zirconium grades. At the "blue brittle" temperature 720°K, the c.p.Zr uniform elongation curve shows a tendency for a minimum. The maximum value of uniform elongation at 625°K is due to a minimum value of q at this temperature due to the dynamic strain aging effects. The other two zirconium grades conform to high values of q throughout this temperature interval and therefore their uniform elongation curves show less variation. Above 750°K, dynamic recovery effects are appreciable, q increases resulting in smaller uniform elongations in all three zirconium grades. Comparing the c.p.Zr data with those of c.p.Ti in Fig. 53, it is noted that above 900°K, the uniform elongation of c.p.Ti is almost zero while in c.p.Zr it has a finite value around 0.05.

This difference can be explained in terms of the deformation stage behavior shown in Figs. 76 and 77. In these figures, the deformation behavior of c.p.Zr and c.p.Ti is analysed by the Crussard-Jaoul method at three representative temperatures. At the lower temperature limit of the DSA temperature range, at its center and at the higher limit of the DSA range. The values of the constants n and q evaluated for the different stages in Figs. 76 and 77 are given in Table IV.
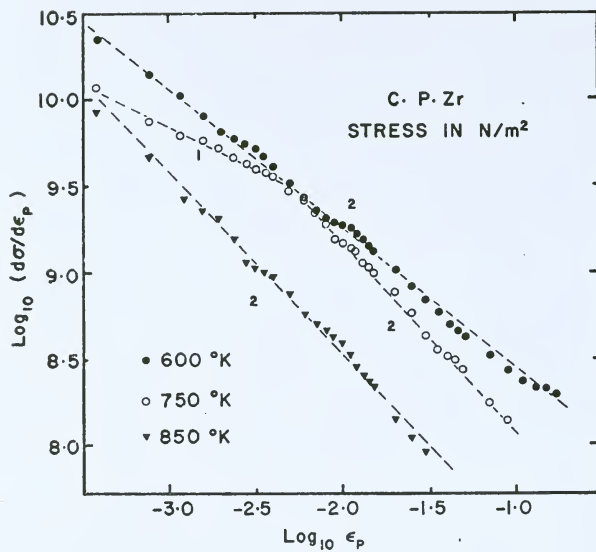
Fig. 76. The Crussard-Jaoul plots for c.p.Zr at 600, 750 and 850°K.
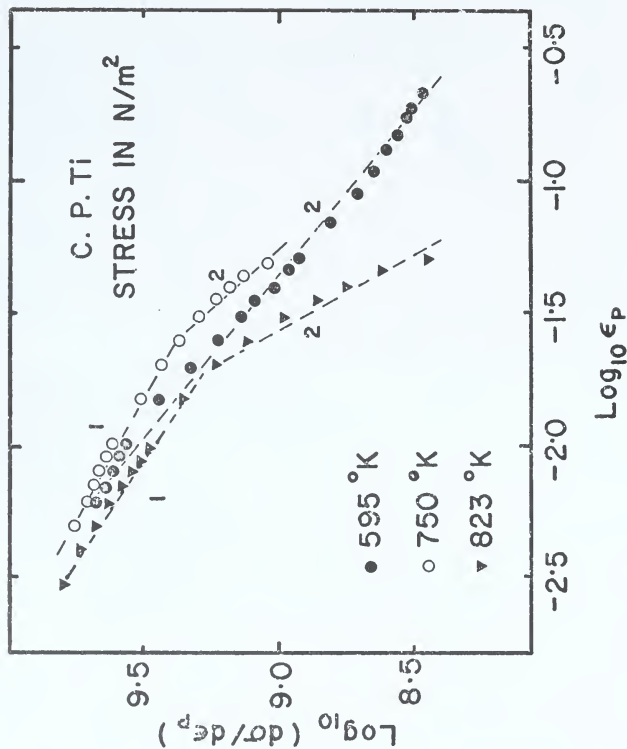
Fig. 77. The Crussard-Jaoul plots for c.p. Ti at 595, 750 and 823°K.

Table IV

The Constants n and q from the Crussard-Jaoul Plots
in the DSA Interval of C.P.Ti and C.P.Zr

Temperature	C.P.Zr			C.P.Ti		
	Stage No.	n	q	Stage No.	n	q
$600°$K	1	0.16	0.84	1	0.22	0.78
$750°$K	1	0.33	0.67	1	0.43	0.57
	2	-0.11	1.11	2	-0.09	1.09
$850°$K	1	-0.05	1.05	---	-----	----
$823°$K	--	----	----	1	0.35	0.65
	--	----	----	2	-0.77	1.77

Note that at any constant temperature the absolute magnitude of work hardening is higher in titanium than in zirconium.

At 600°K both c.p.Zr (Fig. 76) and c.p.Ti (Fig. 77) show a single stage behavior. As compared to the c.p.Ti data, the c.p.Zr data results in a lower n and higher q. At 750°K, both c.p.Zr and c.p.Ti data show a two stage behavior. Again the corresponding stages in c.p.Zr have lower n and higher q values. At 850°K, whereas c.p.Zr shows a single stage, the c.p.Ti specimen shows two stages with the second stage having a large negative n and high q. A high value of q in the second stage of c.p.Ti data at 850°K induces necking sooner in c.p.Ti. Thus the presence of a second stage with a large q explains the small (almost zero) uniform elongations in c.p.Ti above 850°K. Since the c.p.Zr data do not show such break into a second stage, the uniform elongation of c.p.Zr is finite at high temperatures.

The factors affecting the necking strain are the ductility level of a metal (reduction in area[116]), its strain rate sensitivity and the strain rate dependent work hardening. As will be discussed in the following section, the anomalous work hardening phenomena are negligible in zirconium and therefore only the first two factors need be considered. In this regard compare the strain rate sensitivity curves in Fig. 46 to the necking strain curves in Fig. 58 . Note that the corresponding c.p. and h.p.Zr curves are similar in shape. Near 450°K, the c.p.Zr curve has a maximum strain rate sensitivity corresponding to a maximum necking strain. The other

two zirconium grades that do not exhibit pronounced strain rate sensitivity maximum near 450°K, also do not have a very well-defined necking strain maximum in that temperature range. At the blue brittle temperature 720°K, the c.p.Zr necking strain shows a pronounced minimum. However, at this temperature, the absolute values of uniform and total elongations of c.p.Zr are 0.12 and 0.27 respectively, about double those reported for c.p.Ti[76] at its blue brittle temperature. These results support the conclusion that dynamic strain aging effects are less pronounced in zirconium than in titanium.

The proof offered in Fig.66 that the strain rate dependent work hardening rate peak in c.p.Zr is very weak supports an earlier conclusion[21] that the blue brittle ductility minimum and the rapid rise in necking strain above the blue brittle temperature are primarily associated with sharp changes in the strain rate sensitivity near the strain rate sensitivity minimum (Fig.46). On the other hand in c.p.Ti the blue brittle phenomena are probably associated both with the strain rate sensitivity minimum and the rate dependent work hardening.

The temperatures of the ductility minimum in Fig.56 and the strain rate sensitivity minimum (Fig.46) do not coincide as might be expected from the earlier results.[21] This is due to the fact that the blue brittle minimum is strain rate dependent and the strain rates employed in the two sets of measurements do not conform. Necking increases the strain rate in the neck. However the curves in Fig. 46 were obtained by decreasing the strain rate from the value employed to obtain the data in Fig.56.

The Work Hardening : The data presented in Fig.66 clearly demonstrate that the interstitials present in the c.p.Zr do not produce a work hardening rate peak. On the other hand a pronounced work hardening rate peak is observed in titanium at 760°K (Fig.64). Such a peak signifies a higher rate of dislocation density accumulation at the peak temperature compared to a temperature either lower or higher than the peak temperature. This peak is absent in h.p.Ti implying that the rise in dislocation density at the peak temperature is due to the interaction between the interstitials and the dislocations. The interaction is most likely to be the im- mobilization of dislocations by the impurity atoms. On the the basis of Fig. 67, it can be concluded that the intersti- tial-dislocation interaction is almost equally strong in ti- tanium and steel but is very weak in zirconium. This conclu- sion is supported by the fact that the Portevin-LeChatelier effect is observed in titanium and steel but is very weak or missing in zirconium.

Although the level of work hardening rate of h.o.Zr is higher (Fig.68) than that of c.p.Zr, even this most impure grade of zirconium fails to reveal a work hardening rate peak implying the insignificance of dynamic strain aging in zirconium. The higher level of work hardening of h.o.Zr may be due to the high iron content of this material.

The rapid falloff at high temperatures of the average work hardening rate of the three zirconium grades may be asso- ciated with an increase in dynamic recovery due to increasing

effectiveness of high temperature recovery (climb). A comparison of the three zirconium curves in Figs. 65 and 68 reveals that the temperature at which the average work hardening rate starts decreasing rapidly is lower in h.p.Zr (600°K) than in the other two grades of zirconium (750°K). This observation conforms to a retarding effect of impurity concentration on the rate of dynamic recovery.

The continuous decrease of the work hardening rate of h.p.Zr (Fig. 65) over the entire temperature range 77 to 1000° K is roughly similar to that of h.p.Ti and a fcc metal like silver (Fig. 64) where dynamic recovery has a pronounced effect on the deformation behavior.

The above differences in the work hardening behavior of titanium and zirconium can be examined from a more quantitative point of view by analysing the stress-strain data by the Crussard-Jaoul method. This is deemed appropriate for the present case as we are considering annealed metals covering a wide stress range. (See Figs. 76 and 77 and Table IV.) From these figures, we note that the work hardening rate level at any given temperature is always higher in titanium than in zirconium. At 600°K, although both c.p.Ti and c.p.Zr specimens show a single stage behavior, titanium has a lower q and a higher work hardening level resulting in a greater value of $(1/E).(\Delta\sigma/\Delta\epsilon_p)$ at 600°K for c.p.Ti than c.p.Zr (Fig. 67). At 750°K, again the corresponding stages of c.p.Ti have lower q values with higher work hardening rate level giving rise to a peak value of $(1/E).(\Delta\sigma/\Delta\epsilon_p)$ for c.p.Ti. After

increasing the temperature to 850°K, the c.p.Zr stress-strain curve goes back to a single stage behavior while c.p.Ti data continues to show two stage behavior with a second stage of increasing q values. Due to this the c.p.Ti work hardening rate parameter $(1/E).(\Delta\sigma\Delta\epsilon_p)$ decreases rapidly with increasing temperature above the peak temperature.

The Portevin-LeChatelier Effect : The Portevin-LeChatelier effect manifests itself as serrations on the stress-strain curve. This is due to the inhomogeneous deformation in the form of Luder's bands that nucleate in the gage section of the specimen. These bands[117] may propagate under rising load (Type A) or may not appear to propagate(Type B). Various complex combinations of these types are normally observed in practice. It is evident that discontinuous yielding is strongly associated with dislocation locking or immobilization as in the case of Type A band, plastic deformation does not occur behind a band moving under rising load or as in the case of Type B bands, deformation ceases in each band when the load drops.

Serrated plastic flow was not observed in the present zirconium specimens and has been reported in the past in only one investigation.[20] This is a strong evidence that the ability of impurities to immobilize or pin the dislocations in zirconium is not strong. This conclusion is further supported by the fact that yield points were not observed in the present zirconium grades. In the literature[118] small yield points have been reported for air-cooled fine grained zirco-

nium specimens. However, these yield points were not ratio-
nalized[118] in terms of strain aging due to their temperature
dependence and their nonreappearance after aging.

The Strain Rate Sensitivity : A strong effect of increasing
the purity on the strain rate sensitivity of zirconium is evi-
dent in Fig. 46. The most significant change occurs below
650°K. Note that with purification the strain rate sensiti-
vity maximum near 450°K is weakened and that the general shape
of the n - T curve of h.p.Zr roughly approximates that of
pure silver shown in Fig. 47. Similar n against T behaviors
have been reported for copper[101,119-120] and gold[121] and may
be taken as representative of fcc metals that show little or
no dynamic strain aging effects.

The data of Fig. 46 clearly show that the strain rate
dependence of the flow stress at low temperatures in the c.p.
Zr is largely determined by the impurity concentration.
These curves thus offer a direct confirmation for the conclu-
sion[29-32] that below 650°K the rate controlling deformation
mechanism in zirconium is the overcoming of interstitial atom
barriers. They also imply that in the absence of impurities
the rate controlling mechanism in zirconium below 650°K may
be like that of a fcc metal, as previously implied by Mills
and Craig,[31] and thus probably dislocation intersections.

Though there is a similar tendency[122] for concentration
dependence on the strain rate sensitivity peak at 425°K in
titanium (Fig. 42), the effect is not as pronounced as in
zirconium (Fig. 46). There are reasons to believe that the

present high purity grade of titanium is not pure enough to remove this peak. The deviations in the yield stress data of h.p.Ti (Fig.72) and the large temperature dependence of the yield stress of h.p.Ti below 500°K (Fig.71) imply the presence of a considerable amout of impurities in h.p.Ti (though not enough to produce the work hardening effect). Therefore it is believed that an investigation of a higher purity titanium grade is necessary to check if the strain rate sensitivity peak can be eliminated by purification. However from the trend of the titanium data and extending the zirconium results, it is possible to state that the hypothesis[77,87,123-125] that the rate controlling thermally activated deformation mechanism in titanium at low temperatures is the overcoming of the interstitial barriers, is probably correct.

Above 700°K, the strain rate sensitivity of zirconium (Fig.46) depends less on the impurity concentration. The rapid rise of n with temperature in this range is also apparent in the silver data in Fig.47. In both metals the work hardening rate becomes very small at elevated temperatures. This conforms to the development, during deformation, of a stable substructure whose cell size is determined by the temperature and strain rate. At the same time, while the flow stress becomes nearly independent of stress (almost zero work hardening rate) it becomes strongly dependent on the strain rate. This structure dependence of the flow stress is reflected in Fig. 47 by the marked dependence of n on the

starting grain size of the silver specimens.

The strain rate sensitivity minimum in the dynamic strain aging interval can now be rationalized.[19] From the definition of the strain rate sensitivity Eq. (4), it is seen that when n approaches zero, the flow stress becomes strain rate independent. Since the flow stress is normally related to the dislocation velocity, a strain rate independent flow stress implies a strain rate independent dislocation velocity. Such a relationship between dislocation velocity and strain rate is possible if the model proposed by McCormick[126] to explain the onset of serrated flow is generalized.[19] This assumes that the dislocation velocity during dynamic strain aging is largely controlled by the diffusion rate of the impurity atoms. This follows from the assumption that a dislocation waiting to be thermally activated at a penetrable obstacle should become immobilized if it waits longer than the time, t_i, necessary to immobilize it as a result of the formation of solute atmospheres. In effect this requires that the average dislocation velocity be equal or greater than

$$v = (1/t_i) \tag{19}$$

where l is the average distance between penetrable obstacles. In this relation t_i, the time to immobilize a dislocation, is primarily a function of the diffusion rate of impurities and therefore independent of the applied strain rate.

It is important to note that Eq. (19) is based on a steady state deformation. This implies that the steady state

strain rate sensitivity n" should be indicative of the sig-
nificance of DSA in a metal. In this regard it is worth not-
ing that n" in zirconium (Fig. 46) does fall to about 0.02
at the strain rate sensitivity minimum. This suggests that
interstitial atoms do have an influence on the dislocation
velocity in zirconium. However their effect is certainly
less than that in c.p.Ti where n" is effectively zero.

5.12 Comparison of DSA Effects in Ti, Zr and Steel

Since an unique parameter to evaluate the significance
of dynamic strain aging in metals is not available, probably
the most appropriate way of comparing DSA effects in metals
is to consider all the major manifestations of dynamic strain
aging individually.

Serrated yielding or the Portevin-LeChatelier effect is
strong in steels, it is present in titanium to a lesser ex-
tent in titanium and is almost absent in zirconium. Consis-
tent with this fact is the presence of yield points in steel
and titanium and their absence in zirconium. Abnormal and
strain rate dependent work hardening is present almost to
the same extent in steel and titanium and is absent in zir-
conium (Fig. 67). Strain rate sensitivity minimum in the
dynamic strain aging interval is observed in all three metals.
Transients after a strain rate change are observed in the
stress-strain diagrams of steel and titanium, but are absent
in zirconium. Yield stress or flow stress plateaus on a flow

stress-temperature diagram are observed in steel and titanium data. They are also recorded in the zirconium data though to a lesser degree. The blue brittle elongation minimum is present in steel and titanium data significantly and is not so pronounced in zirconium.

Based on the above stated observations, it can be concluded that dynamic strain aging effects are significant and comparable in titanium and steel. The DSA effects are weak, however, in zirconium. This implies that while impurities (interstitials) interact strongly with dislocations in steel and titanium, this interaction is weak in zirconium. This conclusion is in agreement with the observations of Tyson[32] who showed that at room temperature the interstitials O and N affect the flow stress of titanium to a greater extent compared to their effect on the flow stress of zirconium.

5.13 Strain Rate Sensitivity Minimum as a Measure of Significance of DSA

The present results on the deformation of titanium and zirconium indicate that the strain rate sensitivity minimum is a good measure of DSA effects provided the strain rate sensitivity is calculated from the extrapolated steady state flow stress level. For titanium, that shows significant DSA effects, has a n"value of zero at the minimum while zirconium that does not show DSA effects significantly, n" at the DSA minimum is 0.02.

5.14 Effect of Prestraining in DSA Interval

That in the DSA interval of titanium the interstitials interact strongly with dislocations and immobilize them is supported by the fact that yield points appear in the specimens prestrained in DSA interval (Fig. 75). Note that the specimen without the prestrain does not exhibit yield point behavior. A typical work softening behavior, where the specimen necks and fractures at considerably lower elongation after prestraining is not observed in titanium implying that contrary to the steel behavior[75] the dislocation substructure introduced by the prestraining in the DSA range is relatively stable at room temperature. On the other hand prestraining in the dynamic strain aging interval does not increase the yield stress or the ultimate tensile strength of titanium to any appreciable extent and therefore, unlike steel,[73,74] this method cannot probably be used as a strengthening mechanism.

5.15 The Cottrell-Stokes Law in Titanium and Zirconium

It is shown by the present results on h.p.Zr that the temperature variations of the work hardening rate and strain rate sensitivity approach those of a fcc metal. A similar trend, to a lesser degree, is also observed in h.p.Ti data. Since the Cottrell-Stokes law is generally obeyed by fcc metals, it would imply that the deformation of a sufficiently pure zirconium and titanium would follow this law. That this

is true below room temperature is shown by the results in
Figs. 44, 45, 48 and 49. There seems to be an effect of
twinning in this connection as deformation twinning occurs
in these metals below room temperature. These results are
consistent with earlier results on zirconium[20] and cadmium[127]
which show that the Cottrell-Stokes law is obeyed when defor-
mation occurs by both slip and twinning.

5.16 Effect of Prestraining at 77°K

The improvement in the yield stress and the ultimate
tensile strength of titanium, especially at the high purity
level, due to a 77°K prestrain is remarkable (Figs. 73 and 74).
The important point is that this strengthening is not accom-
panied by a loss of ductility normally associated with the
work softening. The $\{11\bar{2}2\}$, $\{11\bar{2}4\}$ and $\{10\bar{1}2\}$ deformation
twins introduced during prestraining grow during room tempera-
ture deformation. Therefore, prestraining at 77°K can be
used as a strengthening mechanism for titanium.

CHAPTER VI
CONCLUSIONS

1. Deformation twinning is significant in the low temperature deformation of several grades of titanium over a range of texture and grain sizes.

2. Deformation twinning is also important in the low temperature deformation of high purity zirconium.

3. The linear work hardening rate and high uniform elongations observed in h.p.Ti and h.p.Zr at $77°K$ are associated with a high rate of deformation twinning.

4. The changes in the work hardening behavior indicated by Crussard-Jaoul plots of $77°K$ stress-strain data of titanium and zirconium correspond closely to changes in evolution of twin structure.

5. Impurities have a stronger effect in suppressing deformation twinning in zirconium than in titanium.

6. Due to the Luder's plateau, deformation of h.p.Ti is complex at low strains. For strains above 0.01, twin nucleation is dominant. For h.p.Zr, twin growth appears to be more significant above 0.05 strain.

7. Deformation twinning is more prominent in Ti than in Zr. It accounts for about 30 percent of the total strain in h.p.Ti, while the corresponding contribution in h.p.Zr is only about 10 percent.

169

8.   Both the Crussard-Jaoul analysis and the one based on the Swift equation are in qualitative agreement in revealing the number and extent of the stages of a zirconium stress-strain curve.

9.   Transverse and longitudinal zirconium specimens exhibit basically different types of stress-strain behavior, as exemplified by differences in the number of stages and the values of the parameters descriptive of the stages.

10. Above approximately 500 to 600°K the longitudinal zirconium stress-strain curve can be approximated by a single stage. In this range deformation primarily occurs by prism slip. In specimens where twinning or kinking are important deformation features, multi-stage behavior was observed.

11. The basic zirconium stress-strain curve is generally one in which the stress-strain curve slope (work hardening rate) tends to decrease rapidly with increasing stress (or strain). The rate of this decrease is much more rapid than in a typical fcc metal such as nickel or copper.

12. In high purity titanium specimens the dynamic strain aging phenomena are either eliminated or drastically reduced. These include : the Portevin-LeChatelier effect, the "blue brittle" elongation minimum and the anomalous work hardening phenomena.

13. The tendency for the shapes of the stress-strain curves of commercial purity titanium to vary widely with temperature and strain rate is due largely to dynamic strain aging.

14.   Impurities have a strong effect on the work hardening rate of titanium and act to increase it over a wide range of temperatures. The work hardening rate tends to maximize at a temperature (or temperatures) whose value depends on the strain rate.

15.   In titanium, dynamic strain aging has a very strong effect on the amount of uniform elongation. At elevated temperatures this parameter tends to become very small, implying that impurities induce early necking.

16.   At high temperatures, dynamic strain aging produces large necking strains in c.p.Ti suggesting that DSA increases the strain rate dependence of the flow stress.

17.   Dynamic strain aging effects are insignificant in zirconium.

18.   The work hardening characteristics and the rate dependence of the flow stress of pure zirconium and pure titanium approach   the behavior of a fcc metal.

19.   While the blue brittle effect in zirconium is probably primarily due to the low strain rate sensitivity in the DSA region, this effect in titanium is probably due to a combined effect of the strain rate dependent work hardening rate and the low strain rate sensitivity.

20.   In terms of the work hardening rate peak magnitude, the dynamic strain aging effect is strong and comparable in steel and titanium. It is very weak in zirconium.

21.   The Portevin-LeChatelier effect is strong in steel, less pronounced in titanium and is absent in zirconium.

22. Impurities interact strongly with dislocations in titanium. In zirconium, however, this interaction is weak.

23. The strain rate sensitivity minimum in the DSA region is a good measure of the magnitude of DSA effects, provided an extrapolated steady state load value after the strain rate change is used to calculate the strain rate sensitivity.

24. Below $600°K$, the rate controlling thermally activated deformation mechanism in zirconium is probably the dislocations overcoming the interstitial barrier atoms. Same mechanism probably operates in titanium at low temperatures.

25. Titanium and zirconium obey the Cottrell-Stokes law below room temperature where the deformation occurs by slip and twinning.

26. Prestraining at $77°K$ results in a considerable increase in the room temperature yield stress and ultimate tensile strength of titanium without any appreciable loss of ductility.

27. In c.p.Ti, although the structure obtained by a prestrain in the dynamic strain aging region is relatively stable at room temperature, such a prestrain does not increase the room temperature strength appreciably.

BIBLIOGRAPHY

1. R. N. Orava, G. Stone and H. Conrad : _Trans. ASM_, 1966, vol. 59, p. 171.

2. R. L. Jones and H. Conrad : _Acta Met._, 1967, vol. 15, p. 649.

3. R. L. Jones and H. Conrad : _Scripta Met._, 1968, vol. 2, p. 239.

4. H. Conrad and R. Jones : _The Science, Technology and Application of Titanium_, R. Jaffee and N. Promisel, eds., p. 489, Pergamon Press, New York, 1970.

5. F. D. Rosi and F. C. Perkins : _J. Metals_, 1953, vol. 5, p. 1083.

6. E. B. Kula and T. S. DeSisto : Am. Soc. Testing Mater., Spec. Tech. Publ., 1966, p. 387.

7. H. R. Burrier, Jr., M. F. Amateau and E. A. Steigerwald : Air Force Materials Laboratory, AFML-TR-65-239, July 1965.

8. F. D. Rosi and F. C. Perkins : _Trans. ASM,_ 1953, vol. 45, p. 972.

9. Y. Lii, V. Ramachandran and R. E. Reed-Hill : _Met. Trans.,_ 1970, vol. 1, p. 447.

10. R. J. Wasilewski : _Trans. ASM_, 1963, vol. 56, p. 221.

11. A. T. Santhanam : Ph. D. Dissertation, University of Florida, 1971.

12. W. R. Kiessel and W. J. Sinnott : _Trans. TMS-AIME_, 1953, vol. 197, p. 331.

13. R. L. Jones : _Scripta Met._, 1968, vol. 2, p. 345.

14. J. W. Suiter : _J. Inst. Metals,_ 1954-55, vol. 83, p. 460.

15. N. G. Turner and W. T. Roberts : _J. less-common Metals,_ 1968, vol. 16, p. 37.

16. J. D. Baird : _Metals Mater. Metall. Rev.,_ 1971, vol. 5, p. 149.

17. S. N. Monteiro, A. T. Santhanam and R. E. Reed-Hill : _The Science, Technology and Application of Titanium,_ R. Jaffee and N. Promisel, eds., p. 503, Pergamon Press, New York, 1970.

18. A. T. Santhanam and R. E. Reed-Hill : _Scripta Met._, 1970, vol. 4, p. 529.

19. R. E. Reed-Hill :"On the Dynamics of Dislocation Pinning during Dynamic Strain Aging," Technical Report to the Army Research Office, Durham (AROD), N. Carolina, April 25, 1973.

20. B. Ramaswami and G. B. Craig : _Trans. TMS-AIME_, 1967, vol. 239, p. 1226.

21. V. Ramachandran and R. E. Reed-Hill : _Met. Trans._, 1970, vol. 1, p. 2105.

22. C. R. Simcoe and D. E. Thomas :"The tensile properties of zirconium alloys at fabrication temperatures and strain rates," WAPD-51, Westinghouse Atomic Power Division, Pittsburgh, Pa., 1952.

23. D. Lee : _Met. Trans._, 1970, vol. 1, p. 1607.

24. L. S. Rubenstein, J. G. Goodwin and F. L. Shubert : _Trans. ASM_, 1961, vol. 54, p. 20.

25. D. Lee : _Trans. ASM_, 1968, vol. 61, p. 742.

26. L. G. Bell : _Canad. Met. Quart._, 1963, vol. 2, p. 119.

27. W. R. Tyson : _J. Nucl. Mat._, 1967, vol. 24, p. 101.

28. D. Lee and W. A. Backofen : _Trans. TMS-AIME_, 1967, vol. 239, p. 1034.

29. W. R. Tyson and G. B. Craig : _Canad. Met. Quart._, 1968, vol. 7, p. 119.

30. P. Soo and G. T. Higgins : _Acta Met._, 1968, vol. 16, p. 177.

31. D. Mills and G. B. Craig : _Trans. TMS-AIME_, 1968, vol. 242, p. 1881.

32. W. R. Tyson : _Canad. Met. Quart._, 1967, vol. 6, p. 301.

33. J. J. Holmes : _J. Nucl. Mat._, 1964, vol. 13, p. 137.

34. K. G. Samual and P. Rodriguez :"Deformation mechanisms in Zircaloy-2 at low temperatures," To appear in _Trans. Indian Inst.Met._

35. P. Feltham : _J. Inst. Metals_, 1961, vol. 89, p. 210.

36. F. Guiu and P. L. Pratt : _Phys. Stat. Sol._, 1964, vol. 6, p. 111.

37. P. Rodriguez : _J. Mat. Sci._, 1968, vol. 3, p. 452.

38. J. C. M. Li : _Canad. J. Phys._, 1967, vol. 54, p. 493.

39. I. Gupta and J. C. M. Li : _Mat. Sci. Engr._, 1970, vol. 6, p. 20.

40. I. Gupta and J. C. M. Li : _Met. Trans._, 1970, vol. 1, p. 2323.

41. D. Lee and E. W. Hart : _Met. Trans._, 1971, vol. 2, p. 1245.

42. A. T. Santhanam, V. Ramachandran and R. E. Reed-Hill : _Met. Trans._, 1970, vol. 1, p. 2593.

43. P. D. Gupta : _Trans. Indian Inst. Met._, December 1970, p. 22.

44. J. D. Lubhan : _Trans. AIME_, 1949, vol. 185, p. 702.

45. J. D. Lubhan : _Trans. ASM_, 1952, vol. 44, p. 643.

46. C. W. MacGregor and J. C. Fisher : _J. App. Mechanics_, 1946, vol. 13, A-11.

47. J. W. Pugh : _Trans. ASM_, 1955, vol. 47, p. 984.

48. P. L. Raffo : _Met. Trans._, 1970, vol. 1, p. 835.

49. J. W. Pugh : _Trans. ASM_, 1956, vol. 48, p. 677.

50. J. W. Pugh : _Trans. AIME_, 1957, vol. 209, p. 1243.

51. A. Seeger : _Dislocations and Mechanical Properties of Crystals_, J. C. Fisher, W. G. Johnston, R. Thomson and T. Vreeland, Jr., eds., 1957, p. 243, John Wiley.

52. E. Macherauch : _Z. Metallkunde_, 1964, vol. 55, p. 60.

53. G. Zankl : _Z. Naturforschg_, 1963, vol. 18a, p. 795.

54. Ch. Schwink and W. Vorbrugg : _Z. Naturforschg,_ 1967, vol. 22a, p. 626.

55. Ch. Schwink and D. Knoppik : _Phys. Stat. Sol._, 1965, vol. 8, p. 729.

56. D. Krause and E. Göttler : Phys. Stat. Sol., 1965, vol. 8, p. 485.

57. U. Essman, M. Rapp and M. Wilkens : Acta Met., 1968, vol. 16, p. 1275.

58. O. Vöhringer and E. Macherauch : Z. Metallkunde, 1967, vol. 58, p. 21.

59. R. E. Reed-Hill, W. R. Cribb and S. N. Monteiro :"Concerning the analysis of tensile stress-strain data using log (dσ/dε_p) versus logσ diagrams," Accepted for publication in Metallurgical Transactions.

60. W. B. Morrison : Met. Trans., 1971, vol. 2, p. 331.

61. Y. Bergstrom and B. Aronsson : Met. Trans., 1970, vol. 1, p. 1029.

62. Y. Bergstrom and B. Aronsson : Met. Trans., 1972, vol. 3, p. 1951.

63. V. S. Arunachalam, S. Pattnaik, S. N. Monteiro and R. E. Reed-Hill : Met. Trans., 1972, vol. 3, p. 1009.

64. S. N. Monteiro and R. E. Reed-Hill : Met. Trans., 1973, vol. 4, p. 1011.

65. J. H. Hollomon : Trans. AIME, 1945, vol. 162, p. 268.

66. P. Ludwik : Elemente der Technologischen Mechanik, Julius Springer, Berlin, 1909, p. 32.

67. H. W. Swift : J. Mech. Phys. Solids, 1952, vol. 1, p. 1.

68. C. Crussard and B. Jaoul : Rev. Met., 1950, vol. 47, p. 589.

69. C. Crussard : Rev. Met., 1953, vol. 10, p. 697.

70. B. Jaoul : J. Mech. Phys. Solids, 1957, vol. 5, p. 95.

71. R. T. Dehoff and F. N. Rhines : Quantitative Microscopy, McGraw-Hill Inc., 1968.

72. R. E. Reed-Hill and E. P. Dahlberg : Electrochem. Tech., 1966, vol. 4, p. 303.

73. D. J. Lloyd and K. Tangri : Mat. Sci. Engg., 1972, vol. 10, p. 75.

74. I. Gokyu and K. Hashimoto : J. Japan Inst. Met., 1967, vol. 31, p.352.

75. W. P. Longo and R. E. Reed-Hill : Scripta Met., 1972, vol. 6, p. 833.

76. A. M. Garde, A. T. Santhanam and R. E. Reed-Hill : Acta Met., 1972, vol. 20, p. 215.

77. H. Conrad : Acta Met., 1966, vol. 14, p. 1631.

78. V. Ramachandran : Ph. D. Dissertation, University of Florida, 1970.

79. M. L. Picklesimer : "Anodizing as a metallographic technique for zirconium base alloys," ORNL-2296, May 24, 1957, Oak Ridge National Laboratory, Oak Ridge, Tennessee.

80. U. F. Kocks, H. S. Chen, D. A. Rigney and R. J. Schaefer : Work hardening, AIME Met. Conf. Series, J. P. Hirth and J. Weertman, eds., Gordon and Breech Science Publishers, New York, 1968, vol. 46, p. 151.

81. V. Ramachandran, D. H. Baldwin and R. E. Reed-Hill : Met. Trans., 1970, vol. 1, p. 3011.

82. R. P. Carreker, Jr. : Trans. TMS-AIME, 1957, vol. 209, p. 112.

83. S. A. Bradford and O. N. Carlson : Trans. TMS-AIME, 1962, vol. 224, p. 738.

84. A. S. Keh, Y. Nakada and W. C. Leslie : Dislocation Dynamics, A. R. Rosenfield, G. T. Hahn, A. L. Bement, Jr. and R. I. Jaffee, eds., 1968, McGraw-Hill, p. 381.

85. B. J. Brindley and J. T. Barnby : Acta Met., 1966, vol. 14, p. 1765.

86. A. M. Garde and R. E. Reed-Hill : Met. Trans., 1971, vol. 2, p. 2885.

87. G. Sargent and H. Conrad : Scripta Met., 1969, vol. 3, p. 43.

88. A. M. Garde, E. Aigeltinger and R. E. Reed-Hill : Met. Trans., 1973, vol. 4, p. 2461.

89. A. M. Garde, E. Aigeltinger, B. N. Woodruff and R. E. Reed-Hill : " The insignificance of dynamic strain aging in zirconium," to be submitted for publication to Metallurgical Transactions.

90. S. L. Mannan and P. Rodriguez : Trans. Indian Inst. Met., June 1973, p. 49.

91. R. E. Reed-Hill : "The role of deformation twinning in determining the mechanical properties of metals," Paper presented at the 1971 ASM Seminar in Detroit and to be published in the proceedings of the seminar.

92. E. A. Loria, G. H. Keith and E. A. Rowe : "Correlation of yield behavior in electrorefined anadium with interstitial impurities," U. S. Department of the Interior, Bureau of Mines. Report of investigations 6716, 1965.

93. K. S. Raghavan, A. S. Sastri and M. J. Maricinkowski : Trans. TMS-AIME, 1969, vol. 245, p. 1569.

94. C. N. Reid, A. Gilbert and G. T. Hahn : Acta. Met., 1966, vol. 14, p. 975.

95. R. E. Reed-Hill : Review of high temperature materials, 1972, vol. 1, p. 99, Freund Publishing House Ltd., Tel-Aviv, Isreal.

96. A. M. Garde and R. E. Reed-Hill :" A Dual Analysis of Longitudinal and Transverse Zirconium Tensile Stress-Strain Data," Paper presented at ASTM-AIME Symposium on Zirconium in Nuclear Applications, Portland, Oregon, August 21-24, 1973 and accepted for publication in the ASTM-STP covering the proceedings of the Symposium.

97. W. R. Cribb : Unpublished Research, University of Florida.

98. J. L. Martin and R. E. Reed-Hill : Trans. TMS-AIME, 1964, vol. 230, p. 780.

99. K. Ono : Met. Trans., 1972, vol. 3, p. 749.

100. R. E. Reed-Hill, E. R. Buchanan and F. W. Caldwell, Jr. : Trans. TMS-AIME, 1965, vol. 233, p. 1716.

101. A. Nadai and M. J. Manjoine : Trans. Am. Soc. Mech. Engrs., 1941, vol. 63, p. A77.

102. A. T. Santhanam and R. E. Reed-Hill : Met. Trans., 1971, vol. 2, p. 2619.

103. D. H. Avery and J. M. Stuart : Surfaces and Interfaces, J. J. Burke and V. Weiss, eds., 1968, p. 371, Syracuse University Press.

104. J. D. Baird and A. Jamieson :"The Relation between Structure and Mechanical Properties of Metals," National Physical Laboratory Symposium 15, 1963, p. 361, H.M.S.O.

105. D. Kuhlmann-Wilsdorf : <u>Work Hardening</u>, AIME Met. Conf. Series, J. P. Hirth and J. Weertman, eds., Gordon and Breech Science Publishers, 1968, p. 97.

106. J. J. Jonas, H. J. McQueen and W. A. Wong : Iron and Steel Institute Publication 108, 1966, p. 49.

107. J. Glen : <u>J. Iron and Steel Inst.</u>, 1957, vol. 186, part 1, p. 21.

108. J. D. Baird : <u>Iron Steel</u>, 1963, vol. 7, p. 326.

109. S. Hartley : <u>Acta Met.</u>, 1966, vol. 14, p. 1237.

110. M. Hansen and K. Anderko : <u>Constitution of Binary Alloys</u>, 1958, McGraw-Hill, pp. 383, 990, 1069.

111. W. Köster, L. Bangert and M. Evers : <u>Z. Metallkunde</u>, 1956, vol. 47, p. 564.

112. R. J. Wasilewski and G. L. Kehl : <u>Metallurgica</u>, 1954, vol. 50, p. 225.

113. A. T. Santhanam : Unpublished Research.

114. R. J. Wasilewski and G.L. Kehl : <u>J. Inst. Metals</u>, 1954-55, vol. 83, p. 94.

115. D. R. Miller and K. M. Browne : <u>The Science, Technology and Application of Titanium</u>, R. Jaffee and N. Promisel, eds., 1970, Pergamon Press, p. 401.

116. F. J. M. Boratto, P. R. Cetlin and J. T. Veado : <u>Scripta Met.</u>, 1973, vol. 7, p. 1031.

117. P. R. Cetlin, A. S. Gülec and R. E. Reed-Hill : <u>Met. Trans.</u>, 1973, vol. 4, p. 513.

118. D. Weinstein : <u>Electrochem. Tech.</u>, 1966, vol. 4, p. 307.

119. R. P. Carreker, Jr. and W. R. Hubbard, Jr. : <u>Acta Met.</u>, 1953, vol. 1, p. 654.

120. A. Nadai and M. J. Manjoine : <u>Proc. ASTM</u>, 1940, vol. 40, p. 822.

121. P. C. J. Gallagher : <u>Phil. Mag.</u>, 1967, vol. 15, p. 55.

122. A. M. Garde :"The Strain Rate Sensitivity of Titanium," Paper that won the 1972 TMS-AIME Outstanding Student Paper Award.

123. H. Conrad : <u>Canad. J. Phys</u>., 1967, vol. 145, p. 581.

124. K. Okazaki and H. Conrad : <u>Trans. Jap. Inst. Met</u>., 1972, vol. 13, p. 205.

125. K. Okazaki and H. Conrad : <u>Acta Met</u>., 1973, vol. 21, p. 1117.

126. P. G. McCormick: <u>Acta Met</u>., 1972, vol. 20, p. 351.

127. N. R. Risebrough and E. Teghtsoonian : <u>Canad. J. Phys</u>., 1967, vol. 45, p. 591.

BIOGRAPHICAL SKETCH

Anand Madhav Garde was born on January 1, 1945 at Sangli, India. In 1961, after graduating from New English School, Poona-30, India, he joined Fergusson College of the University of Poona where he passed the Pre-Professional Examination in 1963. He received the degree of Bachelor of Technology in Metallurgical Engineering from the Indian Institute of Technology, Bombay-76, India. During 1967-68, he was a graduate student in Ferrous Process Metallurgy at the same Institute.

In the fall of 1968, he came to the USA and received the degree of Master of Science in Metallurgical Engineering from the Syracuse University, Syracuse, New York in June 1970. Since then, he has studied for his doctorate in the Materials Science and Engineering Department of the University of Florida. In 1972, his paper, "The Strain Rate Sensitivity of Titanium," won the TMS-AIME Outstanding Student Paper Award. He is a member of ASM, TMS-AIME and Alpha Sigma Mu.

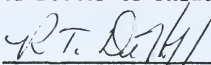He is married to Vandana, formerly Alka Joshi, and they have a one year old daughter, Vinaya.

I certify that I have read this study and that in my opinion it conforms to acceptable standards of scholarly presentation and is fully adequate, in scope and quality, as a dissertation for the degree of Doctor of Philosophy.
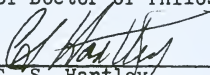
R. E. Reed-Hill, Chairman
Professor of Materials Science
and Engineering

I certify that I have read this study and that in my opinion it conforms to acceptable standards of scholarly presentation and is fully adequate, in scope and quality, as a dissertation for the degree of Doctor of Philosophy.

R. T. Dehoff
Professor of Materials Science
and Engineering

I certify that I have read this study and that in my opinion it conforms to acceptable standards of scholarly presentation and is fully adequate, in scope and quality, as a dissertation for the degree of Doctor of Philosophy.

C. S. Hartley
Associate Professor of Materials
Science and Engineering

I certify that I have read this study and that in my opinion it conforms to acceptable standards of scholarly presentation and is fully adequate, in scope and quality, as a dissertation for the degree of Doctor of Philosophy.

A. K. Varma
Associate Professor of
Mathematics

This dissertation was submitted to the Graduate Faculty of the College of Engineering and to the Graduate Council, and was accepted as partial fulfillment of the requirements for the degree of Doctor of Philosophy.

December, 1973

Wayne H. Chen

Dean, College of Engineering

Dean, Graduate School